

**Investigations into
membrane protrusions
mediated by IRSp53 IMD**

By

Andrew Philip Waller

A thesis submitted to the University of Birmingham for the
degree of DOCTOR OF PHILOSOPHY

School of Biosciences
The University of Birmingham
September 2009

UNIVERSITY OF
BIRMINGHAM

University of Birmingham Research Archive

e-theses repository

This unpublished thesis/dissertation is copyright of the author and/or third parties. The intellectual property rights of the author or third parties in respect of this work are as defined by The Copyright Designs and Patents Act 1988 or as modified by any successor legislation.

Any use made of information contained in this thesis/dissertation must be in accordance with that legislation and must be properly acknowledged. Further distribution or reproduction in any format is prohibited without the permission of the copyright holder.

Summary

Cells depend on the actin cytoskeleton and the structures it forms for a wide range of processes. IRSp53 acts downstream of cytoskeleton master regulators Rac and Cdc42 in the formation of lamellipodia and filopodia, respectively. IRSp53 interacts with many other effectors in the formation of these structures, via various protein interaction domains. IRSp53 also contains an IMD (IRSp53/MIM homology domain), which is able to induce formation of filopodia-like structures when overexpressed in cells. Early reports suggested that the IMD exerts its effect by bundling actin filaments. However, the structure of the IMD revealed that it is related to BAR domains, which can induce membrane curvature by binding to membranes. It is still unsure whether IMD activity is dependent on actin or membrane interactions, or both. Data are presented here showing that actin destabilizing drug cytochalasin D prevents extension of IMD protrusions, suggesting a role for actin in this process. Fluorescence recovery after photobleaching experiments suggest that a large proportion of IMD is stably associated with the protrusions. Finally, *in vitro* lipid binding experiments suggest that IMD binds to membranes by mainly electrostatic interactions. These findings suggest that IMD activity may depend on interactions with both actin filaments and membranes.

Acknowledgements

I would like to thank my supervisors Klaus Fütterer and Laura Machesky for giving me the opportunity to work with them, and for their advice and support. Thanks to all members of the 8th floor in Biosciences for their advice. Special thanks to John Dawson for help and advice in the lab, and a comfortable camp bed in Glasgow; and Balazs Visegrady for FRET experiments and advice.

Thanks also to Nicola, my parents and friends for love and support.

Thanks to the Scientific Projects Committee at the University of Birmingham for funding.

Abbreviations

Arp2/3	Actin related proteins 2 and 3
AUC	Analytical ultracentrifugation
BAR domain	Bin/Amphiphysin/RVS domain
C ter	Carboxy terminal
CD	Circular dichroism
CM	Carboxy-methyl
CME	Clathrin mediated endocytosis
Cos-7	CV-1 origin SV40 (simian kidney cell line)
CRIB	Cdc42/Rac interactive binding
CytD	Cytochalasin D
DMEM	Dulbecco's modified eagle media
DTT	Dithiothreitol
<i>E. coli</i>	Escherichia coli
EDTA	Ethylenediaminetetraacetic acid
EGF	Epidermal growth factor
EGFP	Enhanced Green Fluorescent Protein
EM	Electron microscopy
F-BAR	Fch-Bin Amphiphysin Rvs
FCS	Foetal calf serum
FRAP	Fluorescence Recovery After Photobleaching
FRET	Förster Resonance Energy Transfer
GFP	Green fluorescent protein
GST	Glutathione-S-transferase
GTP	Guanosine triphosphate
I-BAR	Inverse Bin/Amphiphysin/Rvs
IMD	IRSp53/MIM homology domain
IRSp53	Insulin Receptor Protein of 53 kDa
latB	Latrunculin B
LB	Lurea broth
MIM	Missing in metastasis

N-BAR	N-terminal helix containing BAR
N-WASP.....	Neuronal Wiskott Aldrich syndrome protein
PAGE	Poly acrylamide gel electrophoresis
PBS	Phosphate buffered saline
PC	Phosphatidylcholine
PCR.....	Polymerase chain reaction
PI(4,5)P2	Phosphatidylinositol-4,5-bisphosphate
PS	Phosphatidylserine
PSD.....	Post synaptic density
RCB	Rac binding domain
RFP	Red fluorescent protein
SDS	Sodium dodecyl sulphate
SH3	Src-homology 3 domain
TIRF	Total Internal Reflection Fluorescence
VASP	Vasodilator-stimulated phosphoprotein
WAVE	Wiskott Aldrich verproline homologue

Contents

1	Introduction	1
1.1	Actin dynamics	2
1.2	Small GTPases Rac and Cdc42 regulate formation of actin structures.....	4
1.3	IRSp53	5
1.3.1	Domain structure of IRSp53 isoforms and related proteins	5
1.3.2	IRSp53 interactions downstream of Rac and involvement in lamellipodia	6
1.3.3	IRSp53 interactions downstream of Cdc42 and involvement in filopodia.....	8
1.3.4	IRSp53 in the postsynaptic density and nervous system.....	9
1.4	The IMD	12
1.5	The IMD and BAR domains.....	13
1.5.1	BAR domains	13
1.6	The IMD	15
1.7	Effect of reduction of IRSp53 expression levels.....	19
1.7.1	IRSp53 and <i>E. coli</i> invasion of host gut epithelial cells.....	19
1.7.2	IRSp53 in cancer	20
1.7.3	IRSp53 in genetic diseases	20
1.8	Overview of IRSp53 and IMD role in filopodia formation.....	20
1.9	Project Aims	21
2	Materials and methods.....	23
2.1	Purification of recombinant IMD	24
2.2	Cloning	24
2.2.1	DNA preparations.....	24
2.2.2	Sequencing	24
2.2.3	Polymerase chain reactions	24
2.2.4	Cloning and vectors	24

2.3	Tissue culture and cells	25
2.3.1	Transient transfection of mammalian cells.....	25
2.3.2	Preparation of coverslips	26
2.4	Fluorescence microscopy	26
2.4.1	Epifluorescence imaging	26
2.5	TIRF microscopy.....	27
2.6	FRAP confocal microscopy.....	27
2.7	Cytochalasin D treatment	28
2.8	Recombinant protein expression	28
2.8.1	Cell lysis	28
2.8.2	Affinity chromatography	29
2.8.3	Further purification.....	29
2.9	Gel filtration chromatography	29
2.10	Vesicle production.....	30
2.11	Fluorescence analysis of DiI labelled vesicles.....	30
2.12	Fluorescence microscopy of vesicles.....	30
2.13	Lipid vesicle pelleting assays	30
2.14	Förster resonance energy transfer (FRET)	31
2.15	Affinity purification of anti-IMD antibody	31
2.16	Western blotting	31
2.17	Native Gel Electrophoresis.....	32
2.18	Analytical Ultracentrifugation.....	32
3	Generation of DNA constructs	33
3.1	Introduction	34
3.2	Cloning strategy.....	34
3.2.1	Primer design and selection of restriction sites	34
3.2.2	Use of the Strataclone intermediate vector system.....	35

3.2.3	Cloning into the destination vector and detection of clones.....	35
3.3	Use of the constructs in this work	35
4	IRSp53 IMD induced cellular protrusions are dynamic, contain actin and are affected by Cytochalasin D.....	39
4.1	Overexpression of IRSp53 IMD in Cos-7 cells.....	40
4.2	Live imaging of IMD in cells.	41
4.3	Cytochalasin D causes retraction of some IMD rich protrusions.....	41
4.4	TIRF microscopy analysis of cells expressing IMD-GFP.....	46
4.5	IMD overexpression phenotype varies with the level and duration of IMD expression.....	54
4.6	Discussion.....	54
4.7	Conclusions and future perspectives	61
5	Fluorescence Recovery after photobleaching studies of IMD rich protrusions.	63
5.1	FRAP analysis of IMD - rich protrusions.....	64
5.2	Cytochalasin D does not affect FRAP profile of IMD-GFP	68
5.3	Cloning of constructs required for further FRAP experiments	68
5.4	Dual fluorophore FRAP – preliminary data	70
5.4.1	IMD-mCherry and GFP.....	70
5.4.2	FRAP of IMD-mCherry and IMD K4E-GFP	70
5.4.3	FRAP of IMD-mCherry and GFP-actin	72
5.5	FRAP of IRSp53-GFP	72
5.6	Discussion.....	74
5.7	Conclusions and future perspectives	76

6	Characterisation of the interaction between the IMD and unilamellar vesicles	77
6.1	Preparation of small unilamellar vesicles.....	78
6.2	Probing the IMD-vesicle interaction by size exclusion chromatography.....	78
6.3	Use of a low velocity centrifugation assay to investigate IMD interactions with lipid vesicles.	79
6.4	Imaging of PS containing vesicles in the absence and presence of IMD	87
6.5	Fluorescence resonance energy transfer (FRET) analysis of IMD-vesicle interaction.....	90
6.6	Discussion.....	92
6.7	Conclusions and future perspectives	100
7	<i>In vitro</i> studies of the IMD	102
7.1	Expression and purification of recombinant IMD.....	103
7.1.1	High affinity chromatography	103
7.1.2	Ion exchange chromatography.....	103
7.2	Expression constructs for truncation mutants of IRSp53	105
7.3	Presence of thrombin cleavage site in IRSp53 1-438.....	107
7.4	Insolubility of IRSp53 truncation constructs.....	109
7.5	Native gel electrophoresis of IRSp53 IMD suggests the IMD is predominantly a dimer in solution.....	112
7.6	Analytical ultracentrifugation studies of IMD dimerisation.....	113
7.7	Affinity purification of a polyclonal antibody raised against IRSp53 IMD.....	116
7.8	Discussion.....	118
8	General Discussion	120
8.1	IRSp53 domain structure and family.....	121
8.2	Phenotype of IRSp53 in the cell and effect of knockdowns.....	122

8.3	IRSp53 and lamellipodia	123
8.4	IRSp53 and filopodia.....	123
8.5	The IMD	125
8.6	The IMD and BAR domains.....	125
8.7	The IMD and actin.....	128
8.8	Open questions for IRSp53 and the IMD	130
9	References	132
10	Appendix.....	142
10.1	PCR Primers	143
10.2	SDS PAGE buffers	144
10.3	Protein purification buffers.....	145
10.4	Western blotting buffers	146

Table of Figures

Figure		Page
1.1	Electron microscopy images of lamellipod and filopod	3
1.2	Domain structure of IMD-family proteins	7
1.1	Table of IRSp53 interacting proteins	10-11
1.3	Outline of IMD structures	14
1.4	BAR domains and the IMD	16
3.1	Generation of PCR products and the intermediate cloning vector	37
3.2	Ligation of the insert into the destination vector	38
3.3	Overview of constructs used	39
4.1	Overexpression of IMD constructs in cells	43
4.2	IMD rich protrusions contain phalloidin staining	44
4.3	cytD treatment of cells overexpressing IMD-GFP	46
4.4	TIRF microscopy of IMD-GFP	48
4.5	Quantification of IMD-GFP dynamics using TIRF microscopy	50
4.6	Analysis of protrusion distribution and extension	51
4.7	TIRF analysis of cytD effects on IMD-GFP protrusions	52-53
4.8	Further effect of cytD on IMD-GFP protrusions	54
4.9	Effects of long term IMD-GFP expression on the cell	56
4.10	Imaging of IRSp53-GFP using TIRF microscopy	57
4.11	Schematic diagram of proposed cytD effect on protrusions	63
5.1	Schematic overview of FRAP experiments	66
5.2	FRAP of IMD-GFP rich protrusions	67
5.3	FRAP of IMD-myc and GFP rich protrusions	68
5.4	FRAP analysis of IMD-GFP protrusions after cytD treatment	70
5.5	FRAP analysis of IMD-mCherry, GFP, IMDK4E-GFP and GFP-actin	72
5.6	FRAP analysis of cells expressing IRSp53-GFP	74
6.1	Preliminary lipid studies	81
6.2	Imaging of IMD-vesicle mixtures and effect of EDTA on pelleting	82

6.3	Variability of lipid pelleting assays	84
6.4	Effects of varying PS concentration on IMD lipid pelleting	86
6.5	Testing IMD interaction with physiological vesicle mixtures	87
6.6	NaCl concentration affects IMD-vesicle interactions	89
6.7	Imaging of vesicles by fluorescence microscopy and EM	90
6.8	FRET analysis of IMD-lipid interactions	92
6.9	Schematic diagram of IMD-vesicle interactions	102
7.1	The GST expression system and IMD purification	105
7.2	IRSp53 truncation proteins	107
7.3	Thrombin cleavage site identification in IRSp53 1-438	109
7.4	Ion exchange chromatography of IRSp53 1-438	111
7.5	Preliminary pulldown experiment with IRSp53 1-289	112
7.6	Native PAGE analysis of IMD	115
7.7	Analytical ultracentrifugation analysis of IMD and Rac	116
7.8	Testing of IRSp53 IMD antibody	118

1 Introduction

The actin cytoskeleton is important for many cellular processes such as adhesion, migration, cell division, phagocytosis, and neuronal outgrowth (May, 2001; May and Machesky, 2001; Millard et al., 2004). Actin filaments are arranged into several distinct structures in the cell including the membrane protrusions, lamellipodia and filopodia, which are shown in Figure 1.1, (Lazarides and Weber, 1974). Lamellipodia are broad membrane protrusions composed of a large number of short, highly branched actin filaments arranged at 70 ° to one another (Svitkina and Borisy, 1999). Filopodia are thin finger like projections which contain parallel bundles of actin filaments, and these often emerge from lamellipodia (Svitkina et al., 2003). A wide range of proteins have evolved to tightly regulate the polymerization of actin into filaments, and to coordinate filaments into these defined structures (Paavilainen et al., 2004; Mattila and Lappalainen, 2008).

Protrusion of membranes for structures such as lamellipodia and filopodia requires energy to overcome membrane tension, and actin polymerization is capable of generating this force (Hill and Kirschner, 1982). Deformation of membranes by direct binding of other proteins may also contribute to overcoming the force necessary to bend membranes (McMahon and Gallop, 2005).

1.1 Actin dynamics

Actin polymerization can proceed *in vitro* given sufficient concentration of ATP-monomers, however this is a slow process, as the nucleation of new filaments - binding of the first two or three monomers - is a slow process (Cooper et al., 1983). However, once the filament has passed this threshold, polymerization can proceed at a high rate, limited by concentration of available monomer (Pollard, 1986). *In vivo* polymerization occurs at a faster rate in cells than is observed *in vitro* (Zigmond, 1993).

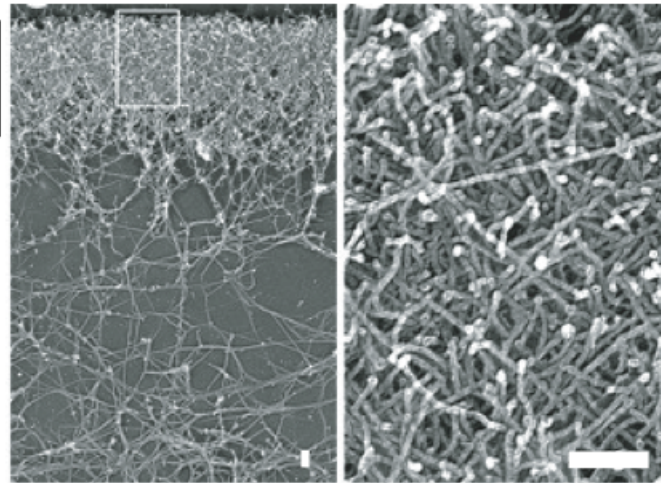
Many different proteins control actin polymerization. Nucleation of new filaments is mediated by different classes of protein. Arp2/3 complex, purified from *Acanthamoeba* contains two components with high similarity to actin monomers, binds to sides of existing filaments and nucleates new actin filaments (Machesky et al., 1994; Mullins et al., 1998).

A Lamellipod

Cell exterior

Lamellipod

Cell interior



B Filopod

Filopod

Cell exterior

Cell edge

Lamellipod

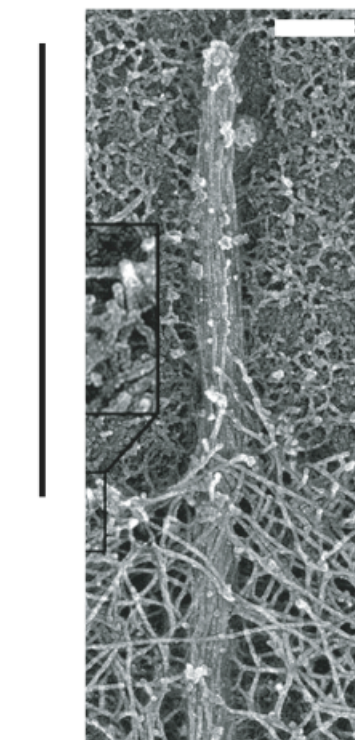


Figure 1.1 Electron microscopy images of a lamellipod and a filopod from (Svitkina et al., 2003). (A) Lamellipodia are broad membrane protrusions characterized by many short, highly branched actin filaments. (B) Filopodia contain long filaments organised in parallel bundles, and often are located at the tips of lamellipodia. Scale bar, 0.2 μ m

New filaments are angled at 70 ° to the existing filament, and this is in agreement with the angled arrays seen in lamellipodia (Mullins et al., 1998). An end-binding model of Arp2/3 complex activity has also been proposed, in which the complex nucleates polymerization at the barbed ends of existing filaments (**Suetsugu et al., 2002**). In filopodia, which consist of unbranched actin filaments, formins and Ena/VASP (Enabled / Vasodilator-stimulated phosphoprotein) proteins localize to the tips, and are essential for filopodia formation (Schirenbeck et al., 2005; Chesarone and Goode, 2009). Formins and Ena/VASP also prevent filament capping, enabling the continued extension of the actin filaments.

1.2 Small GTPases Rac and Cdc42 regulate formation of actin structures

The Rho family small GTPases Rac and Cdc42 act as master switches to direct formation of lamellipodia and filopodia, respectively (Nobes and Hall, 1995; Machesky and Hall, 1997; Ridley, 2001). These proteins bind GTP and possess an intrinsic GTPase activity, which can hydrolyse GTP to GDP. These GTPases are active in the GTP bound state, and inactive in the GDP bound state, and their activity is modified by upstream regulators (Ridley, 2001). GEFs (GTPase exchange factors) upregulate activity as they promote exchange of bound GDP for GTP which is abundant in the cell. GAPs (GTPase activation proteins) inactivate GTPases by enhancing GTP hydrolysis, which leaves the molecule in the inactive, GDP-bound state. Many upstream regulators of GTPases have been characterised, and mutants of Rac and Cdc42 have been generated that exist constitutively in the active or inactive forms. Rac activation leads to formation of lamellipodia by activation of the WAVE (Wiskott Aldrich verproline homologue) complex proteins, which in turn activate Arp2/3 complex, although Rac does not bind to the WAVE complex directly (Miki et al., 1998). Activated Cdc42 also causes Arp2/3 induced actin polymerization, via direct interaction with N-WASP (Neuronal-Wiskott Aldrich Syndrome protein) (Aspenstrom et al., 1996; Symons et al., 1996). Other downstream effectors of Cdc42 include MRCK, serine/threonine kinases and PAK4, (Abo et al., 1998; Leung and Lassam, 1998)

The Insulin Receptor Substrate of 53 kDa (IRSp53) is involved in both lamellipodia and filopodia formation, and binds to both Rac and Cdc42, and is discussed in more detail below (Miki et al., 2000; Krugmann et al., 2001).

1.3 IRSp53

IRSp53 was first characterized in a study searching for phosphorylation targets of the insulin receptor, and was found to be tyrosine phosphorylated in response to insulin *in vivo*, and when incubated with isolated insulin receptor *in vitro* (Yeh et al., 1996). Later studies have revealed IRSp53 to be involved in formation of filopodia-like protrusions (Govind et al., 2001; Krugmann et al., 2001; Bockmann et al., 2002; Soltan et al., 2002; Nakagawa et al., 2003; Millard et al., 2005; Disanza et al., 2006), and also localization to lamellipodial protrusions (Nakagawa et al., 2003). IRSp53 also binds and acts downstream of both Rac and Cdc42, and so is an important factor in the formation of filopodia and lamellipodia (Miki et al., 2000; Govind et al., 2001; Krugmann et al., 2001). A key role of IRSp53 may be as a molecular adaptor, localizing and interacting with various proteins involved in filopodia and lamellipodia. This role is supported by the presence of several protein interaction motifs, and the large number of diverse interaction partners that IRSp53 binds (Table 1.1).

1.3.1 Domain structure of IRSp53 isoforms and related proteins

IRSp53 belongs to a larger family of proteins which share a conserved N terminal IMD (IRSp53 MIM domain), and have varying C terminal regions (Figure 1.2) (Yamagishi et al., 2004; Machesky and Johnston, 2007). The IMD forms a dimer and has lipid and Rac binding capabilities, and is discussed in more detail later on in this chapter. The family of IMD containing proteins is subdivided into two groups, IRSp53-like and MIM-like (Yamagishi et al., 2004). The MIM-like proteins comprise two members, MIM and ABBA, and are characterised by a WASP family-2 (WH2) actin monomer binding domain at the C terminal of the sequence (Yamagishi et al., 2004). Overexpression of MIM, causes lamellipodia – like protrusion at the plasma membrane, and the IMD in isolation induces filopodia-like structures (Woodings et al., 2003; Bompard et al., 2005). The role of the WH2 domain in the context of MIM is still not fully understood, and deletion of the WH2 has no evident effect on the overexpression phenotype (Bompard et al., 2005).

IRSp53, which is the focus for this study, is classified under the IRSp53-like IMD proteins, which also includes insulin receptor tyrosine kinase substrate (IRTKS) and the poorly studied *FLJ22582*. A defining feature of the IRSp53-like family members is the presence of an SH3

domain, which allows binding of many ligands via a proline rich domain (Table 1.1). IRTKS and some longer isoforms of IRSp53 possess a WH2-like domain, although no actin monomer sequestration has been shown (Millard et al., 2007). IRSp53 has a half-CRIB (Cdc42/Rac interactive binding) motif located to the C terminal of the IMD, which binds to active Cdc42 but not Rac (Krugmann et al., 2001). IRSp53 also has several isoforms, which are identical from residues 1-511, and divergent after (Okamura-Oho et al., 2001; Miyahara et al., 2003). The L- (552 residues) and S- (521 residues) forms of IRSp53 are highly expressed in the brain, and the T-form (520 residues) was only found in a cancer line (Okamura-Oho et al., 2001). The 521 amino acid IRSp53 is the most widely studied isoform. This has a PDZ motif at the C terminal, and many interactions with postsynaptic density proteins occur through this (Table 1.1).

1.3.2 IRSp53 interactions downstream of Rac and involvement in lamellipodia

The WAVE complex is known to activate Arp2/3 activation downstream of Rac signalling to form lamellipodia, although there is no direct interaction between Rac and the WAVE complex (Bishop and Hall, 2000). A study done by Miki *et al*, 2000 gave the first indication that IRSp53 could be a link between Rac and its downstream effectors. Yeast two hybrid and pulldown experiments showed that Rac binds to the N terminus of IRSp53 and that WAVE2 binds to the SH3 domain of IRSp53. IRSp53 with no functional SH3 domain was found to reduce lamellipodia formation in cells expressing activated Rac, suggesting that IRSp53 plays an important role in this process. A subsequent study from the same group (Miki and Takenawa, 2002) found that Rac binding to the N terminus was reduced in the full length IRSp53 relative to the N terminus alone, but that this is relieved in presence of WAVE. This may suggest an autoinhibitory conformation in the full length IRSp53, which masks the Rac binding site on the IMD. IRSp53 was also observed to localize to lamellipodia through its IMD (Nakagawa et al., 2003). Interactions of IRSp53 with other proteins implicated in Rac signalling to lamellipodia have also been documented. Two Rac GEFs have been identified as binding partners of IRSp53, suggesting that IRSp53 can function to maintain and amplify Rac signals (Funato et al., 2004; Connolly et al., 2005). Binding of IRSp53 to Eps8 induces Rac activation, presumably through activation of the Eps8-Sos1-Abi1 GEF complex (Funato et al., 2004). This could play a role in local maintenance of the active Rac signal at the tips of

lamellipodia. IRSp53 binding to Rac GEF Tiam1 leads to increased levels of WAVE2 and Rac bound to IRSp53 thereby enhancing activation of the Rac signalling (Connolly et al., 2005). Overexpression of Tiam1 enhances lamellipodia formation in cells, and this was found to be reduced when level of IRSp53 was decreased. This suggests that Tiam1 requires IRSp53 in order to target it to WAVE2 activation. Overexpression of Tiam1 was also found to reduce the number of filopodia present on the cell surface, which may imply that IRSp53 targeting towards the Rac signalling pathway prevented IRSp53 from mediating filopodia formation.

1.3.3 IRSp53 interactions downstream of Cdc42 and involvement in filopodia

Eps8 has already been discussed above in relation to its role as a Rac GEF (Funato et al., 2004). More recently, it has been implicated as a partner for IRSp53 in filopodia formation (Disanza et al., 2006). IRSp53 and Eps8 were found to act synergistically to bundle actin *in vitro*, and to cause formation of filopodia when coexpressed in cells, Filopodia formation by IRSp53 and Eps8 was still possible in cells with N-WASP and Mena knocked out. Cdc42 was also found to promote formation of the complex between IRSp53 and Eps8. This suggests that actin filament bundling alone is sufficient to produce filopodia, possibly in the manner that overexpression of the actin bundling protein fascin is able to induce filopodia (Vignjevic et al., 2006).

Ena/VASP proteins localize to tips of filopodia and lamellipodia, where they are able to promote actin filament elongation and prevent filament capping (Chesarone and Goode, 2009). IRSp53 was found to bind to Mena (Mammalian enabled) a member of the Ena/VASP family (Krugmann et al., 2001). This interaction was found to occur as a result of Cdc42 binding to IRSp53, which suggests that Cdc42 is required to relieve an intramolecular inhibition. IRSp53-Mena binding is likely important for IRSp53 mediation of filopodia, as cells unable to express Mena may not be able to form filopodia (Lim et al., 2008). Formins also localize to the tips of extending actin filaments, and promote filament elongation (Chesarone and Goode, 2009). IRSp53 has been found to bind formins mDia1 (Fujiwara et al., 2000; Lim et al., 2008), and mDia2 via the SH3 domain (Lim et al., 2008). This interaction has not been extensively studied, although mDia2 coexpression with IRSp53 was found to prevent filopodia formation mediated by IRSp53 (Lim et al., 2008).

The study that detected the interaction between IRSp53 and WAVE2, found no interaction with fellow Wiskott Aldrich protein N-WASP, which is a key effector of Cdc42 in filopodia formation (Miki et al., 2000). However, a recent study has found that IRSp53 does interact with N-WASP (Lim et al., 2008). IRSp53 interaction with N-WASP is likely to be an important interaction, as N-WASP knockdown cells were unable to form IRSp53 induced filopodia (Lim et al., 2008).

1.3.4 IRSp53 in the postsynaptic density and nervous system

There have been several investigations into the role IRSp53 plays in the central nervous system. Processes such as neurite outgrowth during nervous system development require the cells to produce many protrusions and migrate accurately in a highly controlled fashion. IRSp53 has been reported to interact with various proteins enriched in the central nervous system, particularly in the post synaptic density (PSD) of synapses (Abbott et al., 1999; Oda et al., 1999; Bockmann et al., 2002; Soltau et al., 2002; Choi et al., 2005). Work done by Abbott and co workers looking into a roles for insulin in the brain by overexpression of insulin receptor, revealed IRSp53, along with other signalling molecules to be colocalized with insulin receptor in the rat brain, particularly in PSD-enriched fractions. IRSp53 was found in two different studies (Soltau et al., 2002; Bompard et al., 2005) to interact and colocalize with members of the ProSAP/Shank postsynaptic density proteins, via the IRSp53 SH3 domain and one of two Proline-rich domains in the shank family. Shank is a signalling molecule enriched in the PSD and known to play a role in dendritic spine outgrowth (Sala et al., 2001). IRSp53 interacts with other PSD proteins via a PDZ domain, and also with actin regulator cortactin, and is involved in maturation and elongation of dendritic spines. Dendritic spines are actin-rich structures similar to filopodia that allow dendrite remodelling and are implicated in nervous system plasticity and learning (Matus, 2000; Hering and Sheng, 2001). In another study, knockdown of IRSp53 was shown to reduce the number and density of dendritic spine outgrowth, and overexpression of a SH3-defective IRSp53 unable to bind Shank, prevented Shank localization to synapses (Choi et al., 2005). These results argue for a

Summary of IRSp53 interacting partners

Protein motif/domain	IRSp53 binding region	Notes	Reference
BAI1 <i>Pro rich domain</i>	SH3	Neuronal growth – link between membrane and cytoskeleton.	(Oda et al., 1999)
Cdc42	CRIB	Found in Y2H search for Cdc42 interacting partners. Possible relief of intramolecular inhibition of SH3.	(Govind et al., 2001)
CIPP <i>PDZ</i>	PDZ binding	Multivalent protein containing 4 PDZ domains. IRSp53 binds to one, leads to reorganization of CIPP	(Alpi et al., 2009)
DRPLA	SH3	Nervous system protein, involved in neurodegeneration.	(Okamura-Oho et al., 1999)
Eps8 <i>Pro rich domain at N ter)</i>	SH3	Eps8 part of Rac GEF complex – Rac positive feedback activation.	(Funato et al., 2004)
Eps8 <i>Pro rich domain (x2)</i>	SH3	Synergistic actin bundling by IRSp53 and Eps8 complex.	(Disanza et al., 2006)
Insulin Receptor 1	Phosphorylation sites unknown	Tyrosine phosphorylation in response to insulin treatment.	(Yeh et al., 1996)
IQ-ArfGEF/BRAG1 <i>Proline rich domain</i>	SH3	IQ-Arf is a GEF for Arf1 and Arf6. Localizes to PSD. Potential role downstream of NMDA receptors	(Sanda et al., 2009)
Kank <i>N ter coiled coil</i>	'Coiled coil' - IMD	Binding inhibits interaction with Rac but not Cdc42; Knockdown of Kank increases lamellipodia formation.	(Roy et al., 2009)
LIN7 <i>L27 and PDZ</i>	PDZ binding	Localization of IRSp53 to tight junctions and Rac activation	(Massari et al., 2009)
MALS <i>PDZ</i>	PDZ binding	Found in Y2H, and colocalization in cells.	(Hori et al., 2003)
mDia <i>FH1 domain</i>	SH3	RhoA dependent interaction.	(Fujiwara et al., 2000)
Mena	SH3 (inhibition by N ter)	Cdc42 necessary for interaction. Mena involved in filopodia formation; focal adhesions.	(Krugmann et al., 2001)
NESH <i>Proline rich domain</i>	SH3	Overexpression of NESH reduces metastasis, IRSp53 binding proposed to reduce IRSp53 mediated WAVE2 activation	(Matsuda et al., 2008)
N-WASP	SH3	This study finds that N-WASP is essential for IRSp53 mediated filopodia.	(Lim et al., 2008)
ProSAP/SHANK <i>Proline rich domain</i>	SH3	Shank involved in postsynaptic density. Link glutamate receptor to cytoskeleton. Links Cdc42 to PSD?	(Bockmann et al., 2002; Soltau et al., 2002)
ProSAP/Shank2 <i>PDZ</i>	SH3	Recruits IRSp53 to PSD and secretory granules	(Redecker et al., 2007)

PSD-95 <i>PDZ</i>	PDZ Binding motif (C ter)	Post synaptic density scaffold protein Role in dendritic spine outgrowth	**CHOI ET AL 2005**
Rac-GTP	IMD	Possibly lower affinity for full length IRSp53 than IMD alone, possibly relieved by WAVE2	(Miki et al., 2000; Millard et al., 2005)
SPIN90 <i>Pro rich domain</i>	SH3	Cooperative Rac activation. Reduction of SPIN90-IRSp53 binding reduces lamellipodia	(Teodorof et al., 2009)
Synaptopodin	SH3, weak binding to IMD	Synaptopodin prevents formation of IRSp53-Cdc42-Mena complex. Also blocks IRSp53 induced filopodia.	(Yanagida-Asanuma et al., 2007)
Tiam1 <i>PH-CC-Ex domain</i>	Overlapping CRIB (243-299).	Tiam1 is a Rac GEF – directs activated Rac to IRSp53.	(Connolly et al., 2005)
Tir; EspFU	IMD SH3	E. coli EHEC proteins Tir and EspFU require IRSp53 to activate N-WASP for pedestal formation.	(Weiss et al., 2009)
WAVE2	SH3	IRSp53 is necessary for WAVE2 complex formation and localization to membrane, but insufficient for WAVE2 activation.	(Abou-Kheir et al., 2008)
WAVE2 <i>Proline rich region</i>	SH3	Linking Rac signalling to WAVE2 activation of Arp2/3 actin polymerization	(Miki et al., 2000)

Key:

Rac/WAVE activation	Cdc42/Filopodia formation	Neuronal / PSD proteins	Other
----------------------------	----------------------------------	--------------------------------	--------------

Table 1.1 A summary of interaction partners of IRSp53. Colour coding as above according to whether it is principally involved in Rac signalling and/or WAVE activation; formation of filopodia; is specific to neuronal systems; or other.

role of IRSp53 as a scaffold protein in this process, localizing Shank to sites of spine outgrowth and potentially linking it to other GTPase signalling. Work done by Choi *et al.*, 2005 also found PSD-95, another component of the PSD binds to IRSp53. This could have implications in upstream Rho GTPase signalling to IRSp53, as PSD-95 is known to associate directly and indirectly with Kalirin-7 (a Rac GEF) and β -PIX (a Rac and Cdc42 – GEF) (Penzes *et al.*, 2001). In agreement with this, knockdown of PSD-95 prevents spine morphogenesis, which may be due to a failure to activate IRSp53, or may have some other off-target effect (Choi *et al.*, 2005).

1.4 The IMD

The N terminal 250 amino acids of IRSp53 constitute the conserved IRSp53/MIM homology domain (IMD) (Yamagishi *et al.*, 2004). Overexpression in cell lines of the IMD causes formation of a large number of filopodia-like protrusions (Yamagishi *et al.*, 2004; Bompard *et al.*, 2005; Millard *et al.*, 2005; Disanza *et al.*, 2006; Suetsugu *et al.*, 2006b; Millard *et al.*, 2007; Saarikangas *et al.*, 2009). Formation of the filopodia-like protrusions (henceforth referred to as protrusions to differentiate from wild-type filopodia) was found not to act upstream of Cdc42 and Rac signalling, as dominant negative forms of these GTPases does not prevent formation of these protrusions, and so the IMD domain is sufficient for generation of these protrusions. The formation of protrusions was initially ascribed to an actin bundling property of the IMD, which was been measured by *in vitro* actin bundle pelleting assays and imaging, (Yamagishi *et al.*, 2004; Bompard *et al.*, 2005; Millard *et al.*, 2005; Disanza *et al.*, 2006).

Further insights into the activity of the IMD came with the discovery of its crystal structure (shown in Figure 1.3) (Millard *et al.*, 2005). The structure revealed that the IMD forms a cigar-shaped dimer made up of 4 α helices per monomer, and measuring 180 Å along its long axis. The IMD probably forms a tight dimer, as the dimer interface buries a large area of $\sim 1350 \text{ \AA}^2$ per monomer. Dimerisation is expected to occur *in vivo* as IRSp53 but not IRSp53 lacking IMD can immunoprecipitate full length IRSp53 (Yamagishi *et al.*, 2004). The IMD is predicted from its structure to form a constitutive dimer, as it has an extensive dimer interface. This was confirmed by a sedimentation equilibrium experiments, in which only a dimer was detected (Millard *et al.*, 2005). Determination of the structure of the IMD also lent

further weight to the theory that IMD can bundle actin filaments when a conserved basic patch located on helix 2 was identified (Figure 1.3). Mutation of this basic patch to reverse the charge was found to abrogate actin filament bundling and binding, and also prevent formation of protrusions when overexpressed in cells (Millard et al., 2005). Electron microscopy analysis of actin bundles showed that the bundles are located a similar distance apart to that of the basic patches (~11 nm), further suggesting that these are responsible for actin bundling.

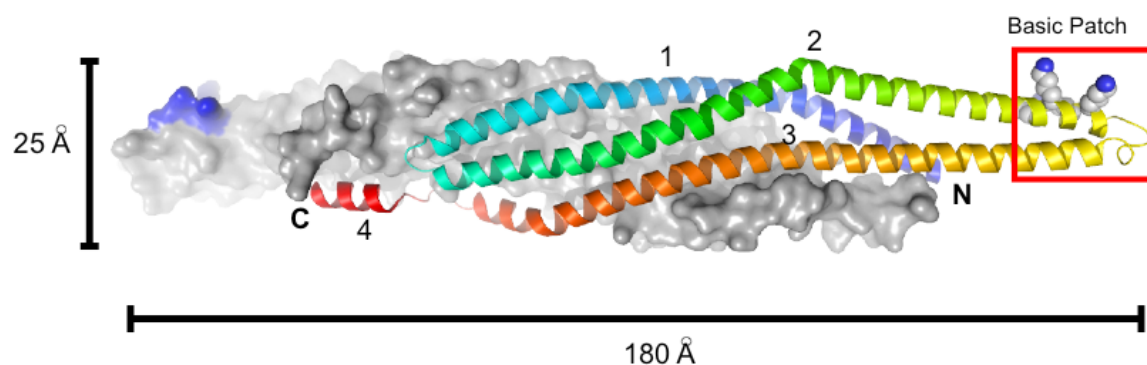
1.5 The IMD and BAR domains

1.5.1 BAR domains

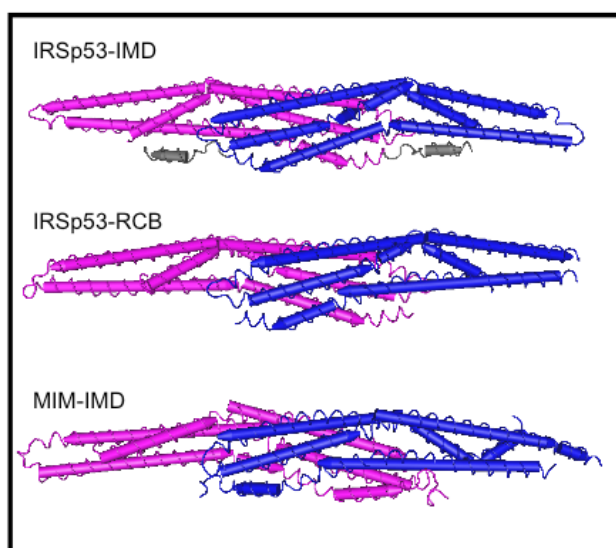
Discovery of the IMD structure revealed a close structural similarity to the membrane-binding BAR domains (Millard et al., 2005). The BAR domain family consists of a number of proteins involved in clathrin mediated endocytosis (CME) and other processes involving membrane curvature (Peter et al., 2004; McMahon and Gallop, 2005). CME requires invagination of the membrane to form a clathrin coated vesicle, and the BAR domains are thought to bind to the forming vesicle and coordinate membrane curvature with other factors.

The acronym BAR refers to the proteins BIN1, Amphiphysin and Rvs, the first proteins in which the domain was characterized (Sivadon et al., 1995; Sakamuro et al., 1996). The ability of BAR domains to tubulate membranes was first noted in amphiphysin (Takei et al., 1999), and endophilin (Farsad et al., 2001). The first structural information to explain this activity of BAR domains was found when the crystal structure of the BAR domain of amphiphysin was solved, revealing its characteristic ‘banana’ shape was determined (Peter et al., 2004). Since then many more members of the BAR domain family have been described (Habermann, 2004; Peter et al., 2004), many of which contain other structural domains downstream of the BAR domain, such as SH3 domains, regulatory domains for GTPases, and phosphatidylinositide binding domains. For example, endophilin binds to dynamin and synaptojanin via its SH3 domain, providing a necessary link between membrane binding mediated by the BAR domain with scission and vesicle uncoating (Ringstad et al., 1997; Slepnev and De Camilli, 2000). Another BAR domain protein, arfaptin, can bind membranes and also to small GTPases Arf and Rac, combining the function of signal transduction with membrane modification (Tarricone et al., 2001). At least two mechanisms for BAR domain

A IRSp53 IMD



B



C

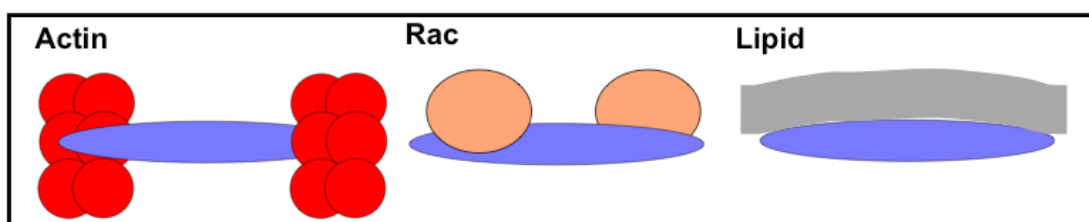


Figure 1.3 Crystal structure of the IMD. (A) Crystal structure of the IRSp53 IMD (PDB accession 1Y20). One monomer in grey, the other blue-red according to sequence progression. Conserved basic region is denoted by blue colouring on left dimer, and side chains on right dimer. Structure rendered by Klaus Fütterer using pymol (pymol.org). (B) Crystal structures of RCB (PDB: 1WDZ) and MIM IMD (PDB: 2D1L). RCB and MIM lack helix 4. Structures rendered using Cn3D. (C) Putative binding sites for actin, Rac and phospholipids, as identified in site directed mutagenesis carried out in previous studies (Suetsugu et al., 2006b; Mattila et al., 2007).

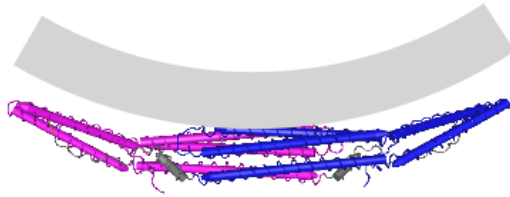
binding to membranes have been established. Conserved positive charges located on the concave face of the dimer are required to bind and deform membranes. These residues are at either end of the dimer, and may be analogous to the basic clusters observed in IMD. A subset of BAR domains possess an amphipathic helix located adjacent to the N terminal of the domain, which can insert into the membrane and may act as a 'wedge' to enhance binding and deformation of the membrane (Gallop et al., 2006; Masuda et al., 2006). Proteins that include this additional helix are termed 'N-BAR' domains. Whereas the binding of the BAR domain alone is an electrostatic interaction, the N-BAR may occur through other interactions, as high salt concentration (250 mM) reduces binding of BAR but not N-BAR domains (Gallop et al., 2006). F-BAR (FCH (Fes and CIP4 homologue)-Bin Amphiphysin and RVS) domains are a relatively new addition to the BAR family (Itoh et al., 2005; Tsujita et al., 2006). F-BAR domains are larger and form tubules with larger diameter than N-BAR domains (Henne et al., 2007).

BAR domains are not thought to demonstrate a high degree of lipid specificity, although some preferences have been observed. For example, lipid specific domains located adjacent may infer specificity, as in the case of sorting nexin-1 which has a Phox homology (PX) domain that specifically binds phosphatidyl inositol phosphates (Peter et al., 2004). However, several BAR domains have been shown to require particular phospholipids for binding. FBP17, F-BAR binds selectively to phosphatidylserine (PS) rather than phosphatidylinositolphosphates. Also, endophilin has been found to tubulate brain lipids more efficiently than synthetic lipid mixtures (Farsad et al., 2001). Lipid tubulation assays for BAR domains tend to be done using brain lipid extracts, and the exact membrane composition required has not been fully investigated.

1.6 The IMD

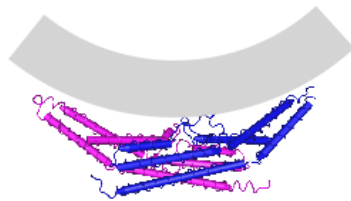
Following the discovery of structural homology between IMD and BAR domains, several studies looking at IMD interaction with phospholipids, and membrane deformation have been carried out (Suetsugu et al., 2006a; Suetsugu et al., 2006b; Mattila et al., 2007; Saarikangas et al., 2009). IMD lipid binding was first detected in work done by Suetsugu and coworkers in

A i F-BAR (Fcho1)



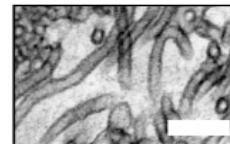
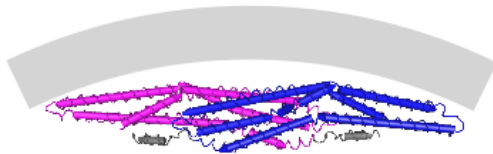
Henne *et al.*, 2007

ii N-BAR (Endophilin)



Masuda *et al.*, 2006

iii IMD



Saarikangas *et al.*, 2009

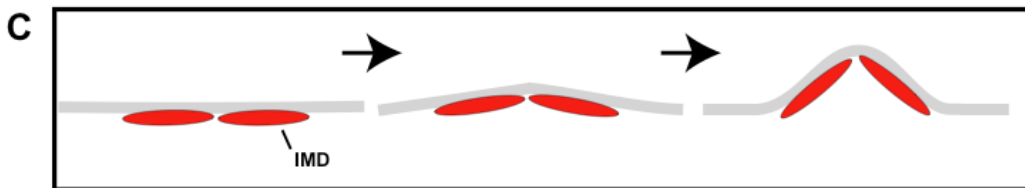
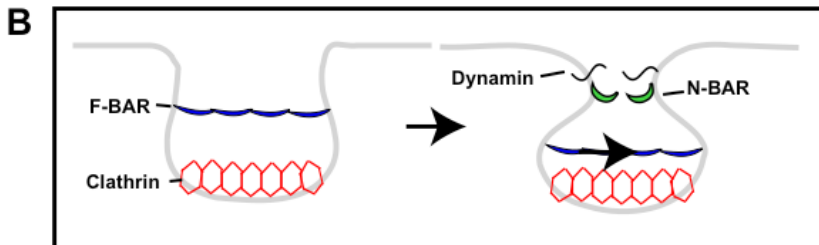


Figure 1.4 BAR domains and the IMD. (A) The F-BAR, N-BAR and IMD domains show structural similarity. Grey lines indicate membranes, to show how each domain binds to membranes. Right: EM images showing the tubules formed after incubation of vesicles with BAR domains. Scale, 200 nm (B) Cartoon of possible role of BAR domains in CME. In early stages, F-BAR can bind to the membrane as it has suitable curvature. As CME progresses, the vesicle neck is drawn in and BAR domains of smaller curvature are able to bind and eventually lead to scission of the vesicle, in association with GTPase dynamin. (C) IMD causes membrane deformation in the opposite orientation to BAR domains.

2006, and the membrane deformation was first shown in a second paper from the same group, also in 2006. These studies found that the RCB (a truncated IMD consisting of 229 residues) interacts with many anionic phospholipids, although the study was focussed on IMD interactions with PIP₃ (phosphatidylinositol-3-phosphate), and also that IMD caused the formation of small membrane deformations when incubated with Folch fraction vesicles. The addition of lipid-modified Rac was found to enhance the formation of these deformations, and GFP-Rac was found to bind to IMD with an affinity of 3.5 μM, comparable to the affinity of Arfaptin-Rac binding (Tarricone et al., 2001). Some competition between Rac and lipid for IMD binding was also observed. In contrast to the PIP₃ requirement seen in the Suetsugu 2006b study, another group found a requirement for PI(4,5P)₂ in vesicles to establish interaction, and no interaction with PIP₃.(Mattila et al., 2007). The strongest interaction was seen with vesicles containing 30 % PI(4,5)P₂, and a striking tubulation of vesicles was also observed, as depicted in Figure 1.1. These images showed tubulation of lipid vesicles, in a manner analogous to BAR domain tubulation, although IMD is thought to bind to the interior of the tubules, rather than the exterior (Figure 1.4). The tubule diameter measured in these experiments was 78 nm, and this is in general agreement with a diameter of 95 nm predicted from the structure. It must be noted, however, that the lipid composition used, including 30 % PI(4,5)P₂ is a membrane with extremely high negative charge, and it is unclear whether such highly charged membranes are encountered in the cell. Tubulation experiments with BAR domains are carried out using brain lipid mixtures, which are likely more physiologically relevant.

Another study has investigated further the vesicle tubulation of a range of IMDs from different species and different proteins (Saarikangas et al., 2009). Different IMDs were found to induce tubules of different diameters, and interestingly different IMDs were found to segregate into separate protrusions when coexpressed in cells. Using lipid-specific dyes, it was found that IMD binding to vesicles causes clustering of PI(4,5)P₂ but not PS, which reinforces the claim of this group that IMD binds PI(4,5)P₂ specifically (Saarikangas et al., 2009). The work done by Saarikangas et al also suggests that the IMD of MIM but not of IRSp53 may deform membranes by a mechanism similar to N-BAR domains, as it possesses a similar N terminal amphipathic helix that helps to stabilise IMD-lipid binding at elevated NaCl concentrations (400 mM). Given that the IMD is proposed to cause membrane

tubulation by binding to the interior (and therefore more highly compacted) side of the protrusion, it is unclear how insertion into this region would lead to the expected membrane bending.

The recent discovery of the membrane binding and deformation capabilities of the IMD have led some researchers to test the requirement for actin in IMD induced protrusions. The observation that filopodia-like protrusions could be formed *in vitro* in vesicles incubated with IMD alone, may suggest that actin is not required for all such protrusions (Mattila et al., 2007; Saarikangas et al., 2009). Data presented in the Mattila 2007 paper suggests that the actin bundling assays done by Millard et al 2005 may be an artefact of the experimental conditions used. In their study, dynamic light scattering (DLS) was used to show that IMD may aggregate at the ionic strength used in the Millard et al, 2005 study, and that apparent actin bundling may be a result of aggregation rather than a physiological actin bundling activity. In the hands of Mattila et al 2007, no bundling activity was observed at 100 mM KCl, and only occurred at 50 mM KCl, where IMD was shown to be extremely prone to aggregation. However, in the study that initially characterised the IMD, the actin bundling assay was carried out in conditions of 100 mM KCl, and bundling was observed (Yamagishi et al., 2004). In another investigation, full length IRSp53 and Eps8 were found to synergistically bundle actin filaments, again in 100 mM KCl (Disanza et al., 2006). These experiments suggest that IRSp53 does have an actin bundling activity *in vitro*. Furthermore, the finding that the bundling activity is enhanced by Eps8, and that coexpression of the two proteins causes the formation of many more protrusions than either protein alone, strongly suggests that IRSp53 mediated actin bundling is important for its activity in filopodia formation.

Several studies have investigated the role of actin in IMD-induced protrusions in cells, and have come to somewhat different conclusions. One study found that that many IMD protrusions contained no detectable actin, and that protrusions persisted after treatment of the cells with actin filament destabilising compound latrunculin B (latB), at 2.5 μ M (Suetsugu et al., 2006a). Suetsugu and coworkers concluded that the protrusions are not at all dependent on actin. Work done in the study by Mattila *et al*, 2007 also treated cells overexpressing IMD with latB, and found that extension of protrusions was inhibited, suggesting that actin is required for extension. IMD induced protrusions were directly imaged using electron

microscopy in another study, and were found to contain actin, although the filaments were disorganised compared to conventional filopodia (Yang et al., 2009). Another experiment in the work done by Yang *et al* demonstrated that filopodia protrusion was almost always accompanied by actin filament protrusion, but that once formed actin filaments sometimes withdrew without causing collapse. This suggests that actin filaments may be required for providing the protrusive force, but that IMD is capable of stabilising the protrusions.

1.7 Effect of reduction of IRSp53 expression levels

Several studies have utilised a knock down strategy to measure the importance of IRSp53 for cellular structures. Choi et al, in a 2005 study, found that reducing levels of IRSp53 in cultured neuronal cells resulted in a decrease in the number and density of dendritic spines, suggesting a role for IRSp53 in initiation of the formation of these structures, which are similar to filopodia. Disanza et al, in a 2006 study used RNAi to examine the effects of knockdown of IRSp53 on formation of filopodia by active Cdc42, and observed a decrease of around 40 % in the number of filopodia formed. A decrease in N-WASP induced filopodia of around 80 % was observed when IRSp53 was knocked out using RNAi, which suggests that IRSp53 is a major interactor in N-WASP induced filopodia formation (Lim et al., 2008). In the same study, it was reported that no filopodia were observed cells lacking N-WASP, and so these data suggest that IRSp53 is an important component of filopodia. Suetsugu and coworkers, in a 2006 study, also found that reduction of cellular IRSp53 by RNAi reduced cell ruffling and lamellipodia formation in response to active Rac (Suetsugu et al., 2006b).

1.7.1 IRSp53 and *E. coli* invasion of host gut epithelial cells

IRSp53 has been implicated in several disease states. IRSp53 and IRTKS have both been implicated in *E. coli* infection of the mammalian gut epithelium (Morita-Ishihara et al., 2009; Vingadassalom et al., 2009; Weiss et al., 2009; Crepin et al., 2010). Two pathogenic *E. coli* serotypes, EHEC (enterohaemorrhagic *E. coli*), and EPEC (enteropathogenic *E. coli*), enter the gut epithelium via a hijacking of the host signalling pathways and the actin cytoskeleton, resulting in the formation of entry sites that include polymerised actin adjacent to the site of entry (Frankel and Phillips, 2008). This is mediated by the insertion of a bacterial protein, Tir, into the apical membrane of the host gut epithelial cells. Tir proteins cluster in the

membrane, and signal to actin polymerization mediated by N-WASP, by various pathways . IRSp53 and IMD family member IRTKS have both been implicated in activation downstream of Tir (Vingadassalom et al., 2009; Weiss et al., 2009).

1.7.2 IRSp53 in cancer

The involvement of IRSp53 involvement in cancer has also been investigated. In one study, inhibition of IRSp53-Eps8 complex formation was found to decrease the motility and invasiveness of HT1080 fibrosarcoma cells (Funato et al., 2004). A mutated isoform of IRSp53 which varies at its C terminal has only been detected in a cancer cell line (Okamura-Oho et al., 1999). However, no subsequent study has investigated this further.

1.7.3 IRSp53 in genetic diseases

The first identification of IRSp53 in humans was as a binding partner of Brain-specific angiogenesis inhibitor (Bai1), a which is a p53 target mostly expressed in neurons (Oda et al., 1999). IRSp53 also interacts with the DRPLA gene product, atrophin-1, which is implicated in DRPLA, (dentatorubral-pallidoluysian atrophy), a neurodegenerative disease (Okamura-Oho et al., 1999). DRPLA is observed in individuals with extended repeat regions in this gene, and IRSp53 binding may be regulated by CAG repeat length, suggesting that the interaction with IRSp53 may be implicated in this disorder.

1.8 Overview of IRSp53 and IMD role in filopodia formation.

Work done so far on IRSp53 implicates it as an important component of cell signalling to lamellipodia and filopodia. Earlier studies suggested that its main role was in signalling from Rac and Cdc42, and acting as a scaffold, assembling complexes of proteins at the site required. The discovery of the IMD as a separate domain able to induce filopodia-like structures in isolation has brought new possibilities to the mode of action of IRSp53. Comparisons of the IMD with the BAR domain family reveals that the principal role of the IMD may be in membrane deformation rather than actin bundling, although this question has not been fully addressed.

1.9 Project Aims

The aims of this project were to investigate the function of the IMD in formation of filopodia-like protrusions, using a number of different approaches.

1. Generation of several fluorescently tagged IMD constructs

In order to allow imaging of IMD in live cells, a series of IMD constructs with fluorescent tags were generated. It was decided to generate IMD constructs with the GFP located at the C terminal of the IMD, due to the N terminal location of the IMD as it is found in IRSp53.

2. Investigation of the requirement for actin in IMD-induced protrusions

In order to investigate the requirement for actin in IMD-induced protrusions, actin destabilizing drug cytochalasin D was used, and the dynamics of the protrusions examined in the presence and absence of the drug. If actin is required for the dynamics of the protrusions in normal cells, this is expected to be altered in cells treated with cytochalasin D

3. Measurement of IMD dynamics in protrusions

At the commencement of this study, little was known about the dynamics of IMD in IMD-induced protrusions, limiting the understanding of how these structures are formed and maintained. Fluorescence recovery after photobleaching (FRAP) studies were carried out in order to measure the dynamics of IMD, IRSp53, actin and the mutant K4E which is defective in the formation of protrusions. Data on the immobile fraction and recovery rate of IMD were obtained. This approach was also combined with the use of cytochalasin D to determine the effect of actin filament disruption on IMD dynamics.

4. Measurement of the lipid binding properties of the IMD

Although the lipid binding property of the IMD appears to be important for its activity, specific details of binding affinities and selectivity is not yet clear. A fluorescence-based lipid-interaction assay was developed, and used to probe the interaction of the

IMD with vesicles having different membrane compositions, and in different ionic strength environments.

5. Purification of truncated IRSp53 constructs and generation of an anti-IMD antibody.

In order to further investigate the various functions of IRSp53, further studies are required, particularly on how the IMD interacts within the context of the full length protein. Three different IRSp53 truncation constructs were devised, generated and purified to facilitate further *in vitro* studies. An anti-IMD antibody was generated to provide more options for future research of the IMD, including specific detection of the protein and immunoprecipitation experiments.

6. Studies of dimerisation status of IMD

In order to address the question of IMD dimerisation status, native gel electrophoresis and sedimentation velocity experiments were carried out.

2 Materials and methods

All reagents were purchased from Sigma-Aldrich, UK unless otherwise stated. Molecular biology protocols and SDS-PAGE were carried out as described in Sambrook, unless otherwise stated (Sambrook, 2000).

2.1 Purification of recombinant IMD

2.2 Cloning

2.2.1 DNA preparations

All DNA preparations were done using Qiagen Mini- or Maxi-Prep Kit, according to the manufacturer's instructions.

2.2.2 Sequencing

All sequencing was done using the Plasmid to Profile service at the University of Birmingham Functional Genomics laboratory.

2.2.3 Polymerase chain reactions

PCR reactions were performed in a total volume of 50 μ l using 10 pmol primers, 10 ng template DNA, 5 μ l 10 x Phusion polymerase buffer (Finnzymes), 1 μ l Phusion polymerase (Finnzymes) and 10 mmol each dATP, dTTP, dCTP, dGTP. A typical PCR reaction was heated to 98 °C for 2 minutes, followed by 30 cycles of 1 minute at 98 °C, 1 minute at 54 °C to anneal, and 1 minute per kilobase of template at 72 °C. Final extension at 72 °C was done for 10 minutes after completion of the cycles

2.2.4 Cloning and vectors

All restriction digests were performed with enzymes from New England Biolabs Inc. Purification of PCR products and purification of DNA from bands extracted from agarose gels were performed using a QIAquick Gel Extraction Kit (Qiagen), according to manufacturer's instructions. Vectors used for cloning and expression were pRK5-HA (N terminal HA tag, Machesky and Insall, 1998), pEGFP N1 and N2 and mCherry N1(fused to C terminal of insert, Clontech), pGEX 4T2 (N terminal fusion to GST for bacterial expression, Amersham). Agar plates were made using 15 g/L agar, 20 g/L LB broth, plus 50 μ g/ml ampicillin or kanamycin, or 30 μ g/ml chloramphenicol as required.

Open reading frames (ORFs) were amplified by PCR (primers used are included in appendix), and purified from agarose gel after electrophoresis. Purified PCR products were subjected to restriction digest and DNA purified using a PCR Purification Kit (Qiagen). PCR products were ligated into Strataclone vector pSC-B-amp (Stratagene, USA), which allows ligation of the blunt ended product into the vector. Ligation reactions and transformation were carried out according to manufacturer's instructions, and transformants containing insert were identified by presence of white colonies on β -gal substrate, signifying disruption of the LacZ gene in which the multiple cloning site is located. For final cloning, both the destination vector and Strataclone vector containing insert were subjected to restriction digestion for 1 hour, and the appropriate DNA isolated by gel electrophoresis and gel purification (Qiagen Gel Purification Kit). Vector and insert were ligated overnight at 4 °C using T4 DNA ligase as per manufacturer's instructions. 1 μ l of the ligation reaction was used to transform electrocompetent *E. coli* derived from a DH5 α strain (Invitrogen) or BL21(DE3)-pLysS (Promega) for bacterial expression. Transformants were plated onto selective media containing 50 μ g/ml kanamycin or ampicillin; or 30 μ g/ml chloramphenicol as required. Single colonies were picked and grown in selective media containing appropriate antibiotics, and DNA purified by mini prep. Mini-preps were analyzed by restriction digestion for positive clones, and these were then sequenced.

2.3 Tissue culture and cells

Cells were grown at 37 °C and 5 % CO₂. COS-7 and cell lines were maintained in 75 cm² flasks in Dubecco's Modified Eagle Medium (DMEM; GIBCO Life Technologies, UK), supplemented with 10 % (v/v) foetal calf serum (FCS). Cells were passaged as follows. Media was aspirated, followed by washing with sterile PBS, and cells were removed from the flask surface by incubation with 0.05 % (w/v) trypsin in 2 ml PBS-EDTA for 5-10 mins at 37 °C. Media was added to a total volume of 10 ml replating solution and typically 1 ml of this solution would be used to replat the colony (in 15 ml total volume) in a fresh flask.

2.3.1 Transient transfection of mammalian cells

Cells were transfected with appropriate coding sequences in pRK5 mammalian expression vector, prepared from bacterial cultures by miniprep, or maxiprep. Cells were plated at 5 x 10⁵ per coverslip, left overnight and cell confluence assessed by phase contrast microscopy. 3

μ l of Lipofectamine 2000 (Invitrogen, UK) was added to 100 μ l Serum Free Dulbecco's Modified Eagle Medium (SFM) without antibiotics and incubated for 5 minutes at room temperature. This mix was then added to 0.5 μ g DNA and incubated for 15 minutes at room temperature before addition to cells in media including 10 % serum. Transfected cells were incubated for 18 hours before imaging.

2.3.2 Preparation of coverslips

Coverslips were removed from 6 well plates and subjected to a number of steps, with a PBS wash step between each. Cells were crosslinked to maintain structure for 10 mins in 4 % formaldehyde. Quenching was done by 10 min incubation with 50 mM NH₄Cl, followed by a 4 min permeabilisation step with 0.1 % Triton – X 100 in PBS. For immunofluorescence, cells were incubated for 40 minute with primary (target specific) and secondary (fluorophore-conjugated) antibodies. Rhodamine – conjugated phalloidin was used to stabilise and stain actin filaments.

2.4 Fluorescence microscopy

2.4.1 Epifluorescence imaging

A Zeiss Axioskop2 microscope with a 63x 1.4NA Plan Apochromat lens was used for fluorescent microscopy of fixed cells. Images were captured using a Qimaging 12-bit QICAM with a 0.63x camera lens and Openlab software (Improvision) and saved as 12-bit TIFF files. Images were processed for publication in Adobe Photoshop (Adobe). The image histogram was adjusted to make full use of the available greys, without adjusting gamma, converted to 8-bit and where necessary merged with corresponding images, taken with different fluorescent filters, to make an 8-bit/channel RGB file. Regions of interest were selected from merged images and scale bars were added. Where image size was adjusted for making figures this was done in Photoshop without resampling of the image. For time-lapse microscopy, cells were plated onto a 25mm cover slip in a cell chamber from Medical Systems Corp. (Greenville, NY); the chamber was filled with media or buffer and sealed with a second 25mm cover slip to prevent evaporation and optical aberrations from the meniscus. A Zeiss Axiovert 100 microscope was kept at 37 °C in an incubation chamber custom built for the

microscope (Solent Scientific). Images were captured using a Hamamatsu Orca C4745-12NRB with a 0.5x camera lens and Openlab software (Improvision).

2.5 TIRF microscopy

TIRF was performed on a Nikon Eclipse TE 2000-U microscope equipped with 60x and 100x 1.45 NA Nikon TIRF oil-immersion objectives. The Nikon Epi-fluorescence condenser was replaced with a custom condenser in which laser light was introduced into the illumination pathway directly from the output of a 3.5 μm optical fibre oriented parallel to the optical axis of the microscope. GFP and RFP excitation were performed at 473 nm and 561 nm respectively using individually coupled diode lasers (Omicron) controlled by a DAC 2000 card running MetaMorph (Molecular Devices). All live-cell imaging was performed with a Cascade 512F EMCCD camera (Photometrics UK). For GFP imaging a filter block consisting of a Z 473/10 excitation filter, a 488 RDC dichroic mirror and an ET 525/50M emission filter was used. For dual-colour imaging a dual band-pass filter block (Chroma 59022) was used, combined with an Optical Insights DualView containing 595 nm dichroic, and 525/50 and 630/60 emission filters.

2.6 FRAP confocal microscopy

FRAP was performed using an Olympus FV-1000 laser scanning confocal microscope with a 405 nm laser coupled through the simultaneous scanning port. This microscope configuration had two separate pairs of X- and Y-scanning mirrors which allowed image data to be continuously acquired using 488-nm excitation while a small region of the sample was independently photobleached using a 405-nm laser. The image acquisition rate was 1.107 s per frame, with typically 6 frames of data acquisition prior to a 1-frame photobleach event. Photobleaching was performed using the 'cyclone' bleach function, in which the laser starts in the middle of a circle and processes outward in a spiral pattern. Bleach size was between 0.5 and 4 μm . Photobleaching was performed at sufficient laser intensity to achieve at least 50 % bleaching where possible. Scanning was performed at zoom 2-4 (0.412-0.206 μm per pixel) using an NA 1.1 PLAPO 60x OLSM objective in 12-bit acquisition mode. GFP was imaged over a 500-550 nm and RFP/mCherry over a 600-660 nm emission range. FRAP values were obtained using the measure stack tool in ImageJ. Curves were normalised for bleaching

during imaging with reference to an unbleached area of the cell. The data were fitted with GraphPad Prism 5.0, using a 1 exponential nonlinear regression algorithm with initial fluorescence constrained to 0.

2.7 Cytochalasin D treatment

Cytochalasin was added to the concentrations specified from a 1 mM stock solution in dimethyl sulphoxide (DMSO). DMSO alone was not observed to have any effect on cell morphology in the conditions used.

2.8 Recombinant protein expression

Plasmid pGEX2T containing coding sequences of the IMD of human IRSp53 fused to an N terminal glutathione-S-transferase (GST) tag was transformed into BL21 p LysS *E. coli* (Invitrogen). Cultures were grown in 1 L flasks of LB containing 30 µg/ml chloramphenicol and 50 µg/ml ampicillin at 37 °C to OD600 ~0.4 before inducing expression with 1 mM IPTG under shaking at 25 °C for 18 h. Expression of recombinant protein was assessed by SDS-PAGE, comparing induced and uninduced culture lysates (boiled 15 min in SDS loading buffer), on Coomassie stained polyacrylamide gel. Cells were harvested by centrifugation of 500 ml at 2000 x g for 10 mins followed by resuspension in 40 ml phosphate buffered saline (PBS) and centrifugation at 4000 x g for 10 mins. Pellets were stored at -80 °C prior to use.

2.8.1 Cell lysis

Pellets were resuspended in 20 ml Lysis Buffer I (see appendix) at room temperature, and 20 mg lysozyme was added. The lysate was then incubated on a rotator for 20 min at room temperature. Following this, 8 ml Lysis Buffer II (at 4 °C) was added and the sample incubated on a rotator at 4 °C for a further 10 mins. Cells were sonicated on ice 5 x (10 s on; 5 s off). The lysate was then cleared of debris by centrifugation at 37,000 x g for 30 mins and a sample saved for analysis.

2.8.2 Affinity chromatography

Cleared lysates were incubated for 2 h at 4 °C with glutathione immobilized on agarose beads (2 ml beads per 1 l original culture). The slurry was then passed through columns and the beads washed with 3 column volumes of PBS-DTT-Tween (see appendix), with regular resuspension of the beads using a pipette tip to ensure removal of unbound components. The beads were equilibrated with TRB (see appendix) and the slurry placed in gently rotating tubes and incubated with 60 units thrombin (Calbiochem, UK) at 4 °C for 18 h. Cleaved protein was then eluted into TRB and stored on ice.

2.8.3 Further purification.

Eluted protein was dialysed into CM sepharose loading buffer and applied to a CM sepharose column, bed volume 20 ml. The column was eluted with a linear NaCl gradient from 140 mM to 320 mM, and 3 ml fractions collected. Fractions were analysed for protein content using the Biorad assay - Bradford reagent, (Biorad, UK) was diluted 1 in 5 and 180 µl added to 20 µl sample. Strongly positive fractions were analysed by SDS-PAGE, followed by Coomassie staining, and homogeneous fractions pooled and concentrated using Vivaspinn centrifugal concentrator (Vivascience, Germany). Purity of the concentrated protein was assessed by SDS PAGE, followed by Coomassie staining, and the protein stored in 1 ml aliquots at -80 °C. The protein concentration was estimated by measuring absorbance at 280 nm, with the molar absorption coefficient derived from the protein sequences. The BCA-copper-sulphate assay was also used to measure sample concentration against BSA standards.

2.9 Gel filtration chromatography

A column measuring approximately 48 cm by 1.2 cm was loaded with approximately 32 ml of Sephacryl S-300 resin. The resin was degassed under vacuum prior to pouring, and was packed at a high flow rate of buffer to improve resolution. Prior to each experiment, the column was equilibrated extensively with the buffer (50 mM Tris-Cl, pH 8, 150 mM NaCl). Samples were diluted to a volume of 600 µl, incubated at room temperature for 1 h, and loaded manually onto the column. Once the sample was in the column, buffer was pumped through at a rate of 0.35 ml per minute, and fractions of 0.7 ml were collected and analyzed. Fractions containing the IMD were identified by the Bradford protein assay, and further analyzed using SDS PAGE.

2.10 Vesicle production.

Porcine brain phospholipids (Avanti Polar Lipids, USA) and bovine brain lipid extract (Sigma) were acquired in chloroform. To prepare vesicles, lipid and DiI/DiO were mixed in chloroform and dried under vacuum before rehydration in aqueous buffer (50 mM Tris-Cl, pH 8, 150 mM NaCl), and vortexed to form large multilamellar vesicles. The samples were subjected to five freeze-thaw cycles in liquid nitrogen to disrupt the large multilamellar structures. Vesicles of uniform diameter were made by seven passages through a Lipex extruder (Northern Lipids) containing polycarbonate filters (Whatman, USA) with pore size 200 nm, at pressure of up to 600 psi. Final lipid concentration was 2 mM.

2.11 Fluorescence analysis of DiI labelled vesicles.

Fluorescence (excitation. 549 nm; emission. 565 nm) of samples with DiI -containing vesicles was measured in fluorimeter (Photon Technologies International, UK). Where measured, emission wavelength scans were done over the range 560-600 nm, step size 2 nm.

2.12 Fluorescence microscopy of vesicles.

Sample comprising vesicles with IMD was applied to a microscope slide, a coverslip placed on top and sealed in place using clear nail varnish. Microscopy was done as described in imaging section of Materials and Methods. Images were processed using Adobe Photoshop software (Adobe, Inc.).

2.13 Lipid vesicle pelleting assays

Prior to mixing, IMD and lipids were centrifuged for 5 mins at 16,000 x g. Samples were made up to 300 µl final volume, mixed gently by pipette and incubated at room temperature for 20 minutes prior to centrifugation. Samples were centrifuged at 16,100 x g for 30 minutes. Samples were taken immediately before and after centrifugation and fluorescence intensity measured as described above. Samples containing buffer alone were used to subtract background fluorescence signal, and values were corrected for non-IMD induced pelleting (5-15 %).

2.14 Förster resonance energy transfer (FRET)

Briefly, IMD was chemically labelled with fluorescent probe IEDANS, which was bound covalently to exposed cysteine residues. IEDANS has peak excitation of 350 nm and emission 420-490 nm. Fluorescence acceptor was DiO lipophilic fluorophore, at concentration of 25 µg/mg of lipid. DiO has excitation and emission peaks at 484 and 501 nm, respectively. FRET measurements were carried out according to protocols described previously (Visegrady et al., 2004).

2.15 Affinity purification of anti-IMD antibody

The antibody was raised in sheep by inoculation with 0.5 mg of IRSp53 IMD, by the Scottish National Blood Service, UK. Pre- and post- inoculated sera were stored at -80 °C until use in affinity purification. Briefly, this was done as follows. Approximately 1 mg of purified IMD was run on SDS PAGE gel and transferred onto nitrocellulose membrane (as described in Western Blotting, below), the membrane stained with Coomassie, and the band containing protein was isolated, cut into small segments and blocked for 30 minutes in PBS containing Tween 0.1 %, BSA 2 %, and washed twice for 10 minutes in PBS - 0.1 % Tween. The membrane was then incubated for 2 h in 10ml PBS - 0.1 % Tween with serum diluted 1 in 10. Wash steps were as follows: 4 washes with PBS - 0.1 % Tween, 3 washes with 1 M KCl, 20 mM Tris-Cl, pH 8 and 3 with PBS. IMD antibody was eluted in the acidic elution: 5 ml 100 mM glycine pH 2.5 for 15 minutes, and immediately neutralised with 0.5 ml Tris-Cl pH 8.8, and BSA added to final concentration 1 % to stabilise the antibody. The elution was then dialysed against PBS containing 1 % BSA to stabilise the antibody and stored at -80 °C.

2.16 Western blotting

Samples were prepared by mixing with 4 x protein loading buffer, and boiled for 5 minutes, before being separated on an SDS PAGE gel. Blotting onto PVDF membrane (Amersham, UK) was done using a Trans-blot SD semidry blotting cell (Biorad, UK). Cells were assembled in the following order. Two sheets blotting paper incubated in Anode I buffer (see appendix) placed on anode, 4 sheets incubated in Anode II buffer; PVDF membrane preincubated in methanol; SDS gel preincubated in Cathode buffer; 6 sheets blotting paper incubated in Cathode buffer. Excess liquid was removed, and the cathode electrode placed on

top. Transfer was carried out at a constant 10 V for 120 minutes. Following transfer, blot was stained with Coomassie to allow clear marking of size markers. Nitrocellulose membranes were blocked overnight in TBS-Tween containing 5 % (w/v) powdered milk (Marvel, UK) at 4 °C and washed for 3 x 10 ml for 15 mins in TBS-Tween. Antisera / antibodies were added to TBS-Tween containing 1 % milk and incubated with the blot at room temperature for 1 hour, before 3 further washes with TBS-Tween. To probe for sheep antibody, anti-sheep antibody conjugated to horse radish peroxidase (HRP) (Jackson Labs) was used at a dilution of 1 in 10,000 in TBS-Tween 1 % milk, and incubated with the blot for 1 hour at room temperature. Blots were developed using SuperSignal West Pico Chemiluminescent Substrate (Pierce, UK), and the image captured using Genesnap software (Syngene, UK).

2.17 Native Gel Electrophoresis

Native conformation electrophoresis was done on a 4-16 % bis-tris gel using the Nativepage Novex Gel system (Invitrogen, UK). Proteins loaded onto the gel were mixed with 4 x loading buffer and Coomassie solution (5 % v/v) was added immediately prior to loading. The gel was set up as per manufacturer's instructions and run at 150 V until the dye front reached the end of the gel. The gels were destained in Coomassie destain solution, and imaged using Genesnap software (Syngene, UK).

2.18 Analytical Ultracentrifugation

Samples were dialysed into AUC Buffer (50 mM Tris-Cl, pH 8; 150 mM NaCl; 5 mM DTT), and analyzed using a Beckmann Coulter XL-I analytical ultracentrifuge equipped with absorbance optics. Two-chamber centrepieces were assembled according to manufacturer's instructions. Sample protein concentration was estimated by BCA assay, and appropriate dilutions made by addition of final dialysate. Reference buffer (dialysate) and sample were loaded into cells as described by manufacturer. Cells were rotated at 3,000 rpm during initial and wavelength scans; measurements at 40,000 rpm with scans every 2 min. Experiments were done at 4 °C unless specified. Data were analysed using Sedfit to calculate $c(S)$ and $c(M)$ distributions, where S is the sedimentation coefficient and M is the molecular mass (Brown and Schuck, 2006).

3 Generation of DNA constructs

3.1 Introduction

Prior to the commencement of studies in cultured cells, a number of DNA constructs comprising different truncations of IRSp53 were designed and generated. For all wild type constructs, the template used was a pRK5-myc mammalian expression construct containing a cDNA encoding human IRSp53 (accession number NP_059344), (received as a gift from Alan Hall). For cloning of the IMD K4E mutant construct in the pRK5 mammalian expression vector was generated from this initial construct by Tom Millard as described in Millard et al, 2005; and this was used as the template for the IMD K4E-GFP construct.

3.2 Cloning strategy

Inserts for constructs were generated by PCR from the original IRSp53 template. Specific primers with 5' restriction endonuclease sites were designed to amplify specific portions of the template DNA (Figure 3.1 A i); primers listed in Appendix. This generates a PCR product that has the appropriate restriction endonuclease sites flanking the insert sequence (Figure 3.1 A ii), and this product is purified from the PCR reaction by agarose gel electrophoresis and subsequent purification (Figure 3.1 A iii).

3.2.1 Primer design and selection of restriction sites

Primer pairs were designed to amplify specific regions of the IRSp53 construct. In the case of the pEGFP vectors, the multiple cloning site into which the insert DNA was ligated is located between the promoter and the downstream GFP. Consequently, at the downstream site the insert must be inserted in the same reading frame as the GFP in the vector to allow formation of a fusion protein. In the case of cloning into pEGFP N2 vector with the EcoRI downstream restriction site, this site is in frame with the downstream GFP. The primer sequence goes from residue 250 directly to the EcoRI site. Where the BamHI restriction site was used to clone into pEGFP N1, the BamHI site in this vector is in reading frame 3, and so two additional bases were added between residue 250 and the restriction site. The bases added were identical to those present in the multiple cloning site prior to cleavage. In the case of full length IRSp53, the downstream primer was designed to omit the stop codon, as its inclusion would prematurely terminate the polypeptide sequence and result in the expression of an untagged IRSp53 protein. In the case of the pGEX4T2 protein expression constructs,

the GST protein tag is located upstream of the multiple cloning site, so the upstream primer was designed to continue the same reading frame from the vector and through the insert. The downstream primer was designed to contain a stop codon, to ensure that the mRNA is not translated beyond the end of the insert, which would result in the addition of extraneous amino acid residues.

3.2.2 Use of the Strataclone intermediate vector system

To facilitate the cloning process, a Strataclone Blunt PCR Cloning kit (Stratagene Inc., USA) was used. An intermediate vector was used. This allows cloning of blunt ended PCR products into a circular vector, as outlined in Figure 3.1. This was then cleaved with the restriction endonucleases specific for the sites flanking the insert (Figure 3.1 C i, ii), and the insert was separated from the vector by agarose gel electrophoresis (Figure 3.1 C iii). The benefit of using the intermediate vector system is that the insert that is released from the vector has been cleaved and has “sticky ends”, and so this improves the efficiency of ligation into the destination vector.

3.2.3 Cloning into the destination vector and detection of clones

The destination vector was cleaved with the restriction enzymes during cleavage of the Strataclone vector, and both insert and destination vector were purified following agarose gel electrophoresis (Figure 3.2 B). Following ligation (Figure 3.2 A i and ii), and transformation, individual colonies were amplified, and the clones examined for positive inserts by gel electrophoresis (Figure 3.2 C). Clones with inserts were selected for sequencing to verify the sequence of the insert.

3.3 Use of the constructs in this work

Chapter 4 describes investigation done with fixed and live Cos-7 cells overexpressing the IMD-GFP and IRSp53-GFP constructs, in epifluorescence and total internal reflection fluorescence (TIRF) microscopy experiments. A pEGFP vector with no insert was used to express GFP alone in control cells. Chapter 5 describes fluorescence recovery after photobleaching (FRAP) experiments carried out on Cos-7 cells which were transfected with IMD-GFP, IMD-mCherry, IRSp53 GFP, and the IMD K4E GFP. A pEGFP vector with no insert was used for GFP-only expression, and a beta actin pEGFP vector was used to visualize actin localization. An overview of the constructs generated is shown in Figure 3.3.

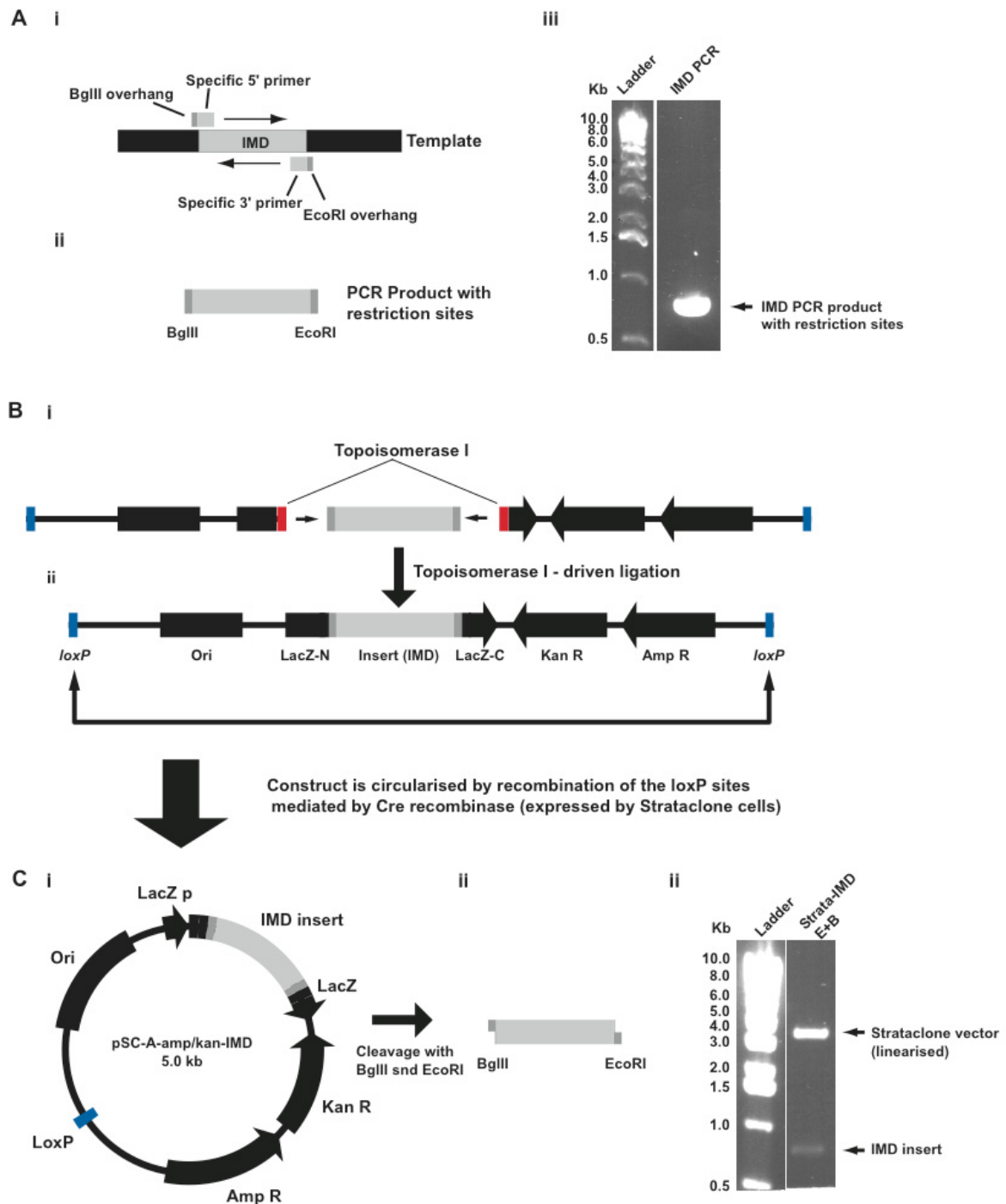


Figure 3.1 Generation of PCR products and use of intermediate cloning vector. (A) (i) a PCR reaction analysed by electrophoresis on a 1 % agarose gel, yield of approximately 1 μ g. (ii) Depiction of the PCR product, with cDNA (light grey) flanked by restriction enzyme sequences (dark grey). (B) Incorporation of the PCR product into the Strataclone vector. (i) The PCR product is ligated to each of the two arms, forming a linear construct (ii), which is then circularised by the Cre enzyme expressed in the bacterial host. (C) (i) The circularised vector, (ii) cartoon of the digested insert and (iii) 1 % agarose gel showing restriction digest of the Strataclone vector and the insert, which is subsequently purified from the gel.

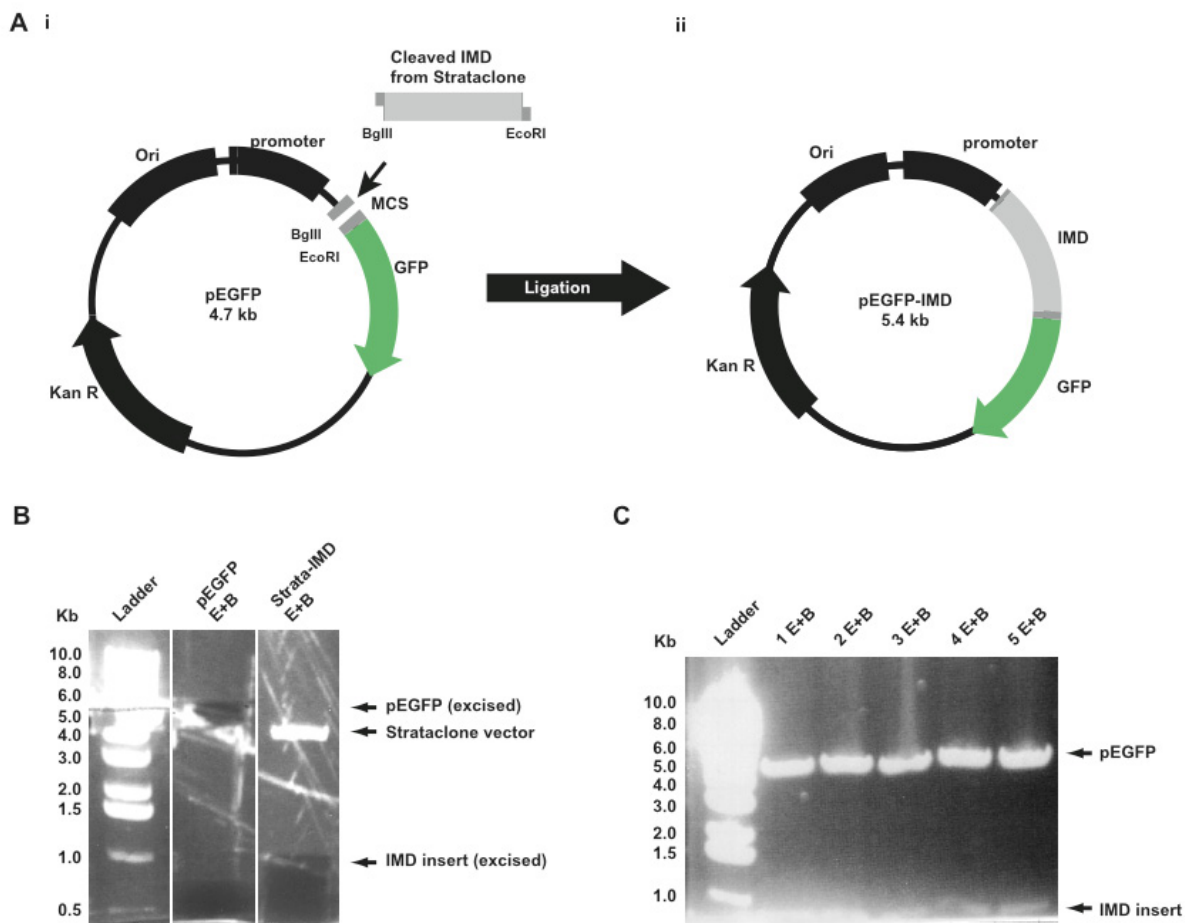
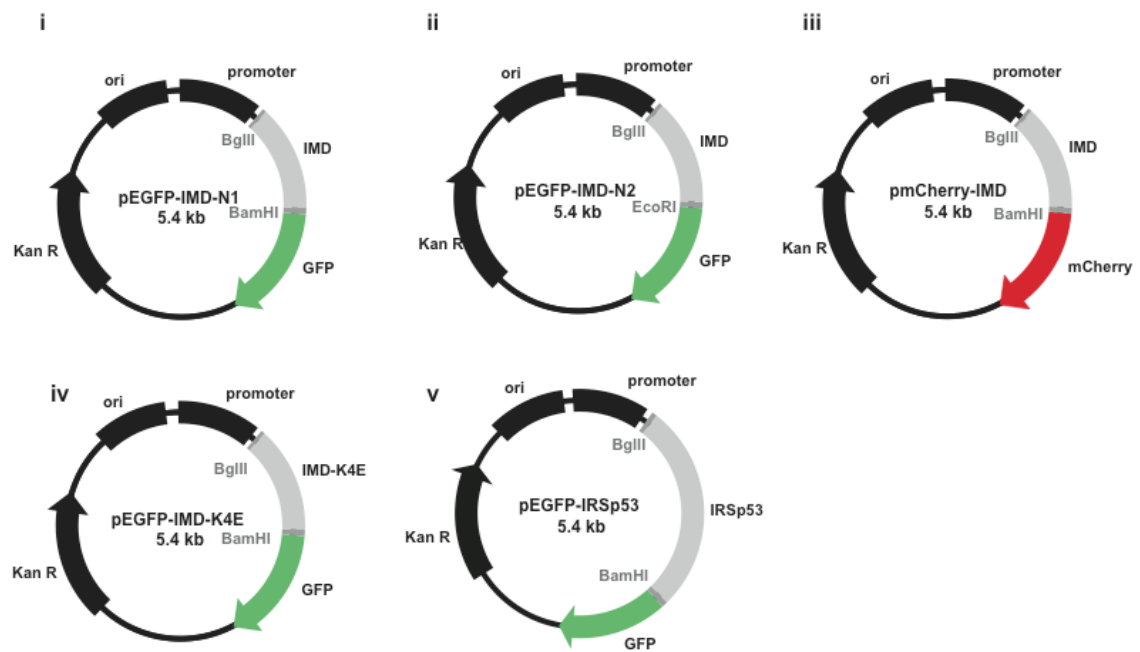


Figure 3.2 Ligation of the insert into the destination vector. (A) Schematic of the cloning procedure. The insert that has been excised from the intermediate vector, and has cleaved restriction sites flanking it, is ligated into the destination vector which has been cleaved with the same restriction enzymes. (B) Agarose gel used to purify the insert and destination vectors, which have been excised. (C) Examination of clones following ligation and transformation was carried out by agarose gel electrophoresis to identify clones containing the insert. Insert sequence was verified by sequencing.

A Mammalian expression vectors



B Bacterial expression vectors

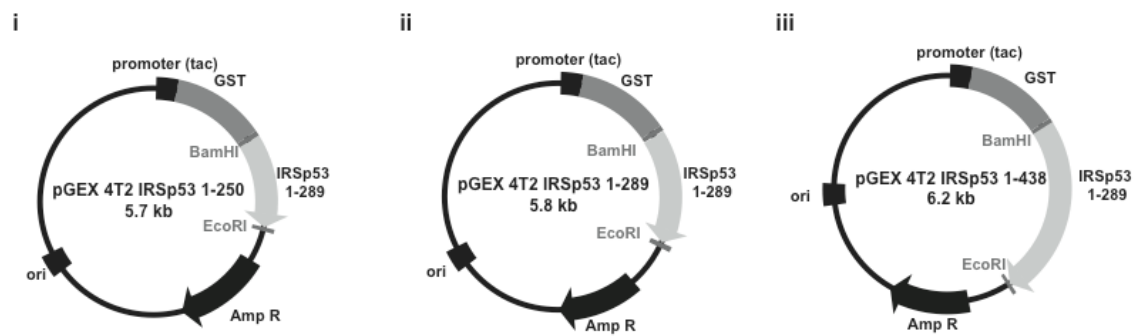


Figure 3.3 Overview of the constructs generated in the present study.

4 IRSp53 IMD induced cellular protrusions are dynamic, contain actin and are affected by Cytochalasin D

Overexpression of either full length IRSp53 or the IMD causes formation of finger-like protrusions reminiscent of filopodia (Govind et al., 2001; Krugmann et al., 2001; Bockmann et al., 2002; Soltau et al., 2002; Nakagawa et al., 2003; Millard et al., 2005; Disanza et al., 2006). Early studies attributed this phenotype to an actin-bundling property of the IMD (Yamagishi et al., 2004; Millard et al., 2005). Subsequent studies have identified that the IMD can bind to and deform anionic phospholipid membranes, in a manner analogous to BAR domains, with which the IMD shares structural similarity (Suetsugu et al., 2006a; Suetsugu et al., 2006b; Mattila et al., 2007; Saarikangas et al., 2009). These studies demonstrate using synthetic lipid vesicles that the IMD is able to induce protrusions in the absence of actin, which resemble the protrusions observed in cells.

Work presented here uses microscopy techniques and the actin filament destabilizing toxin cytochalasin D (cytD) to investigate the importance actin for IMD and IRSp53 induced protrusions in cells.

4.1 Overexpression of IRSp53 IMD in Cos-7 cells

Overexpression of IMD causes a distinctive microspike phenotype that has been described in many studies (Yamagishi et al., 2004; Bompard et al., 2005; Millard et al., 2005; Disanza et al., 2006; Suetsugu et al., 2006b; Millard et al., 2007; Saarikangas et al., 2009; Yang et al., 2009).

Previous investigations done in the Machesky lab have used N terminal HA and myc epitope-tagged IMD constructs. The HA tag is only 9 amino acids long, and so is not expected to change the accessibility of the IMD to its ligands. A typical overexpression phenotype observed is shown in IMD-HA overexpressing cells display many thin finger-like protrusions at the cell periphery, ranging from short spikes that only just protrude from the cell membrane, to longer spikes of around 10 μm in length. This is in marked contrast to cells expressing GFP only as a control, which exhibit a diffuse staining of the cytosol, and have few protrusions at the cell periphery. The protrusions are not obviously distributed in a polarized fashion, protrusions occurring all round the cell periphery. Some protrusions appear to be clustered at particular regions, forming part of a larger projection of the cell edge (**Figure 4.1 A**, arrowheads indicate several such regions).

4.2 Live imaging of IMD in cells.

To improve our understanding of the processes involved in IMD-mediated membrane protrusions, it was desirable to image the activity of IMD in live cells. Prior to this work investigations into the function of the IMD in live cells were limited. Several studies had used full length tagged protein (Nakagawa et al., 2003) a tagged IMD (Yamagishi et al., 2004) or partial IMD (RCB, Rac Binding Domain) (Suetsugu et al., 2006b). These groups all used using fusion constructs with an N terminal tag. A study published during the course of the work described here did use IMD with a C terminal fluorophore tag (Mattila et al., 2007).

A fusion construct of the IMD with EGFP (henceforth referred to as GFP), was generated by cloning into the pEGFP N2 vector, including the GFP at the C terminus. This is in contrast to the earlier studies mentioned above, which contained the GFP tag at the N terminus. In all IMD containing proteins the IMD domain is located at the N terminus, so a C- terminal tag was used in order to avoid potentially deleterious effects of a tag at the N terminus. The IMD-GFP construct showed a similar phenotype to an IMD-HA construct, both qualitatively, and in the number of protrusions formed (**Figure 4.1 A, B**). This suggests that the GFP tag has no marked effect on the activity of overexpressed IMD in these cells and is therefore suitable for further investigations.

4.3 Cytochalasin D causes retraction of some IMD rich protrusions

Preliminary studies were carried out using cells transfected with IMD-myc, which were fixed and stained with Rhodamine-conjugated phalloidin, which binds to and labels actin filaments (Figure 4.2) (Cooper, 1987). These studies confirmed previous studies that found that phalloidin staining is present in all IMD-mediated protrusions (Yamagishi et al., 2004; Millard et al., 2005; Lim et al., 2008; Yang et al., 2009). However, since the presence of actin filaments does not necessarily prove that polymerization is necessary for IMD-mediated protrusions, it was decided to use cytochalasin D to disrupt actin filament dynamics, and investigate the necessity of actin polymerization for IMD-mediated protrusions.

Previous work done to investigate the contribution of actin filaments to IRSp53 function has largely been carried out using latrunculin B (latB), an actin filament destabilizing agent (Suetsugu et al., 2006b; Mattila et al., 2007; Yang et al., 2009). LatB disrupts actin filaments

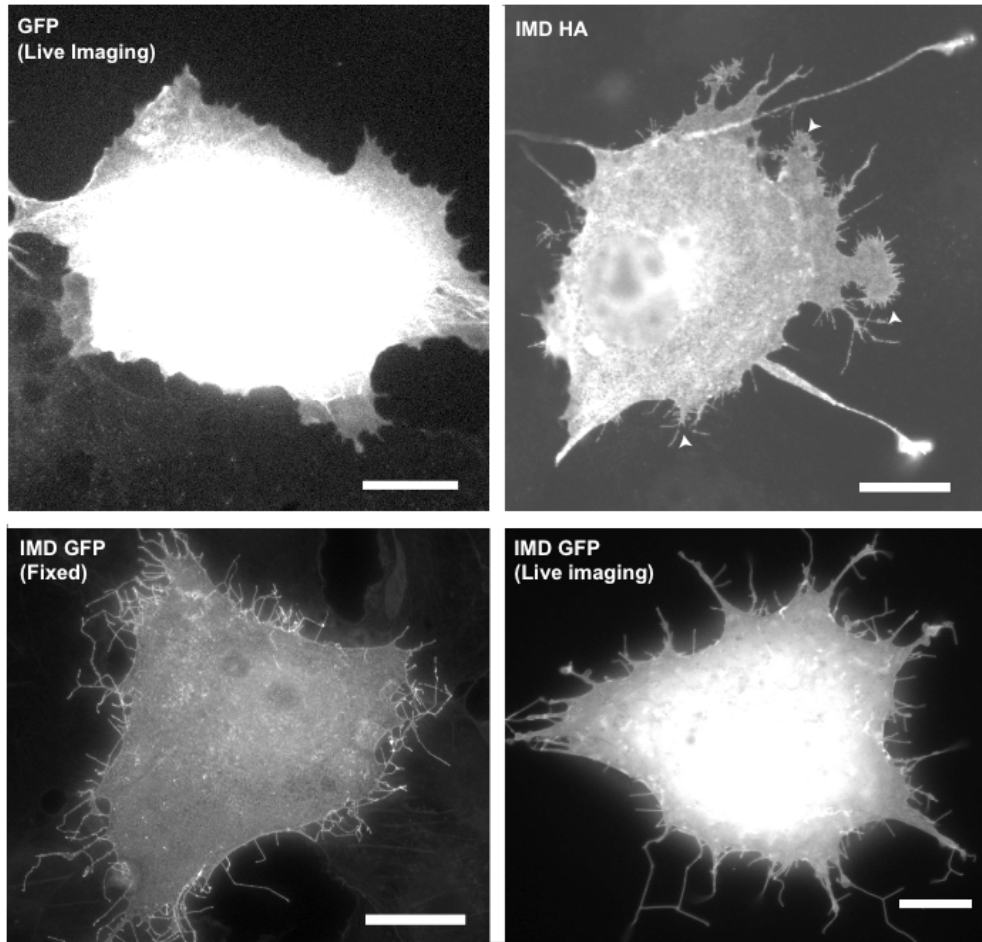
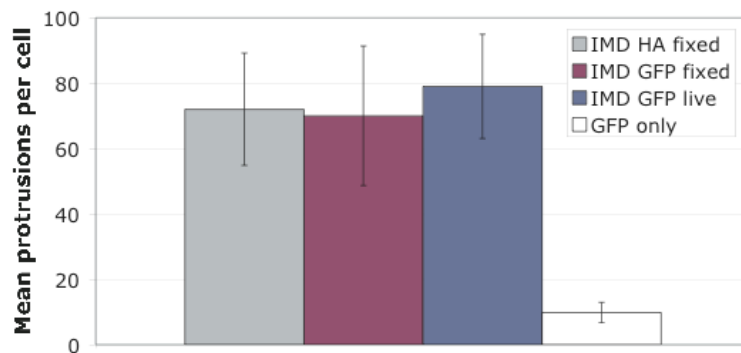
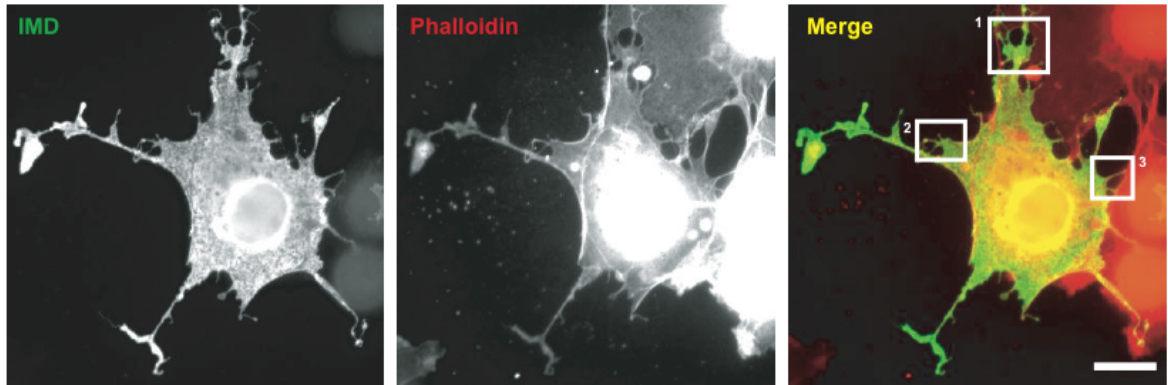
A**B**

Figure 4.1 (A) Cos-7 cells imaged to examine the overexpression of IRSp53 IMD with different C-terminal tags. (i) IMD-HA expressing cells were fixed and stained with anti-HA primary and FITC secondary antibody. IMD-GFP expressing cells were fixed (ii), or imaged in culture (iii). Images are representative of 10 cells viewed on the coverslip, scale bar, 20 μm . (B) chart shows mean number of lateral protrusions per cell for IMD HA, IMD-GFP fixed cells IMD-GFP live cells, and cells expressing GFP only. N = 5, bars +/- standard deviation.

A



B

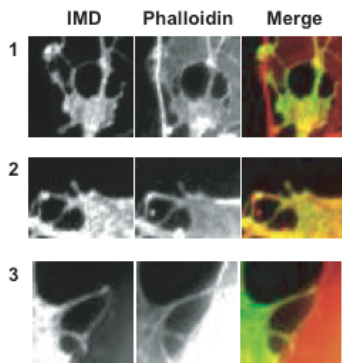


Figure 4.2 IMD rich protrusions contain phalloidin staining. (A) Images of cell transfected with IMD-myc and stained with Rhodamine-conjugated phalloidin to stain actin filament. Phalloidin staining is present in all IMD protrusions. (B) Expanded regions 1-3 marked in the larger image. Scale bar, 20 μm .

by binding to and altering monomeric actin, which can lead to filament depolymerization due to treadmilling (Morton et al., 2000). One study found that protrusions made by the RCB, a truncated form of the IMD, were still maintained after treatment with latB and staining with phalloidin, suggesting that the structures once formed are not dependent on actin filaments (Suetsugu et al., 2006b). Mattila *et al* in their 2007 study found that MIM-IMD filopodia growth was slowed after treatment with latB. In the present study, cytD was used to investigate the importance of actin filaments for existing actin structures. cytD is a cell permeable toxin that binds to the fast growing barbed end of actin filaments preventing elongation, leading to filament disassembly (Cooper, 1987). This provides a tool to investigate whether actin filaments are necessary for IMD - induced protrusions.

Images showing the effect of cytD on IMD-GFP expressing cells are shown in Figure 4.3. Prior to treatment, the cell periphery has a large number of short IMD rich structures, of maximum length approximately 10 μm . They show dynamic lateral movements, presumably due to Brownian motion. Some protrusions show restricted movement, suggesting that they are adhered in some way to the substrate. In addition to the protrusions in the focal plane there are occasional protrusions that come into view from outside the focal plane. There is no obvious effect seen immediately post treatment with cytD, with all protrusions remaining. However there is a marked change beginning at 405 seconds post treatment. During the following 90 seconds the majority of the smaller spikes are lost. Most of the projections shorten slightly but maintain their structural integrity. As the cell edge expands outwards, stationary protrusions become 'consumed' by the moving membrane. By 570 seconds the majority of finger like protrusions initially present, have disappeared and the cell has taken on a smooth shape. Most of the more substantial projecting areas of the cell have a straight appearance. There is no further change in the morphology of the cell from this point to the end of the movie.

Quantification of time-lapse experiments of cells overexpressing IMD-GFP showed that a significant proportion of protrusions was lost in following treatment with cytD (mean 34.2 +/- 9.5 decrease, N=4, P<0.05, paired t test).

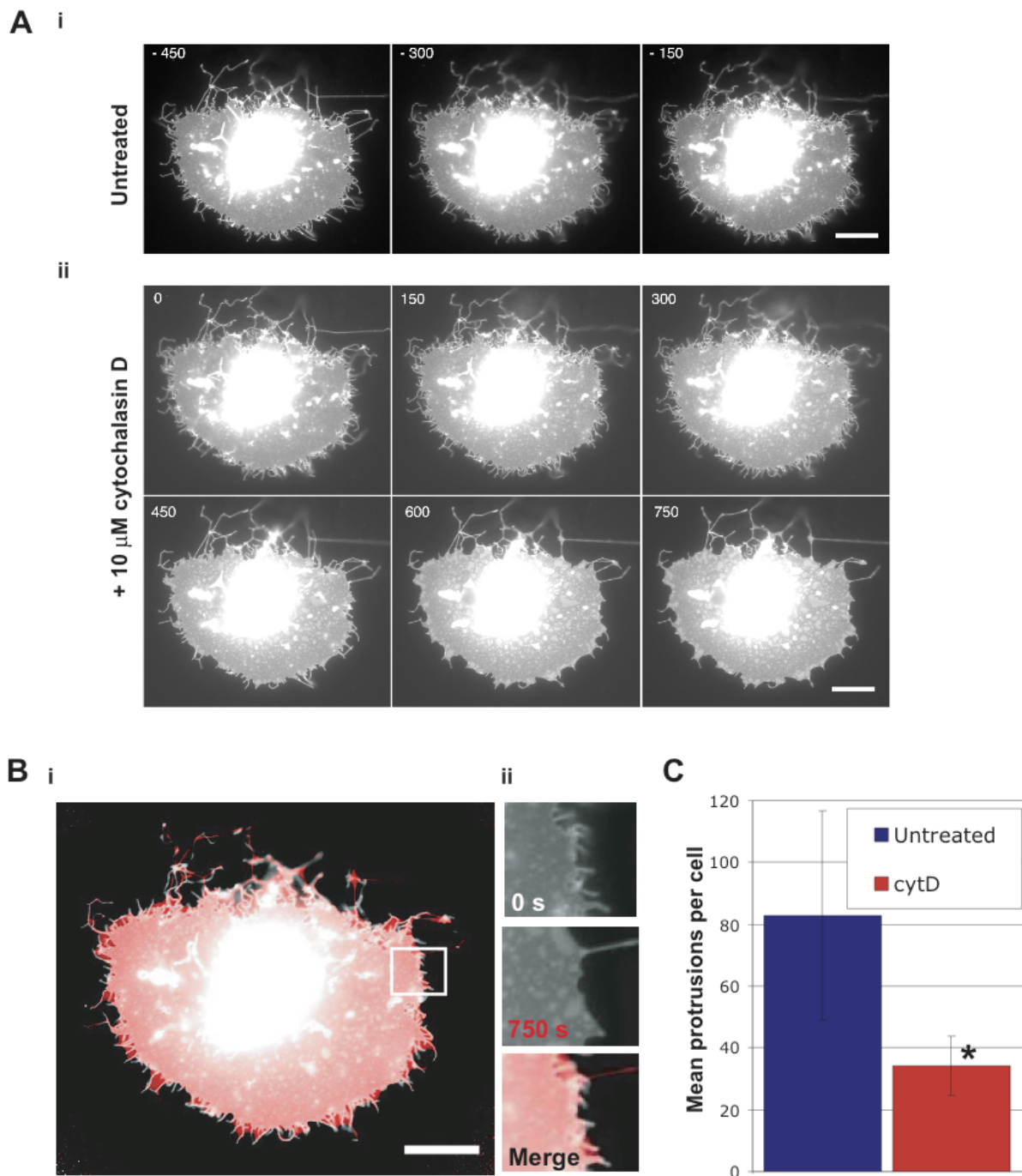


Figure 4.3 cytD treatment reduces the number of IMD – rich protrusions in cells overexpressing IMD GFP. (A) Montages of cell before (i), and directly after (ii) treatment with 10 μ M cytD for 750 seconds. Loss of protrusions is first visible at 450 seconds resulting in the final smooth cell morphology which is seen from 600 seconds until the end of the movie. (B) Merge of the cell prior to cytD treatment (inverted greyscale), and following 750 s of treatment (red). (ii) Magnified area as indicated (i). (C) Mean number of protrusions per cell is significantly reduced following cytD treatment (paired t-test $P < 0.05$, $N = 5$). Frame time indicated in seconds, scale bars 20 μ m. Error bars on graph represent standard deviation.

4.4 TIRF microscopy analysis of cells expressing IMD-GFP

Total internal reflection fluorescence (TIRF) microscopy allows imaging of fluorescent material located within 100 nm of the coverslip on which the specimen rests, and allows detection of fluorescence signal with a high signal to noise ratio (Jaiswal and Simon, 2003). This allows imaging of a higher sensitivity than can be obtained by even confocal microscopy. This technique was employed to investigate the dynamics of protrusions at the ventral surface, as it also allows specific illumination of the area of the cell that is in close proximity to the cover slip, and background fluorescence is reduced.

Figure 4.4 shows a Cos-7 cell expressing IMD-GFP as imaged by TIRF. As was previously observed using widefield fluorescence microscopy, COS7 cells overexpressing IMD-GFP display filopodial protrusions that show dynamic movement. The cell shown in Figure 4.4 has a relatively low level of IMD expression but serves to illustrate several features of IMD protrusion dynamics seen in many cells. In cells expressing GFP alone (Figure 4.4), the ventral surface of the cell is composed of many dynamic regions, and a diffuse GFP signal is observed throughout. In IMD-GFP cells, similar broad areas are also present (Figure 4.4, region 1), however in contrast to cells expressing GFP alone, they have an intense signal at the cell periphery, with little GFP signal detectable in the interior region (Figure 4.4, region 1). As noted earlier, these areas which are already protruding from the cell are often associated with initiation of IMD rich filopodia, both by protrusion outwards, (Figure 4.4 region 1) and also by retraction of this region (Figure 4.4 region 3).

Another characteristic of IMD overexpression observed using TIRF microscopy was the appearance of numerous small foci within the cell (Figure 4.4, C). These foci were observed in the majority of cells imaged, and many show extremely dynamic movement in the z plane, as they were observed to enter and leave the field of view. Some of these foci appeared to be IMD protrusions that are simply dipping in and out of the TIRF field, as occasionally the protrusion would move into the visible field. Others appear to be either foci or tips of protrusions that move into and out of the illuminated field. The density of the foci in foci-containing regions of cells measured, and found to be approximately 0.2 ± 0.043 foci per μm^2 (quantified from 77 μm regions in 5 cells averaged over 4 timepoints). Persistence of

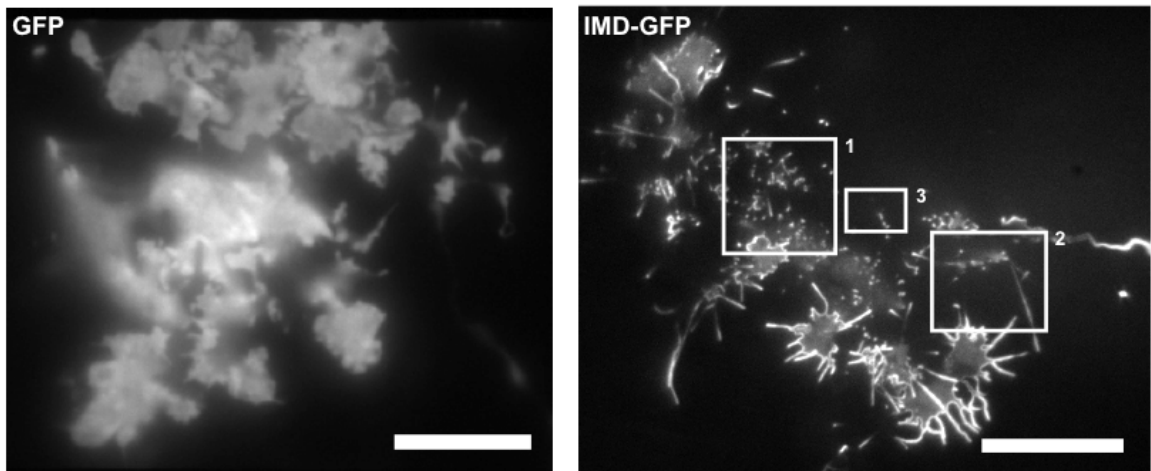
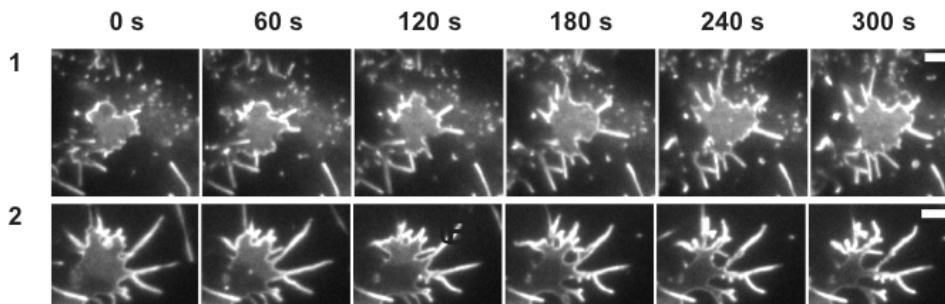
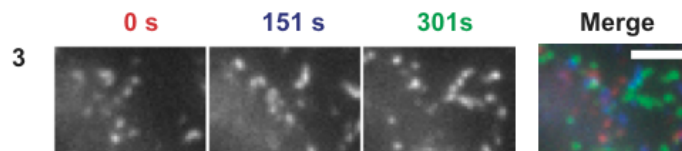
A**B****C**

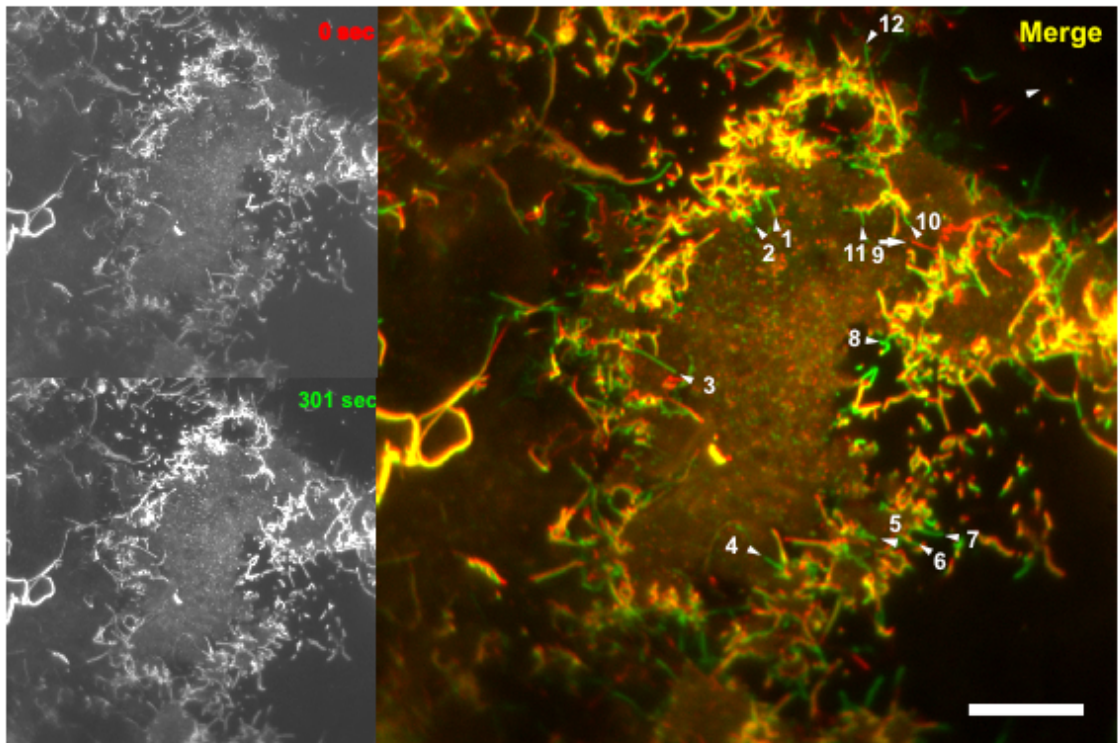
Figure 4.4 Imaging of IMD-GFP - expressing cells using TIRF microscopy. (A) initial image of the movie showing the whole of a cell, (B), montages showing the dynamic movement and growth of IMD rich structures, blown up from regions 1 and 2 highlighted in (A). (C) montage of region 3 expanded. Colour code used to show the dynamically changing localisation of small foci. Scale bars, 20 μm for large image, 5 μm for inserts.

foci that appeared and disappeared over the time courses was measured as 33.5 ± 19.0 s, demonstrating a high degree of variability in persistence (40 foci measured in 4 cells).

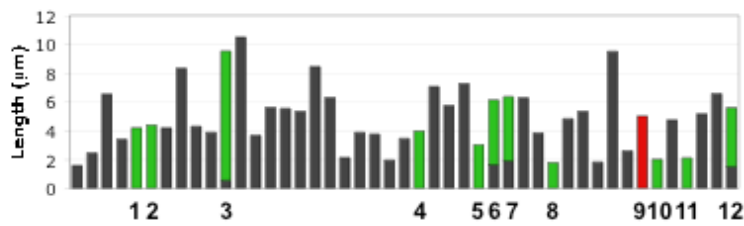
In order to aid the understanding of the nature of the IMD-rich protrusions, the dynamics of protrusions that were fully visible were quantified. IMD protrusion lengths at the start and end of time-lapse experiments (300 s) were measured to detect extension or retraction (Figure 4.5, Figure 4.6). Only a small proportion (mean 11.7 ± 3.3 %, $n=8$ cells) of protrusions observed in most cells showed extension or retraction during imaging. In protrusions that did extend, the mean rate of extension observed was 0.9 ± 0.7 $\mu\text{m}/\text{minute}$ (60 protrusions in 8 cells). The distribution of extending protrusions was analysed by plotting the lengths of protrusions in order of the distribution around the cell periphery (Figure 4.5 B i), and a random distribution was observed. When these data are reordered according to initial protrusion length, protrusion extension is revealed to occur predominantly in shorter existing protrusions and also in *de novo* protrusion formation where no existing protrusion was detected (Figure 4.5 (B ii); Figure 4.6). Retraction of protrusions was only rarely observed (mean 0.75 ± 1.58 % of protrusions, $n=8$ cells).

Next, TIRF microscopy was used to investigate the effect of cytD on IMD-induced protrusions (Figure 4.7). The untreated cell has a large number of IMD rich protrusions, the majority of which appear to be neither extending nor retracting, as opposed to the early extremely dynamic protrusions seen in Figure 4.4. Tips of 18 extending protrusions in 2 cells were measured before and after treatment with 5 μM cytD. Many of these protrusions extend during the course of the images being taken, at a rate of up to 4 μm per minute. Following treatment of the cells with 5 μM cytD protrusion of these structures stopped, and some projections shortened in length (Figure 4.7). Data in graphs represent the mean extension of protrusive structures averaged over 3 cells. Even after addition of 40 μM cytD IMD rich protrusions still remained (Figure 4.8).

A



B i



ii

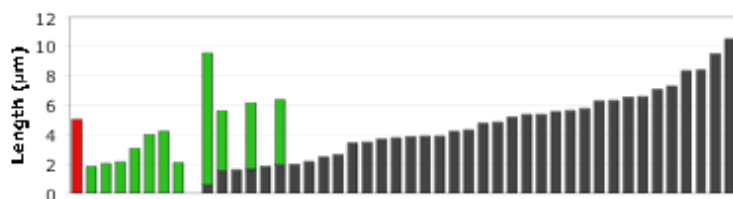


Figure 4.5 Quantification of IMD induced protrusions in TIRF microscopy. (A) IMD-GFP expressing cells were imaged by TIRF microscopy to quantify extending, receding and static protrusions, imaging time, 300 s. In the merged image protrusions that extended are shown in green, shown by arrow heads. Protrusions that showed decrease in length seen in red, shown by arrows. (B) Protrusions were measured, and are shown in the chart in the order they occur around the cell, showing that protrusion length and dynamics are evenly distributed around the cell (i). Black, unchanging portion; green, extension; red, shortening of protrusion. (ii) Data from above arranged in order of increasing initial length of protrusion. Extension occurs preferentially in shorter and undetectable protrusions. Scale bar, 20 μm

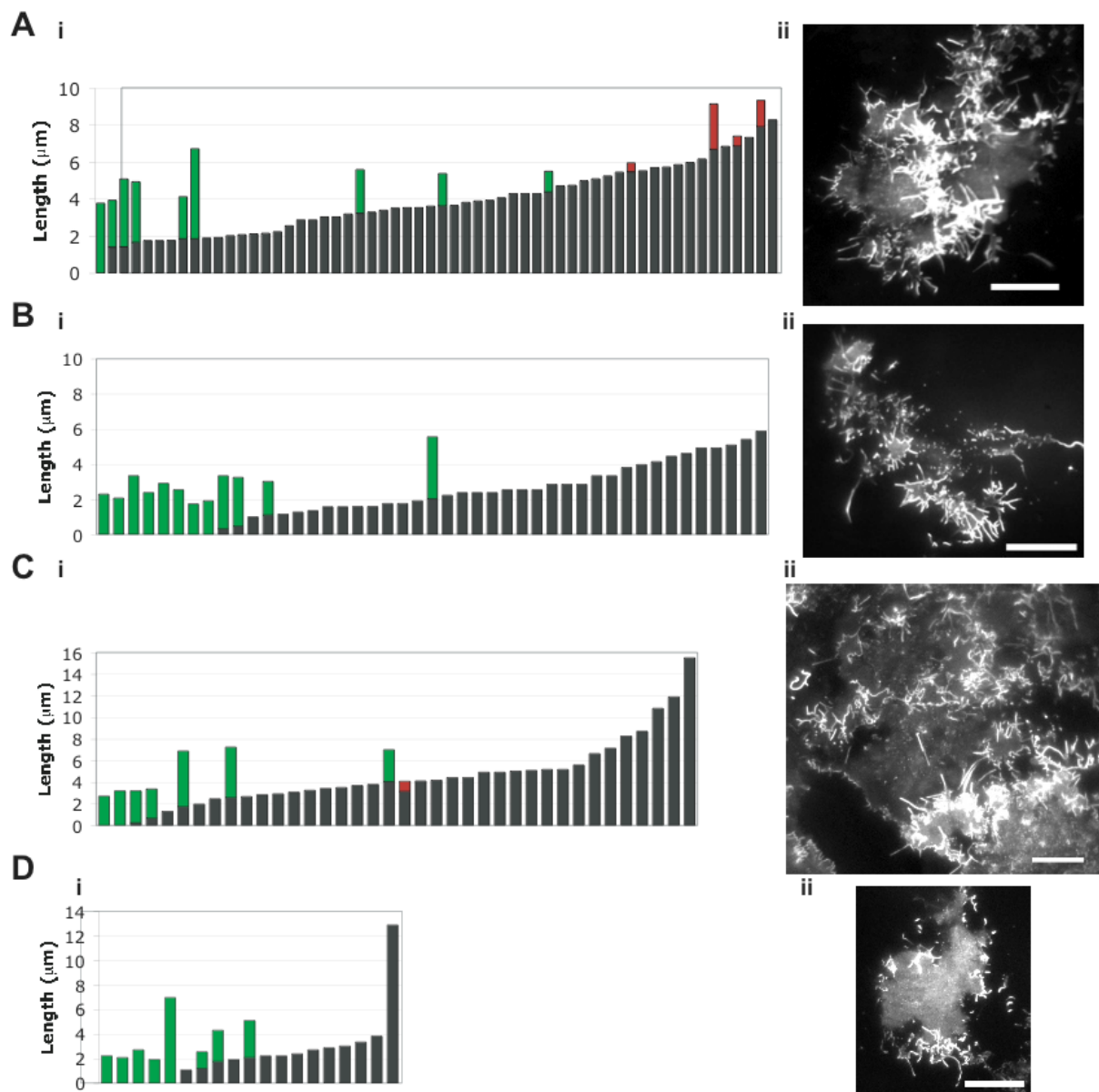
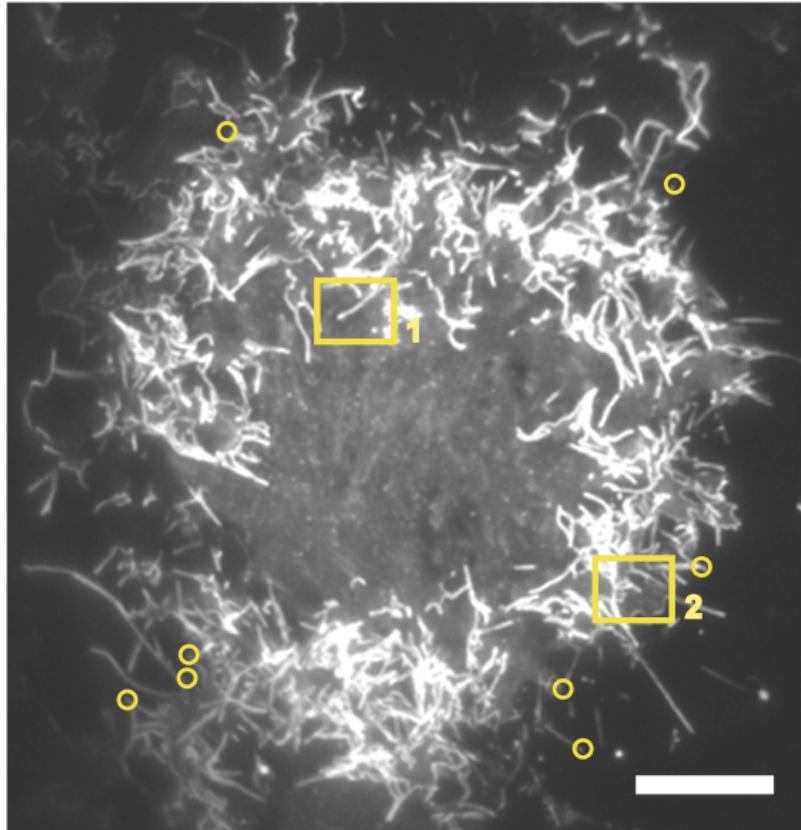
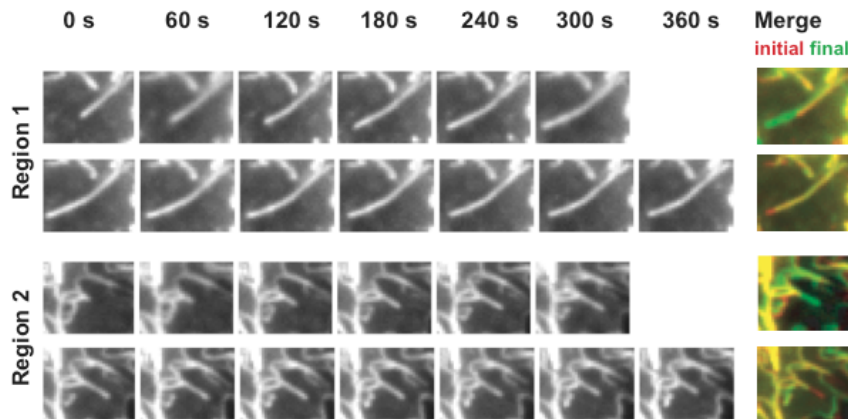


Figure 4.6 IMD-induced protrusion extension occurs preferentially in shorter protrusions, or *de novo*. Protrusion length and change over 300 seconds were measured and the data arranged in order of ascending initial protrusion length. All sufficiently visible protrusions were measured. Scale bars, 20 μm Grey bars represent length of protrusions that does not vary during the time course, green shows amount of protrusion after 300 seconds, red shows retraction observed. A-D show results from different cells, showing that this pattern is consistently observed.

A



B



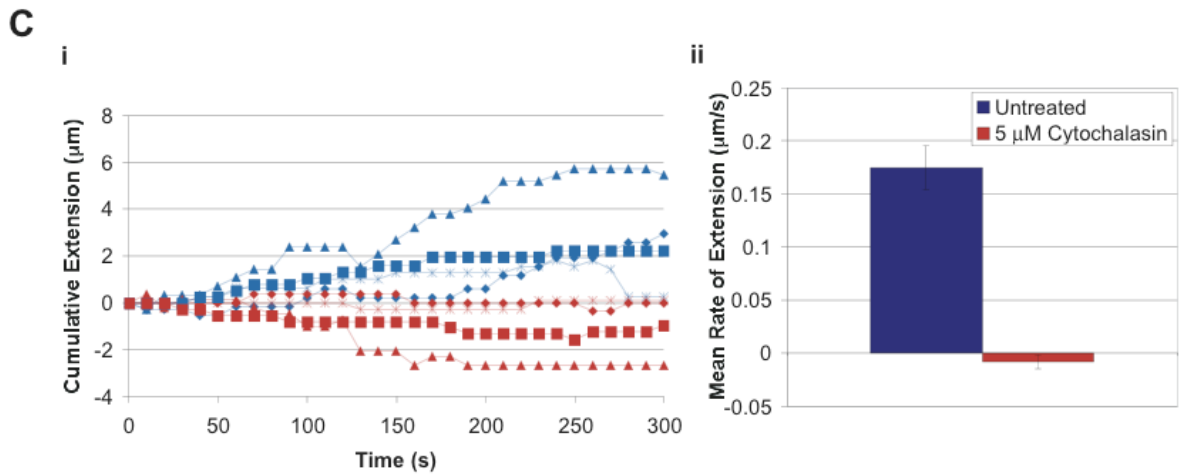


Figure 4.7 Use of TIRF microscopy to observe the effect of cytD on cells expressing IMD-GFP. (A) The whole cell at the outset of the experiment. Cells were imaged for at least 300 s prior to treatment, and 300 s post treatment (B) Montages showing two different regions of the cell before and after treatment with cytD. Protrusions extend prior to treatment, and shorten after exposure to cytD. (C) chart showing extension and retraction of tips of protrusions. (i) Representative protrusions are shown as blue (untreated) and red (after treatment with 5 μ M cytD). (ii) Mean extension of all extending filopodia before and after treatment with cytD, (N=18 protrusions in 2 cells).

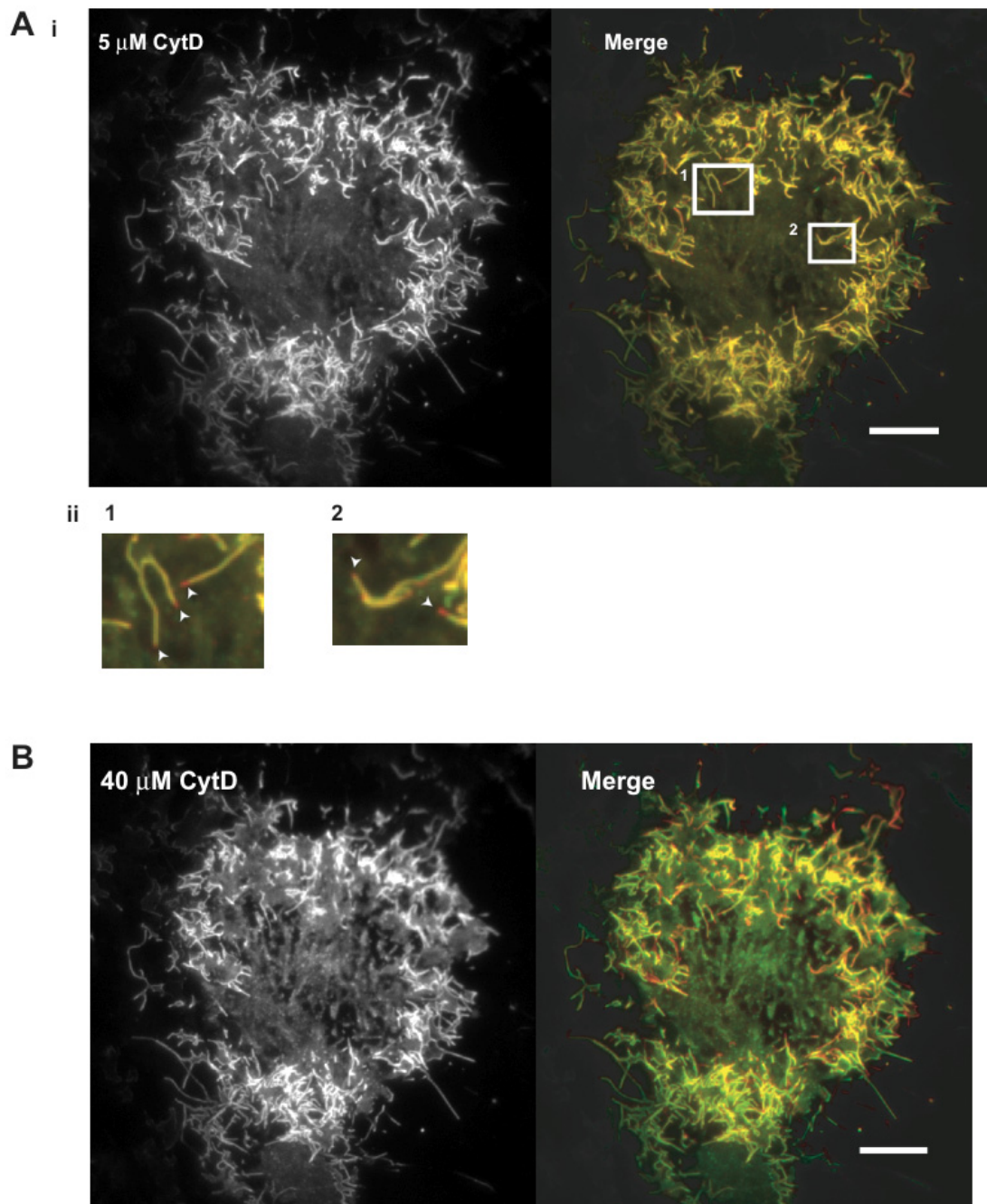


Figure 4.8 Effect of cytD on IMD-GFP protrusions. (A) (i) Cell after 450 s incubation with 5 μ M cytD, merge shows pre incubation in red, final frame in green, and slight retraction is shown as red marks (ii). (B) Cell after half hour incubation with cytD (40 μ M). Scale bar, 20 μ m.

4.5 IMD overexpression phenotype varies with the level and duration of IMD expression

The degree of variation in the severity of phenotypes was shown by cells expressing IMD–GFP may be accounted for by variable expression levels. However, cells expressing the construct for a longer period of time show a more severe phenotype. With increased levels of IMD and time more and more of the cell becomes taken up by tubulated structures. Expression levels vary from cell to cell, and are not totally dependent on time transfected. A representative cell that had been overexpressing IMD-GFP for 48 hours is shown in Figure 4.9. The cell body is mostly eliminated, as most of the membrane is taken up by protrusion formation.

4.6 Discussion

The role of actin in IRSp53 induced filopod formation remains unclear. IRSp53 involvement in filopodia formation was first discovered in (Krugmann et al., 2001). Many proteins are now known to have direct interactions with IRSp53, including several proteins known to be involved in filopodia formation N-WASP, Eps8, Mena, mDia2; and Cdc42; the global regulator for filopodia (Fujiwara et al., 2000; Krugmann et al., 2001; Nakagawa et al., 2003; Lim et al., 2008). Initially the role of IRSp53 in filopodia was thought to be to coordinate some or all of these factors. However, the discovery that the IMD is able to generate filopodia-like protrusions independently of these proteins suggests that the IMD is able to induce protrusions directly (Yamagishi et al., 2004). As the IMD was found to bind and bundle actin *in vitro*, and mutations abrogating this actin binding also prevented protrusion formation *in vivo*, it was proposed that IMD was able to bundle actin in cells leading to filopodia formation (Yamagishi et al., 2004; Millard et al., 2005). More recently, IMD has been found to bind to and deform phospholipid membranes, in the absence of actin (Yamagishi et al., 2004; Millard et al., 2005; Suetsugu et al., 2006a; Suetsugu et al., 2006b; Mattila et al., 2007; Saarikangas et al., 2009). The actin bundling property of the IMD has also been called into question (Mattila et al., 2007), as the conditions used in the *in vitro*

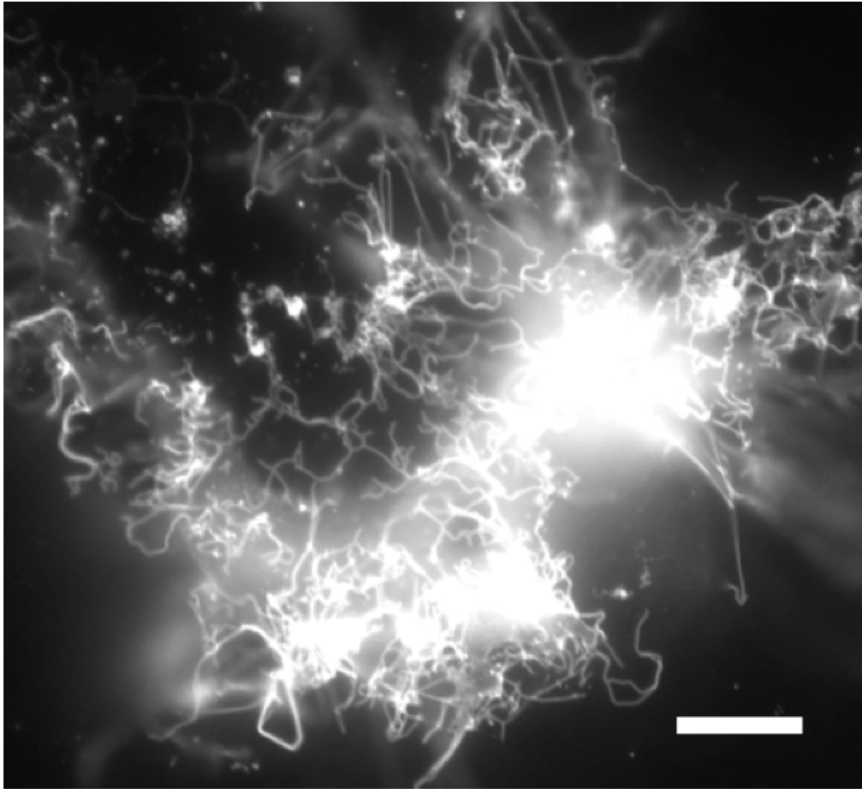


Figure 4.9 Long term IMD expression leads to an extremely severe phenotype. Extended overexpression of IMD leads to severe tubulation of the cell, with very little of the cell body remaining. Protrusions are difficult to measure but appear to be very long. This image was captured using epifluorescence microscopy. Scale, 20 μm

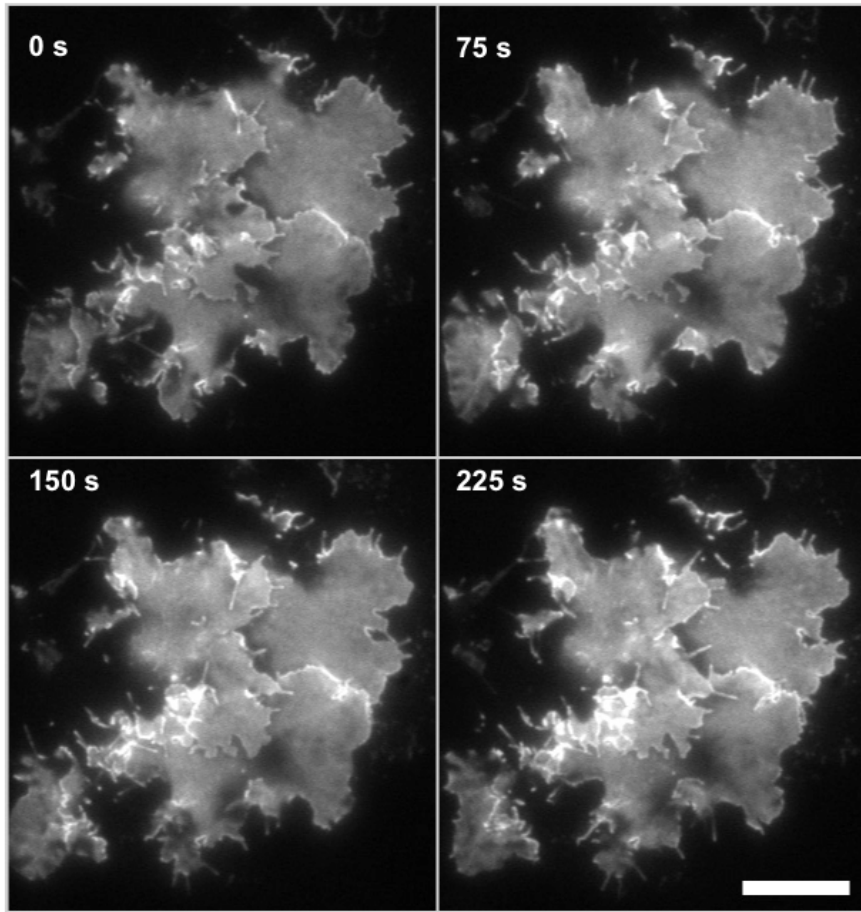


Figure 4.10 Cell expressing IRSp53-GFP and imaged using TIRF microscopy. IRSp53 protrusions were less persistent than IMD. In contrast to IMD expressing cells, much more fluorescence signal is observed in the body of the cell. Scale bar, 20 μm .

measurements may cause aggregation of the IMD, although this is the subject of some doubt. A recent study however, has reopened the debate on the role of actin in IMD induced filopodia-like protrusions, using EM to determine the presence of actin within these structures (Yang et al., 2009).

Here, data presented show that cytD disrupts nascent protrusions and prevents protrusion elongation, but does not cause collapse of most IMD containing protrusions. Data from TIRF microscopy experiments are also shown, which may help to improve our understanding of the way in which these protrusions are formed.

Having demonstrated that the IMD-GFP construct induces the expected IMD phenotype with many finger like protrusions around the cell edge (**Figure 4.1**), TIRF microscopy was used to image the ventral surface of the cell (Figure 4.4, Figure 4.5). Because TIRF microscopy allows imaging of only the 100 nm slice adjacent to the coverslip, it presents a strikingly different view of the cell from conventional epifluorescence or confocal microscopy. It particularly allows imaging of structures that are directly under the cell body and that would normally have a high level of background fluorescence from cytosolic GFP. In cells expressing GFP only there is detectable fluorescence signal visible on the whole bottom surface of the cell (Figure 4.4). This indicates that the body of the cell and some of the cytosol are sufficiently close to the coverslip to be imaged by TIRF (100 nm). When IMD-GFP was expressed, even at high levels, very little diffuse signal was observed in the central region of the cell (Figure 4.4, Figure 4.5, Figure 4.7). Overexpressed IRSp53-GFP showed a higher level of GFP staining in the central regions of the cell more reminiscent of GFP alone than IMD GFP (Figure 4.10). In cells transfected with IRSp53-GFP there appeared to be fewer protrusions than with IMD alone, and when protrusions were formed they did not appear to become increasingly pronounced, as was the case for IMD-GFP induced protrusions. The low levels of IMD-GFP in the cytosol suggest that very little IMD is free, and perhaps is all associated with the membrane at sites of protrusions. Curved regions at the edge of the cell may provide more favourable binding than the centre, and the IMD-rich edges of broad protrusions seen in Figure 4.4 suggest that a large amount of IMD does bind in these regions. Another possibility is that the cell body is pushed away from the coverslip by this protrusive action, thereby removing the cell body from the illuminated region. In contrast,

there may be a higher proportion of IRSp53 in the cytoplasm, perhaps because in the context of the full-length protein the IMD is unable to bind membranes and requires another component to activate it. This may explain why IRSp53 expression appears to induce a less severe phenotype than the IMD in these experiments. Another characteristic of IRSp53 induced protrusions is that they appear to be straighter and more rigid than IMD induced protrusions. This could be due to full-length IRSp53 being capable of binding to other proteins involved in filopodia formation and actin bundling such as the interaction with Eps8 via the SH3 domain, leading to protrusions that are more actin rich (Disanza et al., 2006). However, as these experiments have focussed primarily on IMD, more studies of IRSp53 are required in order to determine the differences between full length IRSp53 and IMD alone.

The IMD-GFP foci that displayed rapid movement and (Figure 4.4 C) were observed in IMD-GFP cells. The nature of these foci is not clear, and has not been reported for IMD before, although they are of a similar appearance to that of endocytosis components observed by TIRF (Rappoport et al., 2004). Similar foci have been observed in *Dictyostelium* when overexpressing IRSp53-GFP. It can be speculated that these foci represent localised areas of IMD binding, and are precursors to protrusion formation. Closer study of these foci using a more rapid capture time would add to our understanding of the activity of the IMD prior to formation of protrusions. With longer time period movies the moment of initial protrusion and the initial steps could be elucidated. In contrast to endocytosis, where endocytic events are marked by disappearance of the complex from the TIRF field, IMD causes outward protrusion of the membrane, and so any such activity is more easily detected. This suggests that TIRF could be a useful tool in improving our understanding of the initiation of IMD induced protrusions.

Cytochalasin D inhibits actin polymerization by binding to the barbed end of filaments with 1:1 stoichiometry (Sampath and Pollard, 1991). Over time this can lead to filament disassembly due to hydrolysis of ATP to ADP actin. As such it has been used in various studies to prevent filament polymerization and also to disrupt filaments. Here, cytD was used at high concentration to attempt to cause large-scale actin filament depolymerization in order to observe the effect on IMD induced protrusions. Concentrations of 5–40 μM were used, which have been shown to cause rounding up of cells, presumably due to actin

depolymerization. Some rounding up was seen in cells imaged by epifluorescence, and small protrusions were lost although larger protrusions still persisted (Figure 4.3). Retraction of the cell body was also observed, which also suggests that actin cytoskeleton depolymerization occurs, or there may be a phototoxic effect observed with the higher light intensity used in epifluorescence. When cells were observed by TIRF, such large scale effects on the cell body were not seen, even at 40 μM cytD, and for long duration (Figure 4.8). This may be due in large part to the fact that the cell body is not visible using TIRF, as discussed above. As discussed above, a subset (approximately 11 %) of protrusions per cell appear to grow at any given time. All such protrusions were prevented from growing by addition of cytD, immediately after its addition. Indeed, as shown in Figure 4.8 (A), many protrusions showed a small reduction in size after cytD treatment. However, there was no large-scale loss of IMD rich protrusions. These data suggest that protrusion formation and elongation require actin polymerization, whereas established protrusions are largely unaffected by disruption of the actin cytoskeleton. The effect could also be an indirect one, with a relaxation of the cytoskeleton leading to a reduction of outward pressure exerted on the cell membrane.

Electron microscopy imaging has shown that IMD can induce protrusions spontaneously when incubated with phospholipid membranes in the absence of F-actin (Suetsugu et al., 2006a; Suetsugu et al., 2006b; Mattila et al., 2007), with the latter finding that Rac is also required. However, with the exception of the latter study, which uses a truncated IMD domain, the consensus is that actin polymerization is required for this activity in cells. Work done by Mattila et al, 2007 showed that latB (at 0.5 μM) reduces the number of extending protrusions in cells, and Yang et al, 2009 found that latB at higher concentrations (2 μM) caused cells to round up entirely. Data presented here support the findings from Mattila et al (2007) in that disruption of cytoskeleton dynamics stopped protrusion extension. However even after incubation with 40 μM cytD (Figure 4.8), the cells are not totally rounded and most IMD rich protrusions are still visible. The differences observed could therefore be due to the different modes of action of cytD and latB, and this should be further investigated. The finding that actin is required for maintenance of IMD protrusions is partly contradicted by other data presented in the study by Yang et al, 2009. They observed that actin filaments sometimes withdraw from protrusions, which do not collapse, and also that a small proportion of IMD containing protrusions do not contain actin. latB at high concentrations may therefore

change other conditions within the cell resulting in rounding up. Presence of polymerized actin in protrusions was not examined in the experiments reported here, and this would aid in the interpretation of the data. However, taking into account the marked effect on the protrusions observed after addition of cytD, and such high levels of cytD were tested that it was assumed that actin filament disruption was occurring. The small reduction in length observed in many protrusions in response to cytD may be accounted for by a reduction in pressure applied by actin filaments at the tips as polymerization is halted, causing a small amount of elastic retraction of the membrane. Retraction of this sort was seen in protrusions that were not actively extending prior to treatment with cytD, which suggests that many protrusions may be under tension from actin filaments.

There are a number of questions raised by these studies which warrant further investigation before a conclusion can be drawn. In many of the movies analyzed, measurement of all protrusions was not possible due to a large degree of overlapping being present. Future studies should make more efforts to analyze cells with lower expression levels, and also optimise the length of time between transfection and imaging. This would especially facilitate observation of new protrusion formation, as this was often occluded by other existing protrusions. Longer imaging times would be able to add much to the understanding of the process of IMD induced protrusion, and it would be extremely instructive to image cells from before their first protrusions are seen. Preliminary experiments were done into this, and GFP expression was first detected approximately 6 hours post transfection. As mentioned above, it would be desirable to verify actin depolymerization by fixing cells and staining with labelled phalloidin. This could be in combination with use of a range of concentrations of cytD, and more careful analysis to observe the effects on the actin cytoskeleton to more closely observe the effects.

TIRF microscopy has proven to be a useful tool in the study of IMD induced protrusions, and further studies with this technique could prove fruitful. Especially intriguing is the apparent difference between IMD-GFP and IRSp53-GFP as observed using TIRF.

4.7 Conclusions and future perspectives

Here it was demonstrated that actin destabilising drug cytochalasin D (cytD) disrupts formation and extension of membrane protrusions, but does not affect existing ones. TIRF imaging of IMD-GFP and IRSp53-GFP is shown, and this has not been previously shown for these constructs. This provided a novel view of the phenotypes of overexpression of these proteins, and has revealed some potentially interesting new phenomena, such as the presence of IMD rich foci. The effects of actin destabilization may suggest a mechanism for IMD protrusion formation similar to that shown in Figure 4.11, whereby the protrusion is stabilised by IMD binding, possibly enabling the maintenance of the protrusion in the absence of filamentous actin.

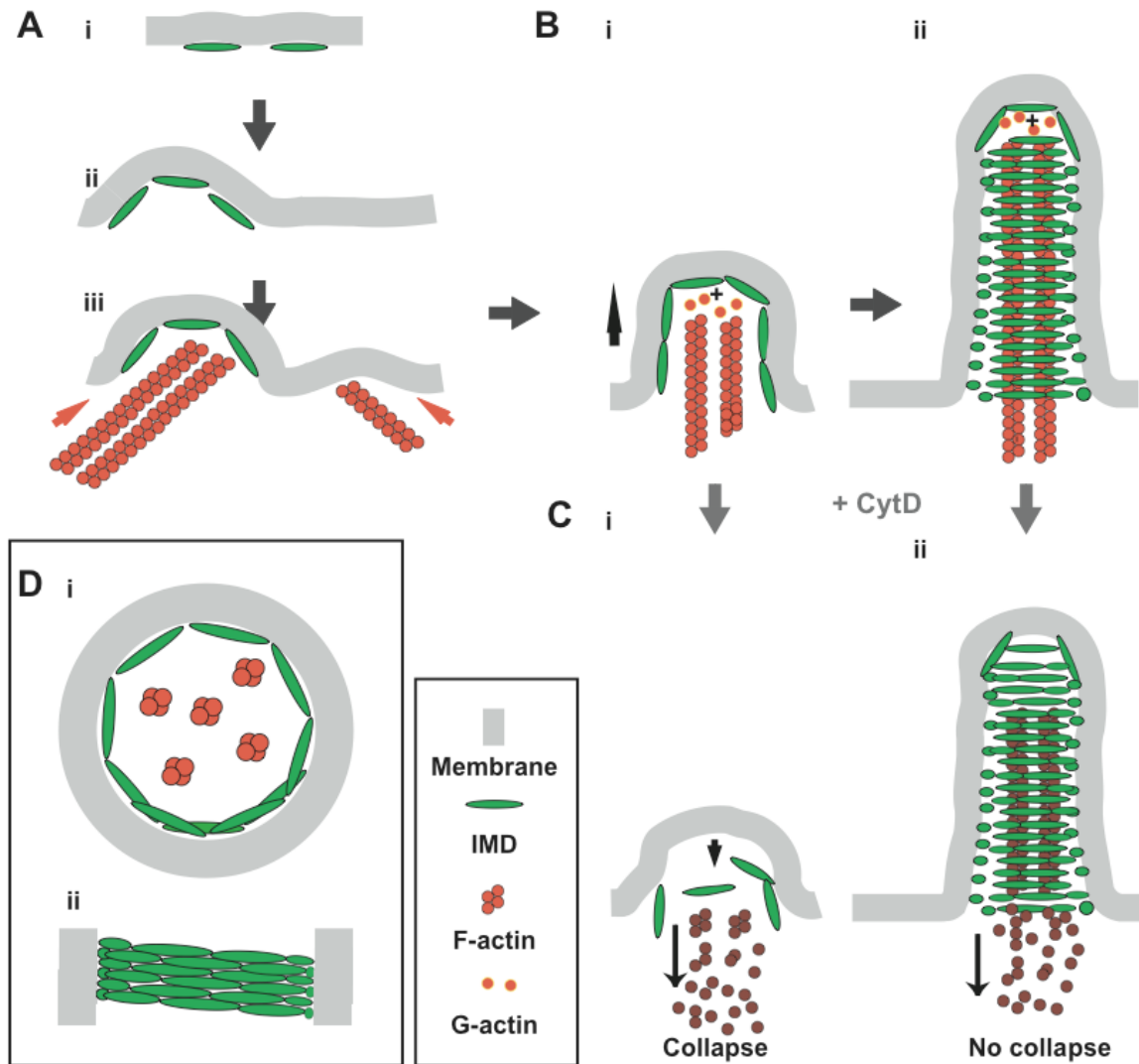


Figure 4.11 Cartoon of proposed mechanism for protrusion induction by IMD, and effect of cytD on protrusions at different stages. (A) Possible initiation steps. (i) IMD binds to the membrane, possibly leading to small local deformation but do not overcome threshold energy required for large scale curvature. (ii) A sufficient local concentration of IMD or other factors initiates more substantial curvature. (iii) Sufficiently curved membrane may be sufficient to ‘capture’ actin filaments. (B) Protrusion formation proceeds, with IMD binding to the membrane during actin based protrusion. (C) (i) Disruption of actin nascent protrusions with little IMD bound may result in collapse. (ii) More established protrusions with IMD stabilisation are able to persist in the absence of actin. (D) Proposed configuration of IMD binding to the inside edge of a protrusion.

5 Fluorescence Recovery after photobleaching studies of IMD rich protrusions.

In order to investigate the role of IMD in membrane protrusions, fluorescence recovery after photobleaching (FRAP) was used. FRAP makes use of a high intensity laser to bleach fluorophores in a specific region of the cell. Recovery of bleached fluorophores from adjacent regions diffuse into the bleached area, and hence the recovery provides information about the time scale of diffusion in specific areas of the cell. A cartoon of the principle of FRAP is shown in Figure 5.1. The rate of recovery (as denoted by the $t_{1/2}$ or half time) gives information about the rate of turnover of the protein attached to the fluorophore. The level of recovery relative to initial fluorescence informs us if there is an immobile fraction of the fluorophore, which is unable to diffuse away after bleaching.

5.1 FRAP analysis of IMD - rich protrusions.

FRAP experiments were carried out on IMD-GFP rich cellular protrusions (Figure 5.2 A), as described in Materials and Methods. It was hypothesized that if IMD forms stable structures in tubules, then there should be a high immobile fraction of IMD in tubules as observed by FRAP. Fluorescence recovery for IMD-GFP followed a characteristic FRAP exponential recovery curve, with an average $t_{1/2}$ of 7.3 ± 3.8 seconds (N=12). Interestingly, mean fluorescence recovery was to an average of 37.5 ± 8.1 % (N=12), suggesting that there is an immobile fraction of around 55-70 %. The mobility of the IMD-GFP in protrusions and in the main body of the cell were compared. Where the majority of the signal is expected to be from IMD-GFP located in the cytoplasm or on the plasma membrane and would be expected to diffuse unimpeded (Figure 5.2 B). IMD-GFP in this region of the cell recovers very rapidly, and has a very different FRAP profile to that observed in protrusions. Due to the extremely rapid recovery of fluorescence, it appears that much of the recovery occurs before the cell is imaged. This rapid exchange prevented accurate modelling of the data and would require further study with a faster rate of image acquisition. However as the $t_{1/2}$ was always below 1 s, and recovery is to approximately 100 %, this suggests that IMD-GFP located in the cytosol/plasma membrane can rapidly diffuse.

Next, it was important to verify that the reduced FRAP recovery time seen in the protrusions is due to IMD-GFP interactions with the protrusion, and not simply due to restricted diffusion as a result of the limited space available. Cells were transfected with an IMD-myc construct

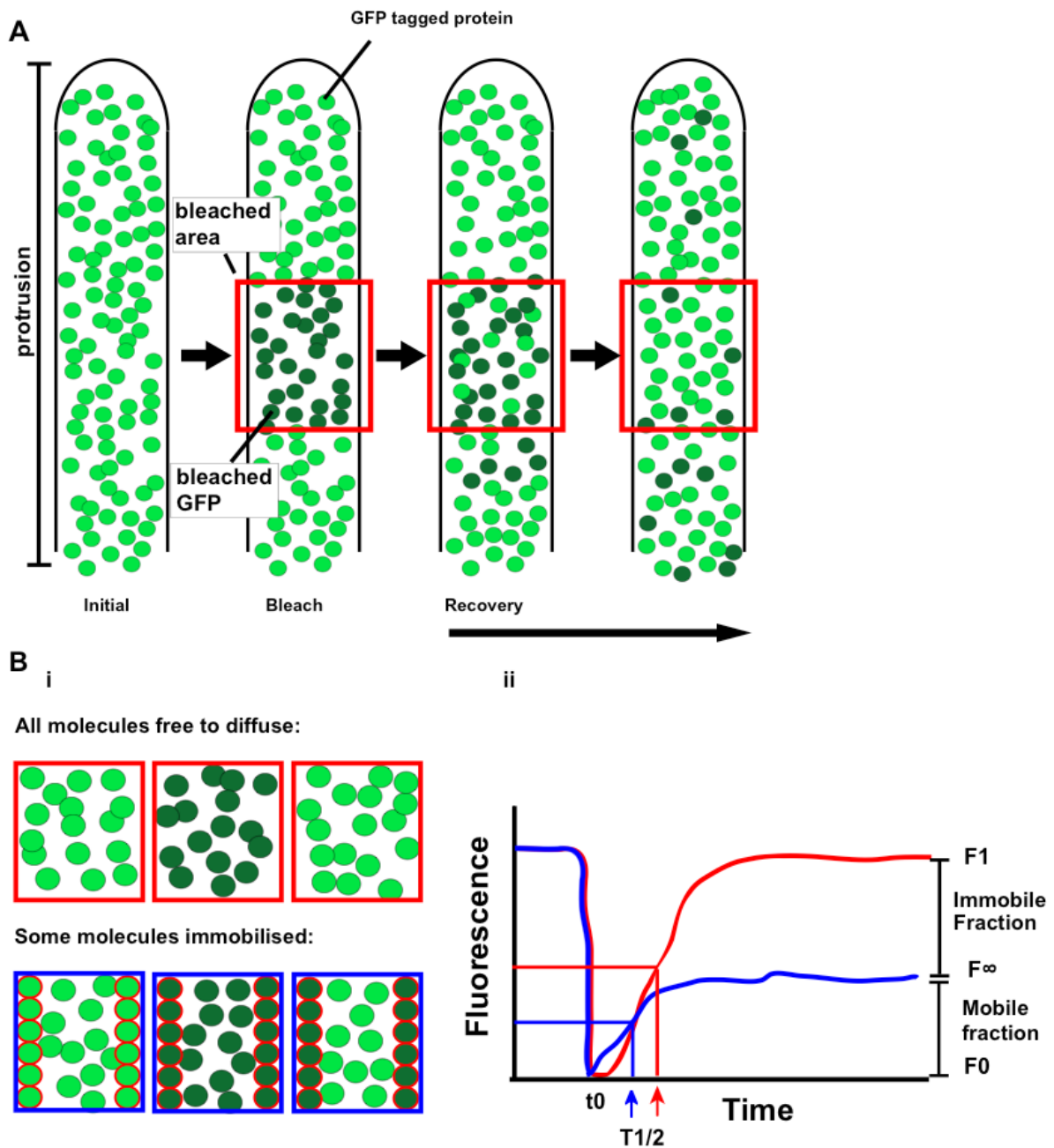


Figure 5.1 Cartoon showing how FRAP was used in the study of IMD dynamics. (A) A protrusion with fluorophore tagged IMD is selected, and a region is bleached using 405 nm laser. The area is imaged before and directly after bleaching to monitor the recovery of fluorescence. (B) (i) Two possible scenarios that can occur after bleaching. If all molecules are free to diffuse, then over time fluorescence recovers to 100 % of initial (red boxes, red trace on graph). If some bleached molecules are unable to diffuse away (blue boxes, blue trace), they form the immobile fraction (outlined in red). This means that recovery is reduced, and the proportion of immobile molecules can be estimated. (ii) Representation of FRAP curve showing $t_{1/2}$, and immobile fraction (see text).

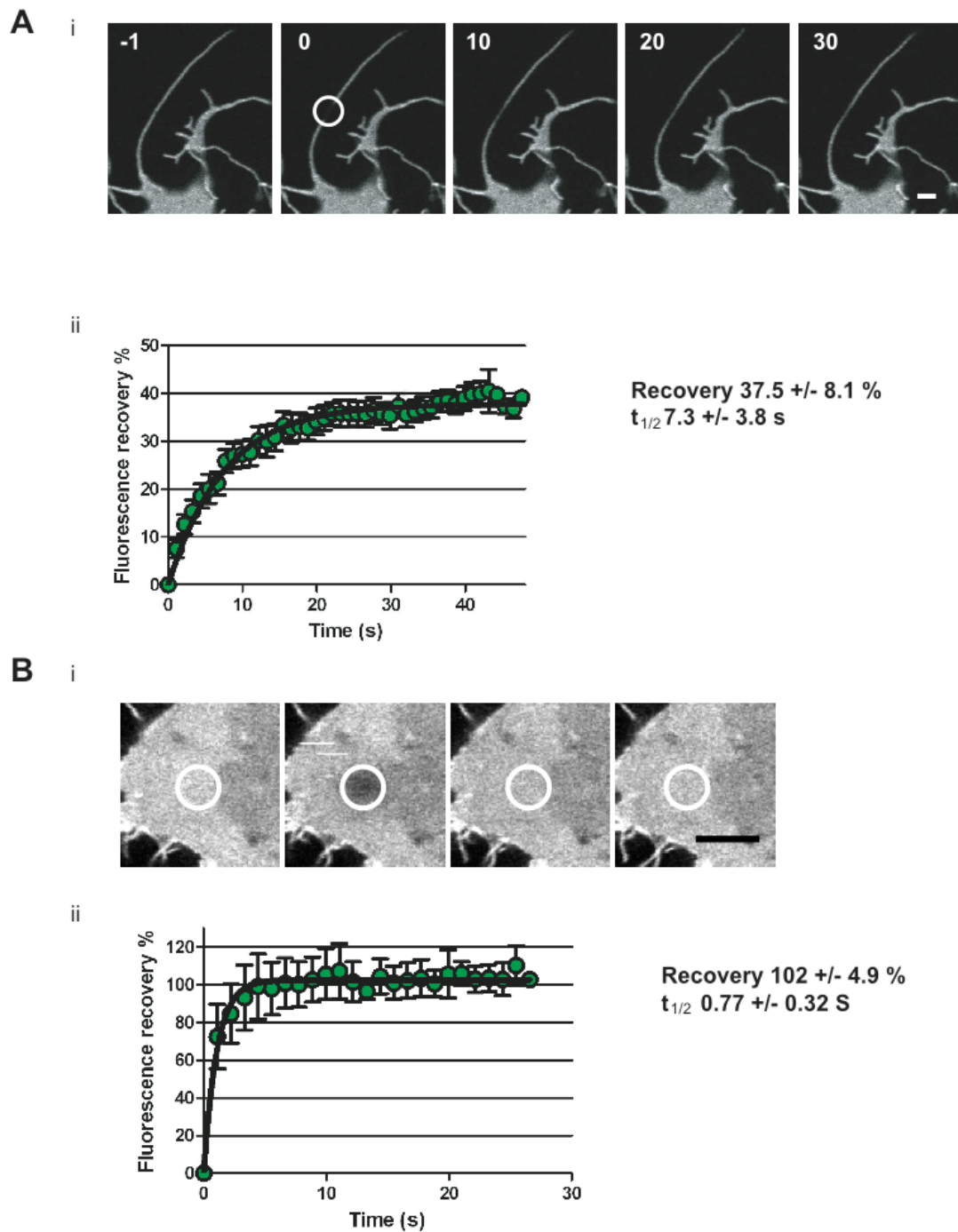
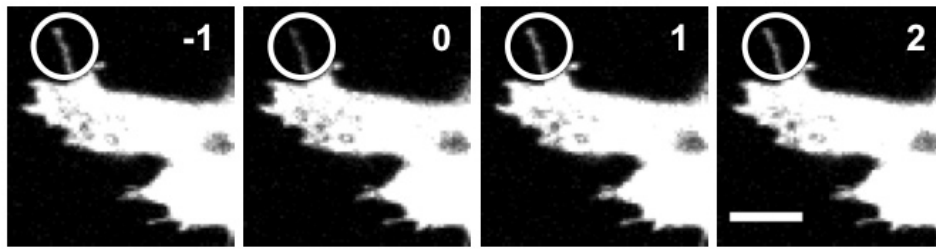


Figure 5.2 FRAP of IMD-GFP induced protrusions. (A) (i) FRAP experiments on IMD GFP protrusions, white circle denotes bleach region. (ii) Mean FRAP data, N=12. Mean recovery and $t_{1/2}$ from individual curve fits. (B) FRAP experiment (ii), and chart (ii) of IMD-GFP located in the cytoplasm, showing rapid recovery of fluorescence signal (N=2). Scale bars, $2 \mu\text{m}$ (A) and $5 \mu\text{m}$ (B). Error bars represent standard deviation.

A i



ii



B

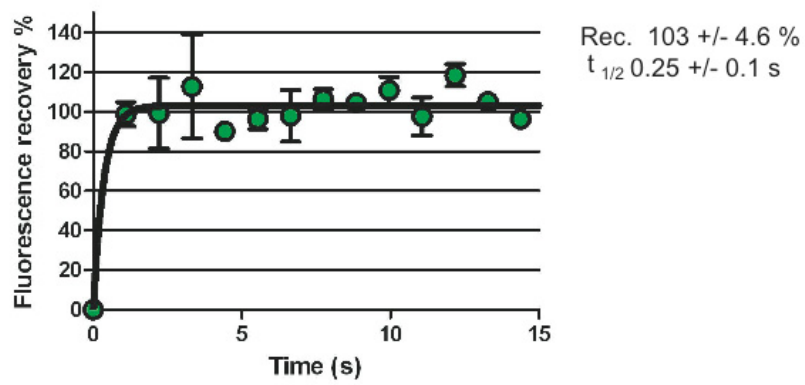


Figure 5.3 FRAP experiments carried out in cells expressing IMD-myc and GFP. (A) FRAP experiment in a protrusion. (B) Mean recovery chart of GFP in thin projection, N=2. Scale bar, 5 μ m

containing no fluorophore, to generate protrusions; and GFP. GFP in isolation is not expected to interact with other molecular components in the protrusion, so would be able to diffuse freely, unless space restriction hindered its movement rate or proportion of recovery would be limited by the dimensions of the protrusion. GFP recovered rapidly when bleached in a protrusion, and recovered to 100 % of its initial fluorescence (Figure 5.3). This suggested that the dimensions of the protrusions do not significantly impede recovery of cytoplasmic molecules, and that the FRAP results of IMD-GFP are due to its interactions with a component of the protrusions.

5.2 Cytochalasin D does not affect FRAP profile of IMD-GFP

Two conflicting mechanisms for IMD activity have been put forward, binding and deforming membranes; and bundling actin (Yamagishi et al., 2004; Mattila et al., 2007). In the previous chapter it was demonstrated that extension of IMD induced protrusions is prevented by cytD, suggesting that actin plays an important role in this process. It was decided to carry out preliminary experiments to determine whether cytD would affect the dynamics of IMD-GFP as measured by FRAP. Cells were treated with 5 μ M cytD for 30 minutes to prevent actin polymerization. Some rounding up and retraction of the cells was observed, although, as seen in experiments in Chapter 3, many IMD-rich protrusions remained. When these cells were used in FRAP experiments, untreated cells had a mean recovery of 52.8 \pm 9.4 % and a $t_{1/2}$ of 7.7 \pm 4.7 s, whereas cells treated with cytD showed a mean recovery of 47.7 \pm 7.0 % and $t_{1/2}$ of 3.7 \pm 1.6 s. These differences are not significantly different (t test, $p > 0.1$) and further experiments with a larger number of replicates will be required to determine whether cytD affects IMD recovery (Figure 5.4 B).

5.3 Cloning of constructs required for further FRAP experiments

To follow up the previous experiments further constructs were generated (Chapter 3). To more properly test the FRAP characteristics of GFP alone, a different coloured IMD tag was required, in order to measure FRAP of different molecules simultaneously to allow direct comparison of FRAP profiles. The IMD-mCherry construct was used for this. To exclude the possibility that GFP alone and IMD-GFP behave differently due to the size difference, a construct with a mutated form of the IMD that does not induce protrusions, IMD K4E was used. This mutant has four key lysine residues mutated to glutamic acid, and does not induce

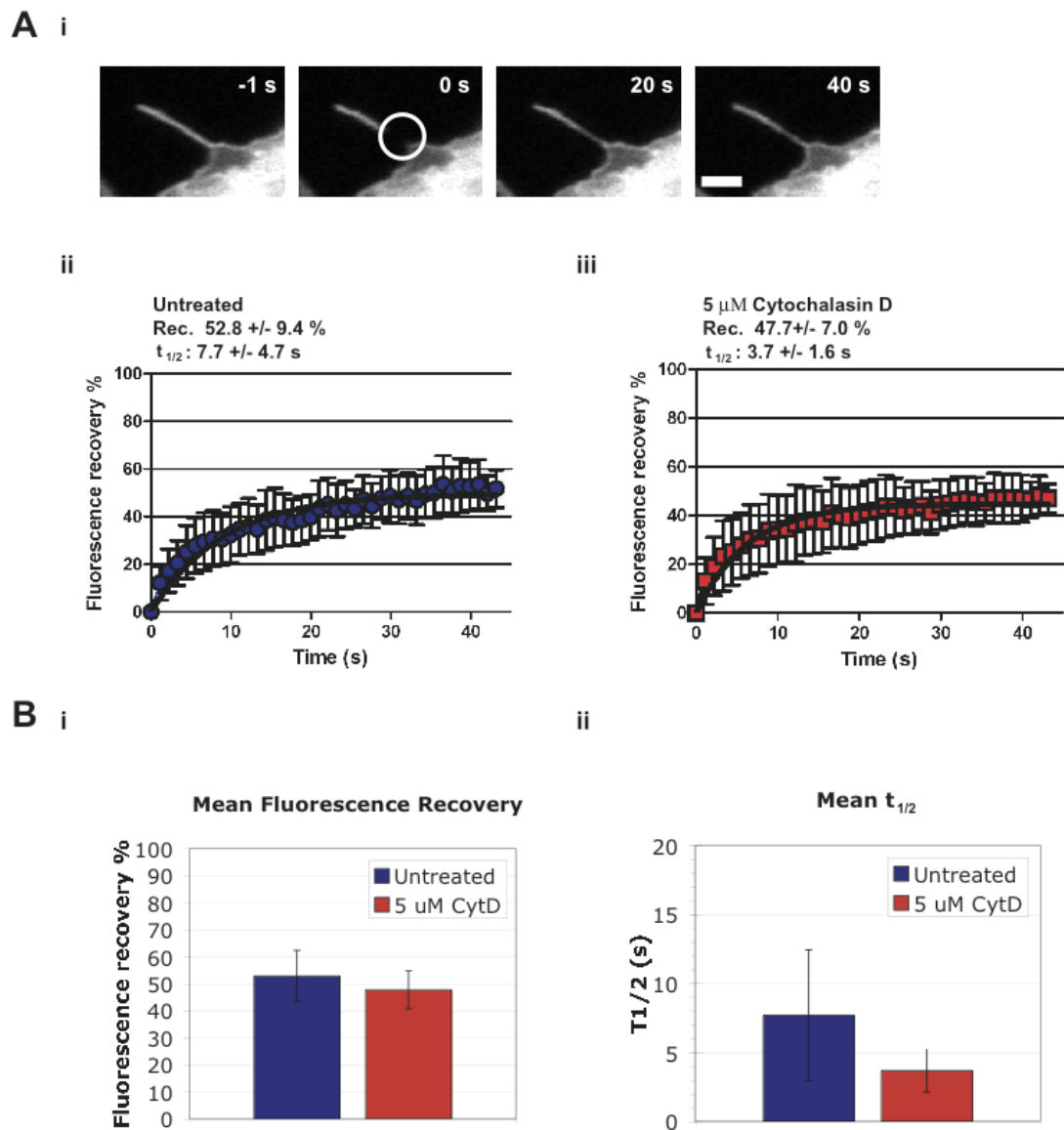


Figure 5.4 Treatment of IMD induced protrusions with cytD does not significantly affect FRAP recovery. (A) FRAP experiment of cell after treatment with 5 μ M cytD – movie (i) and chart (ii). Scale bar, 2 μ m. (B) (i) Recovery time shows no significant effect of cytD on IMD recovery. (ii) Rate of recovery is not significantly different between treated and untreated cells (t-test, $P > 0.1$). $N=5$ protrusions for each condition, all carried out on the same day, error bars represent standard deviation.

protrusions *in vivo* or bundle actin *in vitro* (Millard et al, 2005). Constructs were made by PCR and cloned as described in Chapter 3. When expressed in cells, IMD mCherry was found to have a poorer signal and to undergo rapid bleaching. Most cells showed a less strong IMD expression phenotype, although this was not quantified. Some cells did present the more expected protrusions however, and these showed a FRAP recovery profile similar to IMD-GFP of approx 40-60 %. However, FRAP of shorter protrusions resulted in a recovery to approximately 75 %, indicating that there was still a proportion of 25 % which is immobile.

5.4 Dual fluorophore FRAP – preliminary data

5.4.1 IMD-mCherry and GFP

Earlier experiments showed that GFP diffuses rapidly into thin protrusions, when coexpressed with IMD-myc, with no immobile fraction apparent, suggesting that IMD FRAP recovery is reduced due by its interaction with the membrane (Figure 5.1). Because FRAP recovery varies slightly between different protrusions, a direct comparison of fluorophore-tagged IMD and fluorophore alone in the same protrusion could reveal more about the differences between them. FRAP experiments were therefore done with IMD-Cherry and GFP alone (Figure 5.5). As described above, difficulties were encountered in finding bona fide IMD induced protrusions, and consequently IMD-mCherry showed greater recovery than was seen for IMD-GFP. However, IMD-mCherry was found to have an increased immobile fraction relative to GFP, suggesting that at least a proportion of the IMD still behaves as expected in this case. In all cases, GFP was found to recover at a faster rate than IMD-mCherry (0.6 sec as opposed to 2.6), however this is not statistically significant as analyzed by t test.

5.4.2 FRAP of IMD-mCherry and IMD K4E-GFP

When located in IMD-induced protrusions, GFP is able to recover rapidly and to 100 % of the initial fluorescence intensity, suggesting that the dimensions of the protrusions should provide no impedance to diffusion of molecules into them. However, GFP alone is 27 kDa (Prendergast and Mann, 1978), approximately half the size of IMD-GFP, and so it cannot be excluded that the larger size of the IMD limits its ability to recover into the bleached region. To test this, cells were transfected with IMD-mCherry and IMD K4E-GFP constructs. It was expected that

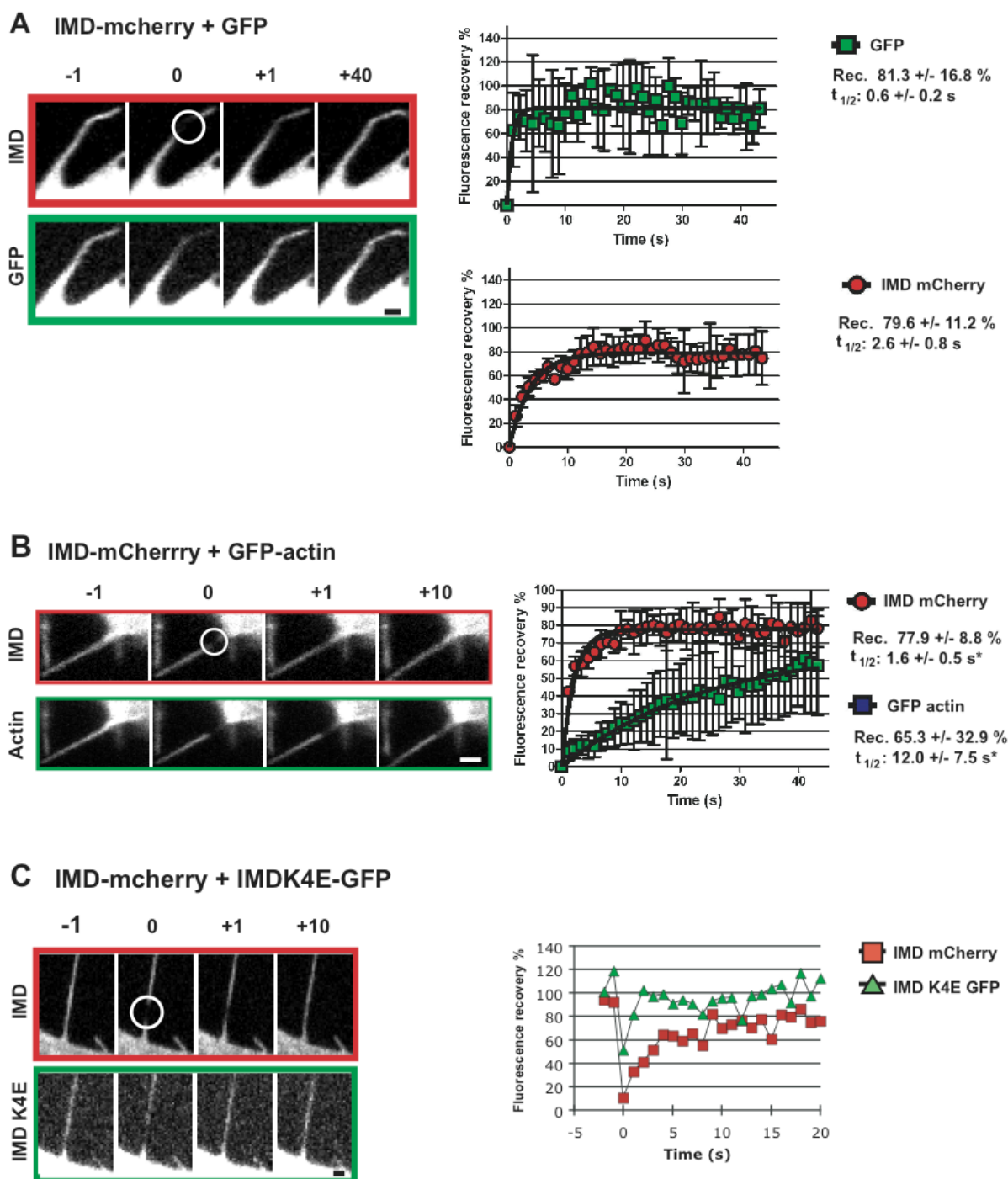


Figure 5.5 Comparative FRAP of IMD mCherry with GFP, IMD K4E mutant, and GFP-actin. (A) IMD mCherry showed slower recovery and larger immobile fraction than GFP alone. (B) Wild type IMD shows delayed recovery compared to IMD K4E where protrusions are observed. (C) IMD shows more rapid recovery than GFP-actin, although it was not possible to fit curves for these data.

IMD-mCherry protrusions would be formed and FRAP analysis of IMD K4E could be performed to detect its dynamics within them. As the mutant does not induce protrusions or bundle actin, it was hypothesized that it would have a similar FRAP profile to GFP. However, co expression of the two constructs resulted in very few cells with very few protrusions, and only one *bona fide* IMD rich protrusion was found. This is shown in Figure 5.5 (C). In this example, there is a clear difference between the recovery of the two components, with IMD-mCherry showing an immobile fraction of approximately 20 %, whilst the IMD K4E recovered extremely rapidly, and to greater than 100 % of initial – this may be attributable to noise in the signal.

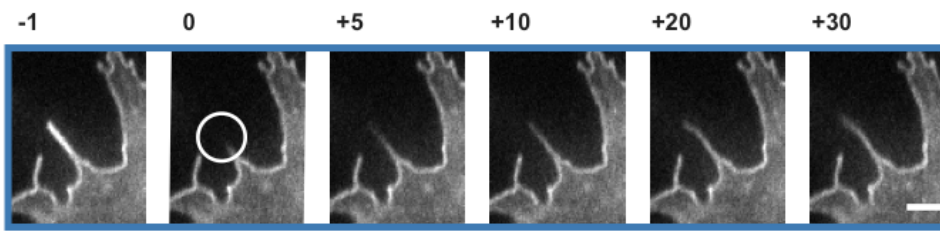
5.4.3 FRAP of IMD-mCherry and GFP-actin

To determine whether we could also study actin dynamics in IMD-induced protrusions, FRAP experiments were done using cells expressing GFP-actin and IMD-mCherry (Figure 5.5 C). Again, only very few protrusions resembling IMD-induced protrusions were detected. However, several experiments showed a different much slower recovery of GFP actin ($t_{1/2}$ 12.0 +/- 7.5 s) than IMD-mCherry (1.6 +/- 0.5 s), N= 4, and this is statistically significant (t test, $p < 0.05$). Actin recovery tended to follow a linear increase rather than the typical exponential increase observed for the other constructs tested, possibly due to unbleached section of the filament moving into the measured area. Follow up experiments could be done to test the FRAP profiles of GFP actin in well defined structures such as stress fibres and filopodia induced by Cdc42 activation, in order to determine whether GFP actin dynamics occur as expected.

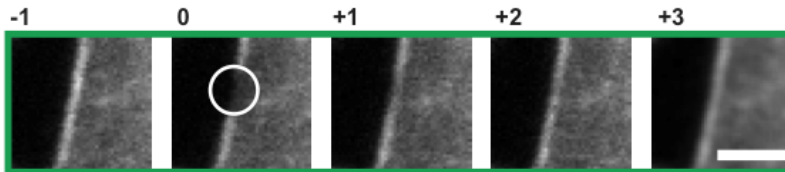
5.5 FRAP of IRSp53-GFP

Several preliminary FRAP experiments were done using the full length IRSp53 construct. In addition to the formation of protrusions, a large amount of signal was observed at the cell edge. FRAP experiments on both protrusions and these high-signal cell edge regions showed similar results in terms of total recovery (edge: 69.1 % \pm 18.0; protrusion 68.4 \pm 11.6 %, N=4), although the cell edge regions had a faster $t_{1/2}$ (mean 0.2 s \pm 0.01 compared to protrusions 3.2 s \pm 3.3, N=4), although this was not statistically significant. This suggests that some IRSp53-GFP is immobilised in some way at the membrane, yet does not induce protrusions.

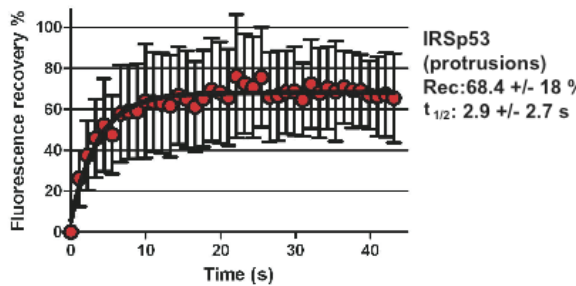
A i IRSp53-GFP protrusion



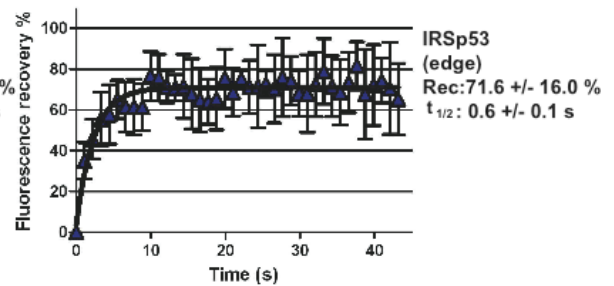
ii IRSp53-GFP cell edge



B i



ii



C

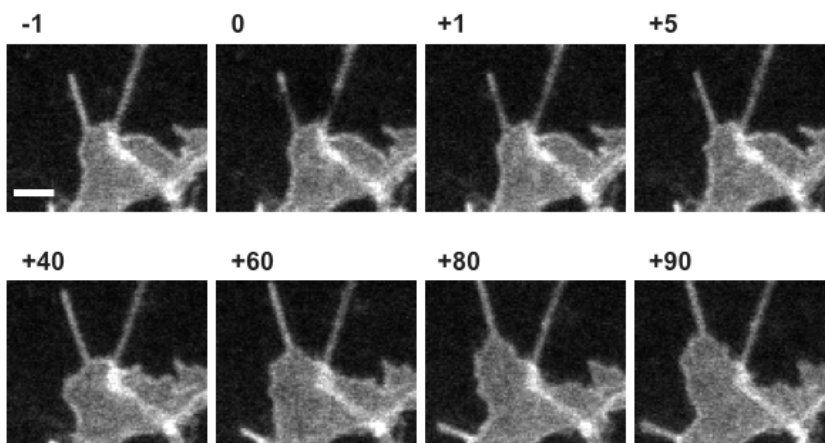


Figure 5.6 FRAP of cells expressing IRSp53-GFP. (A) FRAP done in IRSp53 expressing cells was carried out in both protrusions (i), and regions of the cell periphery (ii). Rapid recovery for cell edge was observed, although this is due to the contribution of cytoplasmic signal recovering. (N=4). (C) Cell showing broad lamellipodia-like movement.

5.6 Discussion

It was expected that if IMD had little or no interaction with protrusion components, then it would show a rapid FRAP recovery profile similar to that seen for free fluorophores. This was found to be the case. A proportion of IMD-GFP located within IMD rich protrusions is stably associated with them, as there is a consistent immobile fraction of 55-70 %. The half time for IMD-GFP recovery is approximately 7.3 sec. Only one study to date has also used FRAP as a technique to examine IMD in protrusions (Saarikangas et al, 2009). In it, they found that IMD with an N terminal GFP tag had a $t_{1/2}$ of 5.2 sec. This correlates well with the $t_{1/2}$ of 7.3 measured in this investigation. However, a higher level of IMD-GFP recovery (approximately 80 %) is observed in the experiments done by Saarikangas *et al*, corresponding to a smaller immobile fraction than was measured in the present study. In some experiments done here with IMD-mCherry FRAP of approximately 80 % was also found. However, as noted above, this FRAP profile was associated with cells showing relatively few protrusions, and one could speculate that the expression level may not have been sufficient to induce IMD protrusions. However, the fact that an immobile fraction was observed strongly suggests that a proportion of IMD-mCherry is associated in some way with the protrusions. Further experiments using the same IMD-mCherry construct have shown an immobile fraction of 63.5 %, which is more consistent with the IMD-GFP data shown here (B. Visegrady, personal communication), suggesting that the GFP and mCherry constructs may actually behave quite similarly and that further repeats of these experiments are needed before we can draw firm conclusions from them.

Delayed recovery of fluorescence as observed for IMD-GFP could have been a result of space and concentration restraints imposed by the dimensions of the protrusions. To control for this, FRAP analysis of GFP in protrusions was done, and it was found that the fluorescence recovered in a rapid and complete fashion comparable to that seen for FRAP experiments done on fluorophore located in the cytosol. In order to correct for the disparity in size between GFP alone and IMD-GFP, FRAP experiments with IMD K4E-GFP coexpressed with IMD-mCherry were carried out, as this is identical in size to IMD-GFP, but is not expected to interact with the membrane or actin filaments. However, only one *bona fide* protrusion was observed, and in this the mutant did show more rapid recovery than wild type IMD, suggesting that it is unable to interact with components of the protrusion, as expected (Figure

5.5). It was not initially considered that the mutant and wild type IMD may have heterodimerized, which may block formation of protrusions, as presumably the IMD requires the basic patches to be present at both ends of the dimer, and a heterodimer with mutant would only possess one. This remains to be determined by further studies.

The final of the dual colour FRAP experiments was with IMD-mCherry and GFP-actin. It was hoped that filamentous actin would show a different FRAP profile to other components due to it being immobilised in filaments, which would restrict its diffusion. Once bleached, the actin did often have an extremely slow recovery, which may signify the presence of filamentous actin, and indicate that this is a reasonable approach. This could be verified by testing the FRAP response of GFP actin in Cdc42 induced filopodia (Figure 5.5 C). As discussed above, further tests need to be done to ensure that the protrusions are generated by IMD, as the cell morphology and FRAP profile for IMD-mCherry was different to that expected for the initial IMD-GFP experiments. However, these experiments demonstrated that filamentous actin can be characterized using FRAP. Simple observation of fluorescently labelled actin in IMD protrusions does not necessarily indicate that it is filamentous, and future studies can use FRAP to determine this. This approach could ideally be used to examine the effects of actin destabilising agents such as latB and cytD, on actin polymerization state in real time. The experiments shown in Figure 5.4 indicate that IMD turnover in protrusions is not affected by cytD. However, as discussed in the previous chapter cytD has multiple effects on the actin cytoskeleton, and so any effect observed can be difficult to interpret. Its effects could be tested by phalloidin staining the cell to selectively stabilise and stain actin filaments, or FRAP of labelled actin as described earlier.

Full length IRSp53 tagged with GFP showed a similar FRAP response to IMD alone, although it had a slightly lower immobile fraction (32 %). This may suggest a higher turnover of IRSp53, and potentially less strong interaction with the protrusion. The presence of IRSp53-GFP at the membrane is consistent with findings that IRSp53 localizes to tips of lamellipodia. (Nakagawa et al, 2003). Although IRSp53 was observed here to localize to membrane in broad lamellipodia-like structures shown in Figure 5.6 A i. And C, this was also observed in some cells for straight non-protruding regions, like the one seen in Figure 5.6 A ii. Further investigations would need to be done in order to determine this.

Another filopodial component which has been investigated by FRAP is actin crosslinking protein fascin (Vignjevic et al., 2006; Aratyn et al., 2007). Interestingly, the recovery half time was found to be less than 10 seconds, which is similar to the values derived from IMD-GFP FRAP shown here. That IMD shares similar initial recovery rates with an actin bundling protein suggests that it may share the actin bundling characteristics required for actin bundling for filopodia. However, whereas an immobile fraction of 55-70 % was observed for IMD, fascin shows a complete recovery within approximately 100 seconds. This suggests that whilst fascin is able to turn over completely, at least a proportion of IMD remains more permanently associated with the protrusion. IMD may bind to protrusions in a stable manner, perhaps oligomerizing in a manner analogous to that of some BAR domains (Henne et al., 2007). These results do not rule out the possibility that IMD may play a role in both actin bundling and membrane binding.

5.7 Conclusions and future perspectives

Here it was shown that GFP-tagged IMD in protrusions has a recovery half time of approximately 8 seconds, and a large apparent immobile fraction of around 55-70 %. IMD-GFP in cytoplasmic regions shows a much more rapid recovery, suggesting that the apparent immobile state of the IMD is related to its presence in the protrusions it induces. Future work should focus on trying to discern between actin and membrane interactions with the IMD. This can be continued by the use of actin destabilizing drugs such as cytD and latB. If IMD is strongly associated with the actin in the protrusions, depolymerization of the filament may lead to increased turnover of IMD. A series of FRAP experiments should also be carried out to elucidate the dynamics of full length IRSp53 in filopodia-like protrusions to determine whether the dynamics vary relative to those of IMD alone. This could also provide information about how much the activity of the IMD contributes to IRSp53-mediated filopodia formation.

6 Characterisation of the interaction between the IMD and unilamellar vesicles

Several recent studies have described interactions between IMD and membrane phospholipids (Suetsugu et al., 2006a; Suetsugu et al., 2006b; Mattila et al., 2007; Saarikangas et al., 2009). The focus of IMD-membrane interactions thus far has been on signalling phospholipids such as PI(4,5)P₂ and PI(4,5,6)P₃, and the interaction has been proposed to be mainly electrostatic. Because IMD overexpression leads to extreme tubulation of overexpressing cells (Chapter 3) irrespective of the presence of localized PI(4,5)P₂. Here, it is investigated whether IMD interacts with more abundant membrane phospholipids, and the interactions are quantified. Phosphatidylserine (PS) lipids were used in these assays, because IMD is known to interact with negatively charged membranes, and PS is present in the inner leaflet of cell membranes (Verkleij et al., 1973; Suetsugu et al., 2006b).

6.1 Preparation of small unilamellar vesicles.

Lipid vesicles were produced by extrusion through a membrane of 200 nm pore size. This method produces unilamellar vesicles with a narrow size distribution. In order to allow tracking of the vesicles during experiments fluorescent lipophilic dye, DiI was used. This allowed vesicle concentration to be quantified by fluorescence spectroscopy. Initially DiI was added to the vesicle mix after extrusion, but the fluorescence profile did not appear as expected (Figure 6.1). Vortexing of the DiI-vesicle mix led to a blue shift of the fluorescence emission spectrum, presumably due to the fluorophore being relocated from an aqueous to a lipophilic environment. The protocol was modified to include the DiI at the organic phase of mixing the lipids, which resulted in the expected fluorescence profile of the dye being observed.

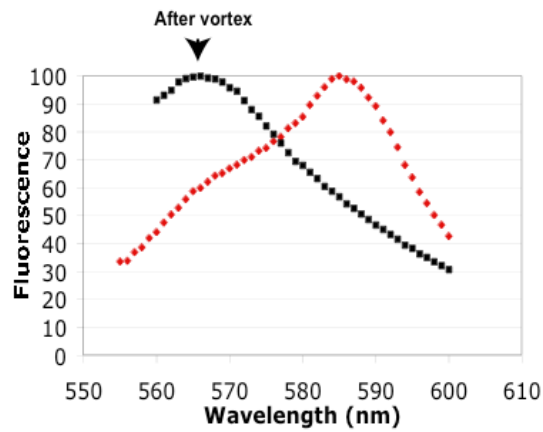
6.2 Probing the IMD-vesicle interaction by size exclusion chromatography.

In order to measure the strength of interaction between IMD and phospholipid membranes, PS and PC (phosphatidylcholine) - containing vesicles were analysed by size exclusion chromatography in the presence and absence of IMD. Gel filtration allows the separation of species of different molecular weight, as smaller species (in this case the IMD) diffuse into the column matrix and taking a convoluted path through the column, whereas larger species (vesicles) are unable to enter into the column matrix, pass through more rapidly and are eluted earlier. The vesicles eluted from the column at approximately fraction 19, and the PS vesicles also had a second peak at fraction 26 (Figure 6.1 B i). Blue dextran has a large molecular

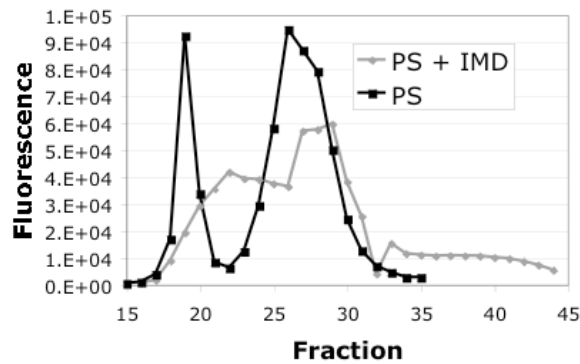
weight of 2,000 kDa, and is not adsorbed onto the column substrate and serves as a marker for the liquid phase. This was also found to elute in similar fractions to the vesicles (fractions 16-21), confirming that the vesicles were also too large to be retarded by the column. IMD alone consistently eluted at fraction 24, and is therefore retarded relative to the vesicles. However, when the mixture of IMD and PS vesicles were added to the column together, no IMD was eluted and there was a reduction in the amount of fluorescence signal detected, in both of the previously observed peaks (Figure 6.1 B ii). In subsequent attempts to repeat this experiment, no IMD was recovered. On closer inspection, there was a residue of the pink lipid at the top of the column, and it became clear that the addition of IMD to PS vesicles was causing aggregation. This was verified by fluorescence microscopy, comparing DiI-containing vesicles with and without adding IMD of vesicles containing DiI (Figure 6.1 C). Following these experiments it was decided that gel filtration chromatography was an unsuitable method for examining the interaction between IMD and lipid vesicles.

6.3 Use of a low velocity centrifugation assay to investigate IMD interactions with lipid vesicles.

Having observed that IMD can cause aggregation of lipid vesicles, which can be detected by measuring fluorescence intensity (Figure 6.1 C), an assay to measure this interaction was derived measuring the partitioning of vesicles between supernatant and pellet in response to incubation with varying concentrations of IMD. The assay is briefly as follows. 200 nm extruded vesicles (66 μ M) labelled with DiI (25 μ g/ml) were incubated with varying concentrations of IMD for 15 minutes, before centrifugation at 16 100 g to remove aggregated lipid from the supernatant. The proportion of lipid lost is calculated from the reduction in fluorescence emission of the supernatant, with 100 % lipid loss occurring when all detectable fluorescence signal is lost from the supernatant. In order to prevent Ca²⁺- or Mg²⁺-induced vesicle aggregation, IMD preparations were dialysed into Ca²⁺/Mg²⁺-free buffers. To verify that all divalent cations are removed in the dialysis conditions used, identical pelleting experiments were carried out with dialysed IMD in presence and absence of EDTA (Figure 6.2 B). These experiments indicated that the dialysis conditions used were sufficient to remove cations from the buffer, and that the pelleting observed is due to IMD. Centrifugation at 16,100 x g for 30 minutes was found to cause some

A

i

B

ii

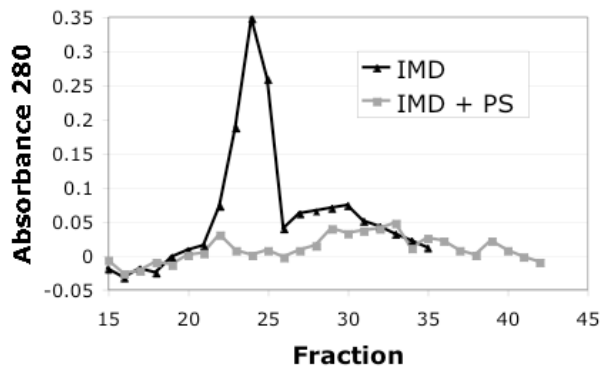


Figure 6.1 (A) Shift of the DiI emission peak as a result of vortexing the DiI-vesicle mixture on fluorescence emission of DiI. 1 mM 200 nm PS vesicles were incubated with 10 $\mu\text{g/ml}$ DiI and analyzed by fluorescence spectroscopy, before (red) and after (black) agitation by vortexing for 1 minute. (B) Gel filtration experiments with 100 % PS vesicles (400 μM) and IMD (40 μM), incubated at 20 $^{\circ}\text{C}$ for 15 minutes. Mixture of IMD and PS leads to a decrease in the amount of PS passing through the column (i), and complete loss of the IMD peak (ii).

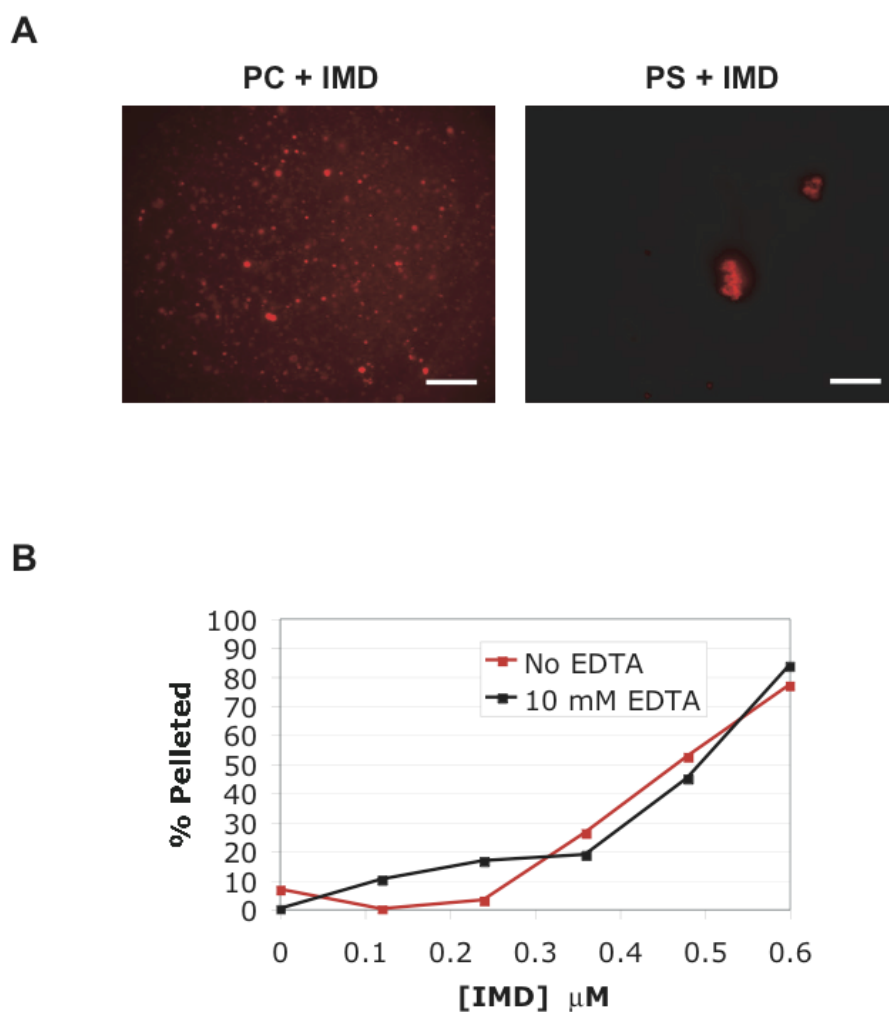


Figure 6.2 (A) Fluorescence microscopy of vesicles following incubation with IMD for 15 minutes, vesicle concentration 400 μM ; IMD 40 μM , in showing aggregation of vesicles in the PS but not the PC sample. Scale bar, 10 μm . **(B)** Pelleting assay done with 66 μM IMD dialysed into buffer lacking divalent cations. The assay was done in presence and absence of EDTA to chelate any residual concentration of divalent cations. The similarity between the curves indicates that the pelleting activity observed is not due to divalent cations and is likely mediated by IMD.

pelleting of vesicles with no IMD present, this was taken into account when calculating amount of lipid pelleted by interaction with IMD. A pre-spin of all lipids and IMD was therefore carried out at the start of each experiment prior to mixing the lipid and protein. The concentration of lipid used in the assays was 66 μM as this concentration was found to reach fully pelleting sediments when incubated with around 1 μM IMD.

Concentration of IMD required to pellet 100 % of the detectable PS varied between different preparations, (Figure 6.3 A). In order to compare data, it was decided to derive a standard measure of pelleting, (k_{pell}), which refers to the concentration of IMD required to pellet half of the vesicles present. The data follow a sigmoidal distribution, and in order to better analyse it attempts were made to convert the data into a linear distribution. To do this a logistic function was applied to the proportion of lipid pelleted: $\log(y/(1-y))$, where y = proportion of lipid lost from the supernatant. The logistic function follows the distribution shown in Figure 6.3 (C), and the inverse function of the logistic function linearises the sigmoidal curve – i.e. if y is 100%-(residual fluorescence in %), then $\log(y/(1-y))$ will be (approximately) linear. However upon applying this function to the data it was found that data points located at the extremities of the distribution do not fit a linear distribution, as the function used caused small variations at either ends of the curve tend to be overemphasized. Data points from the extreme periphery of the distribution were therefore excluded before linear regression analysis (Figure 6.3 B). The concentration of IMD required for pelleting of half of the lipid at this concentration is determined by the intercept of the regression line at the x-axis. As there was some variation in the propensity of the lipid to pellet in absence of IMD, this was taken into account by calculating the estimated lipid concentration after prespin (normalised k_{pell}).

Having developed an assay to measure the interaction of IMD with vesicles, some factors affecting this interaction were probed. Several previous studies had indicated that the IMD interaction with membrane phospholipids is largely electrostatic, and occurs via negatively charged phospholipid headgroups and positively charged areas of the IMD (Suetsugu et al., 2006b; Mattila et al., 2007; Saarikangas et al., 2009). The phosphatidylserine (PS) headgroup carries a negative charge, whereas phosphatidylcholine (PC) is zwitterionic, with no substantial net charge at pH 8.0, and so is not expected to bind to the positively charged regions of the IMD.

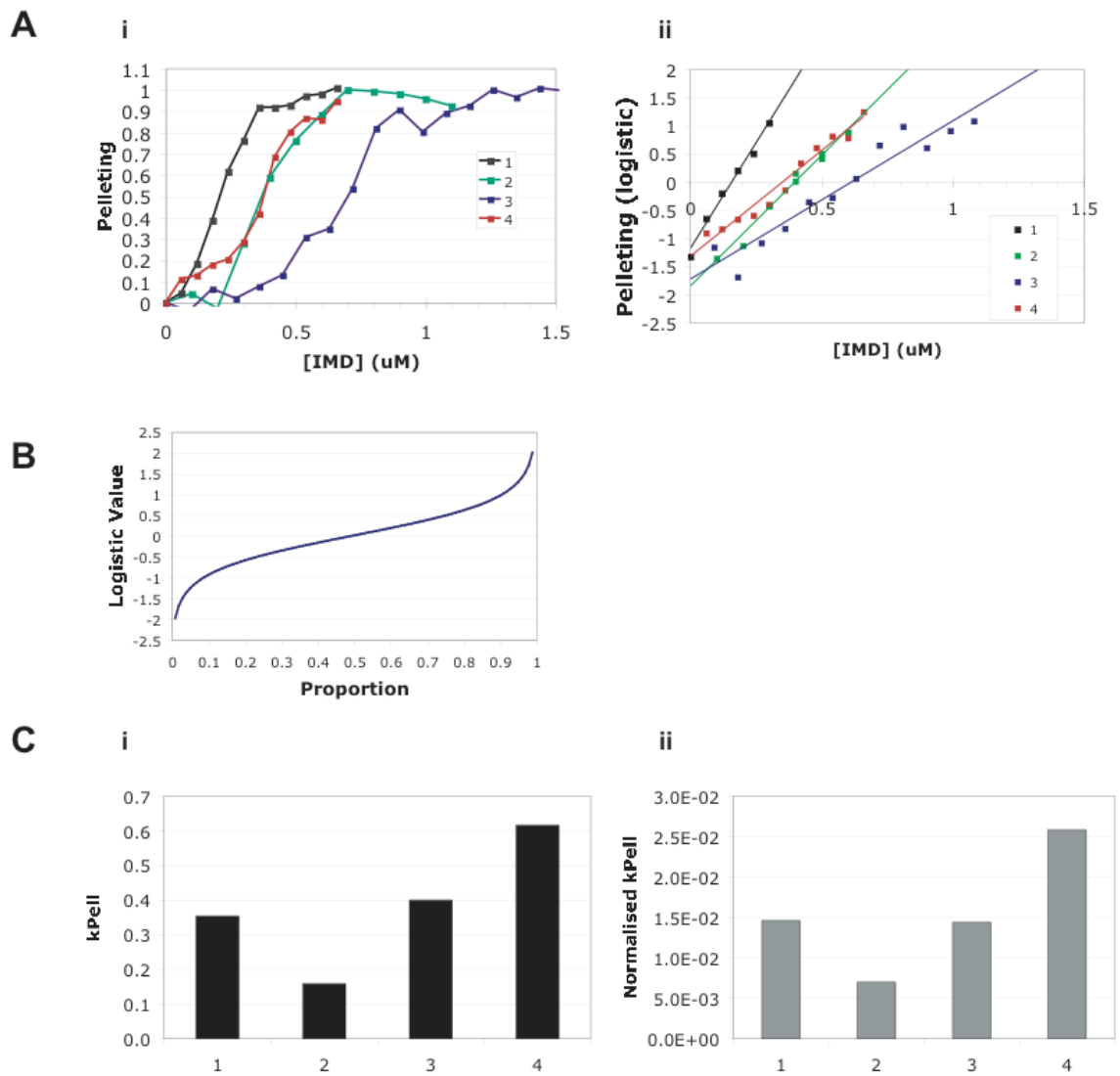


Figure 6.3 (A) (i) Experiments with 100 % PS 200 nm lipid vesicles show a degree of variability between different lipid and protein preparations. Each trace is from a different preparation. (ii) Fitting the sigmoidal curve to a linear distribution. (B) The logistic distribution used in all experiments to generate the linear distribution shown in (A)(ii). Note that 0.5 proportion (50 %) gives a logistic value of 0. (C) Calculated k_{pell} values for each sample. (i) Values as calculated directly from charts; (ii) values normalised to values per μM lipid, to account for intrinsic pelleting in absence of IMD.

Previous experiments indicated that PC does not interact with the IMD (Figure 6.2) and so PC was therefore used to dilute the proportion of PS in the vesicles in these experiments looking at effect of charge density on IMD-vesicle binding. Data from experiments with varying PS proportions are shown in Figure 6.4. 100 % PS and 90 % PS show little difference in their interaction with IMD, whereas lower concentrations of PS 80 % and 70 % require an increased concentration of IMD to remove the same proportion from the supernatant. At PS proportion of 50 %, only a small amount of pelleting is observed at the concentrations used in the other experiments, and approximately 50 % pelleting is observed only at a high IMD concentration of 25 μM . This suggests that IMD affinity for these lipids is so low as to render the interaction unfeasible to measure by this method, and higher concentrations of IMD were not tested.

Having determined that IMD-lipid interactions vary according to negative charge present, it was decided to compare the IMD interactions with PS based vesicles with more physiologically relevant lipid compositions. Two different compositions were used: a brain lipid lysate (Bovine brain Folch fraction I); and a lipid mixture similar to that used in a study that required inner membrane-like lipids - PS 27 %; PI(4,5)P₂ 3 % and PC, PI and PE in a 1:2:2 ratio (Figure 6.5)(Cullen et al., 1995). Vesicles made using these two lipids showed similar pelleting profiles to one another (Figure 6.5 A ii and B ii), with k_{pell} measured to be at 0.9 and 1.1 μM for brain lipid and the lipid mix, respectively. When the lipid mix was directly compared to vesicles containing 100 % PS, a decrease in interaction of 2.9 fold was observed (Figure 6.5 C), suggesting that physiological lipids pellet at similar levels to vesicles containing 80 % PS.

Increasing NaCl concentration reduces the strength of ionic interactions by masking charges, and had been used in similar studies to estimate the strength of protein-lipid interactions (Henne et al., 2007; Saarikangas et al., 2009). Pelleting experiments were done using different NaCl concentrations to investigate whether the interaction that causes pelleting of vesicles is likely to be ionic in nature. Pelleting assays were done at a range of NaCl concentrations between 150 mM and 200 mM (Figure 6.5). An increase in ionic strength of 50 mM (to 200 mM), resulted in a considerable decrease in pelleting - k_{pell} changed from 0.26 to 0.48, representing a decrease in IMD lipid interactions of approximately two-fold. When the

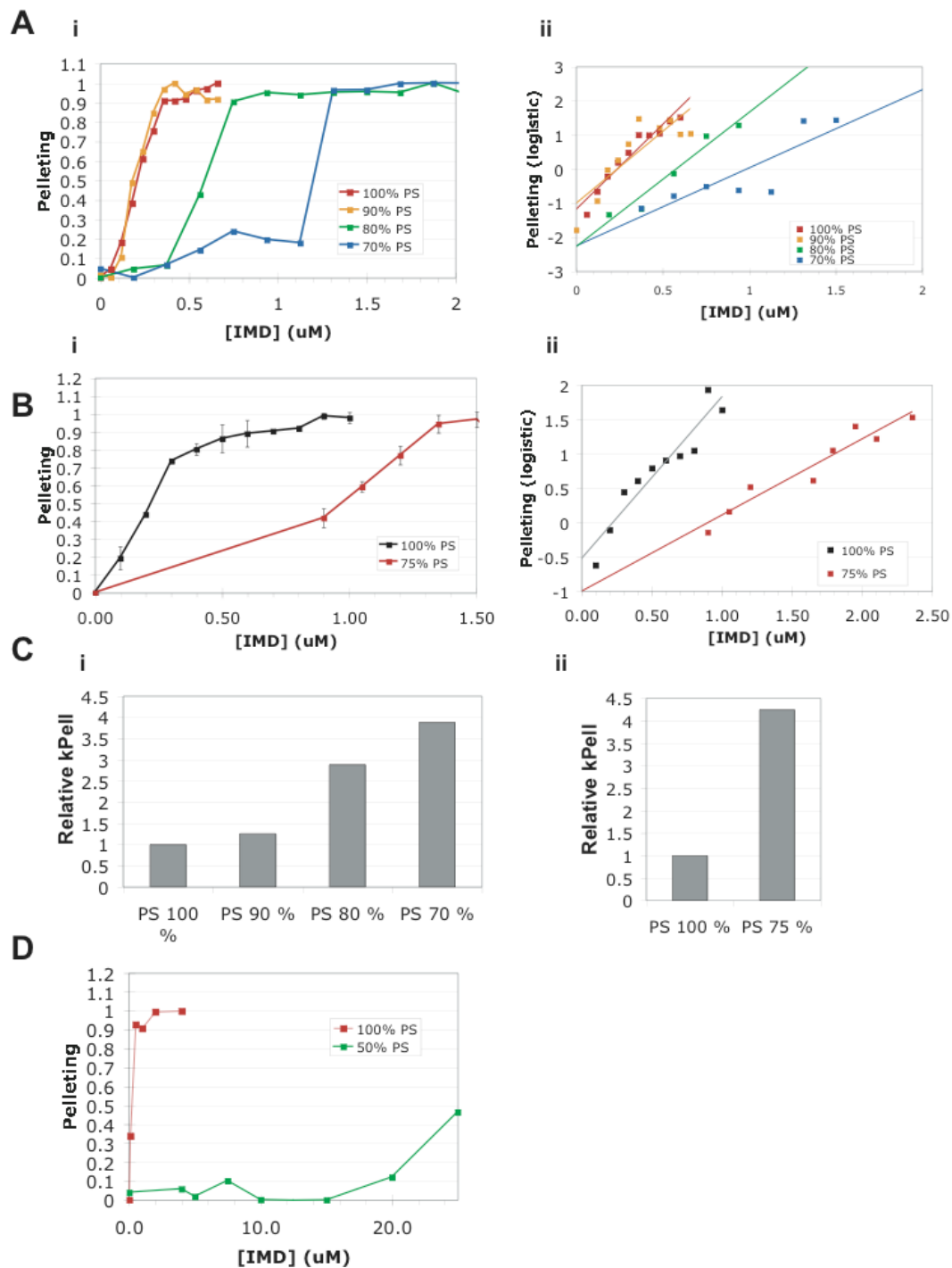


Figure 6.4 Experiments with vesicles containing varying proportions of PS, using PC as a substitute with negligible charge. (A) and (B) (i) show experiments from two separate preparations, and their analysis (ii). (C) k_{pell} values relative to 100 % PS and corrected for intrinsic lipid loss are shown, indicating that IMD affinity for vesicles decreases as the charge is decreased. (D) Vesicles containing 50 % PS show very weak pelleting when incubated with IMD, and a reduction of less than 50% was observed at a concentration of 25 μM IMD.

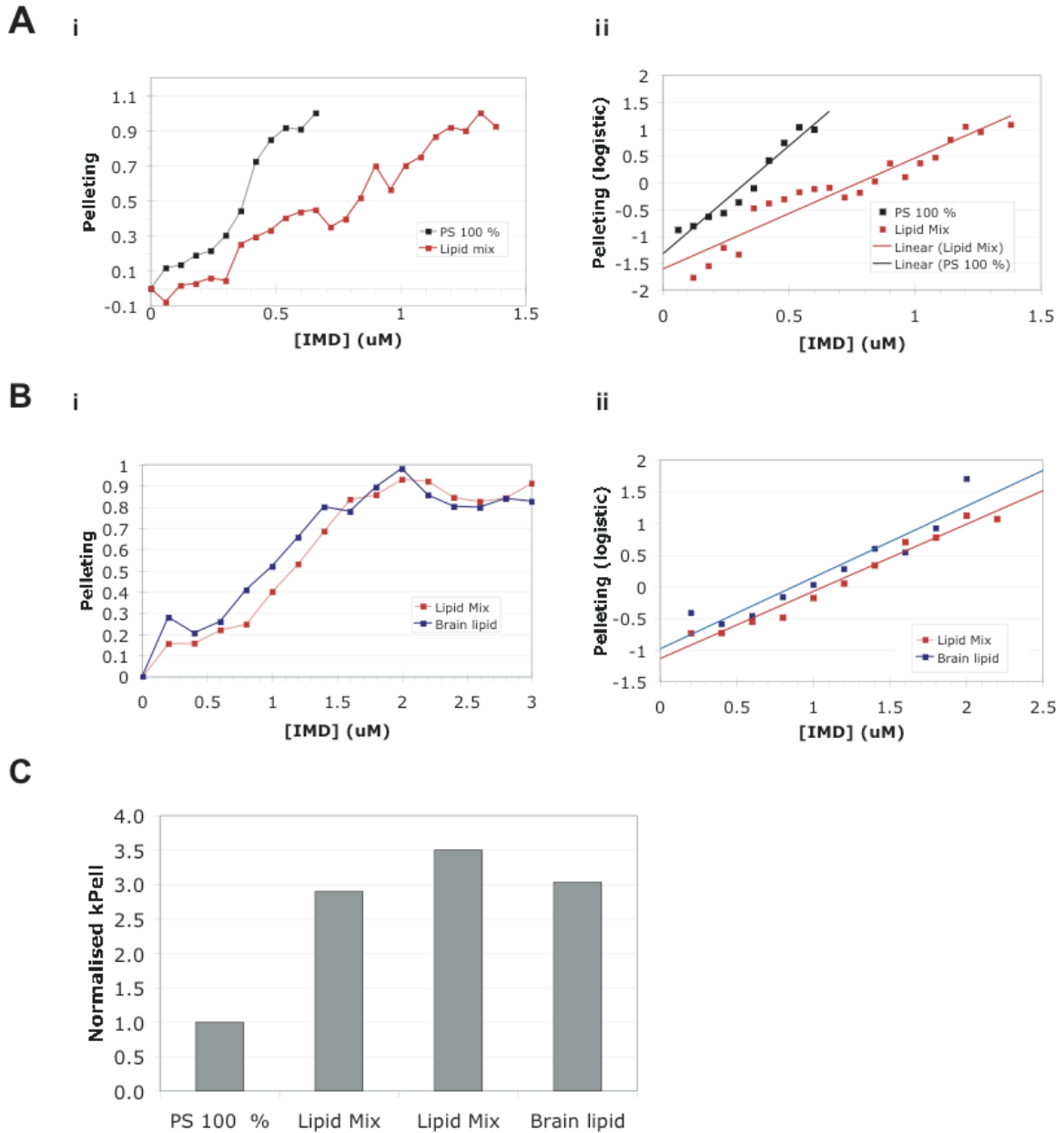


Figure 6.5 Experiments to test the strength of IMD interaction with brain lipids (bovine Folch fraction D) and the synthetic lipid mix (see text). (A) Pelleting assays comparing vesicles made up of 100 % PS with the lipid mix. Degree of pelleting (i) and fitting of data (ii) shown. (B) Comparative pelleting of brain lipids and lipid mix, indicating that both interact with IMD at a similar level. (C) Bar chart showing relative k_{pell} for IMD with brain lipids and lipid mix. Values relative to 100 % PS, and corrected for estimated lipid loss due to pelleting in absence of IMD.

concentration of lipids present is taken into account, this change is around 2.7 fold. This suggests that the interaction is disrupted by increased ionic strength. A slight increase in k_{pell} is observed at NaCl concentration of 170 mM and 190 mM NaCl, but an addition of NaCl to 160 mM had no discernable effect on the pelleting observed. A relatively high amount of pelleting in the absence of IMD was observed in the 200 mM NaCl experiment (approx 53 %), possibly due to the NaCl contributing to lipid pelleting itself. However, even when the half concentration for pelleting is normalised for the amount of lipid present, a decrease in interaction is still observed (Figure 6.6 B).

6.4 Imaging of PS containing vesicles in the absence and presence of IMD

Previous studies of the IMD have used imaging techniques to improve of its activity at the membrane (Suetsugu et al., 2006b; Mattila et al., 2007; Saarikangas et al., 2009). In order to better understand the interactions detected by size exclusion chromatography and the sedimentation assay, PS vesicles were imaged using both fluorescence microscopy and transmission electron microscopy (T-EM). Fluorescence microscopy was used to visualize IMD-induced aggregation at reagent concentrations used in the pelleting experiments described above. Representative images are shown in Figure 6.7. In the image of vesicles with no IMD added, the particles have a diffuse appearance, with different foci of variable apparent size. This is likely to be because the vesicles are suspended in solution and only very few are directly within the focal plane. No aggregation is visible in the absence of IMD. At a concentration of 0.2 μM IMD, aggregates begin to appear in the micron range. It should be noted that at this IMD concentration, aggregation is visible by microscopy yet no reduction of fluorescence is observed in the pelleting assay. At 0.4 μM IMD smaller foci appear, and some coalescence into larger arrays is observed. At the higher IMD concentrations of 1.0, 1.6 and 2.2 μM , where the sedimentation assay shows aggregation of all lipid, increasingly large aggregates of 10 μm are observed.

Fluorescence microscopy provides an overview of levels of aggregation and may help in the interpretation of the pelleting assays. The vesicles can be observed in solution with no fixing process. However, light microscopy offers only limited resolution, and in order to see what occurs at the level of individual vesicles electron microscopy must be used. EM has previously been used to image IMD-vesicle interactions

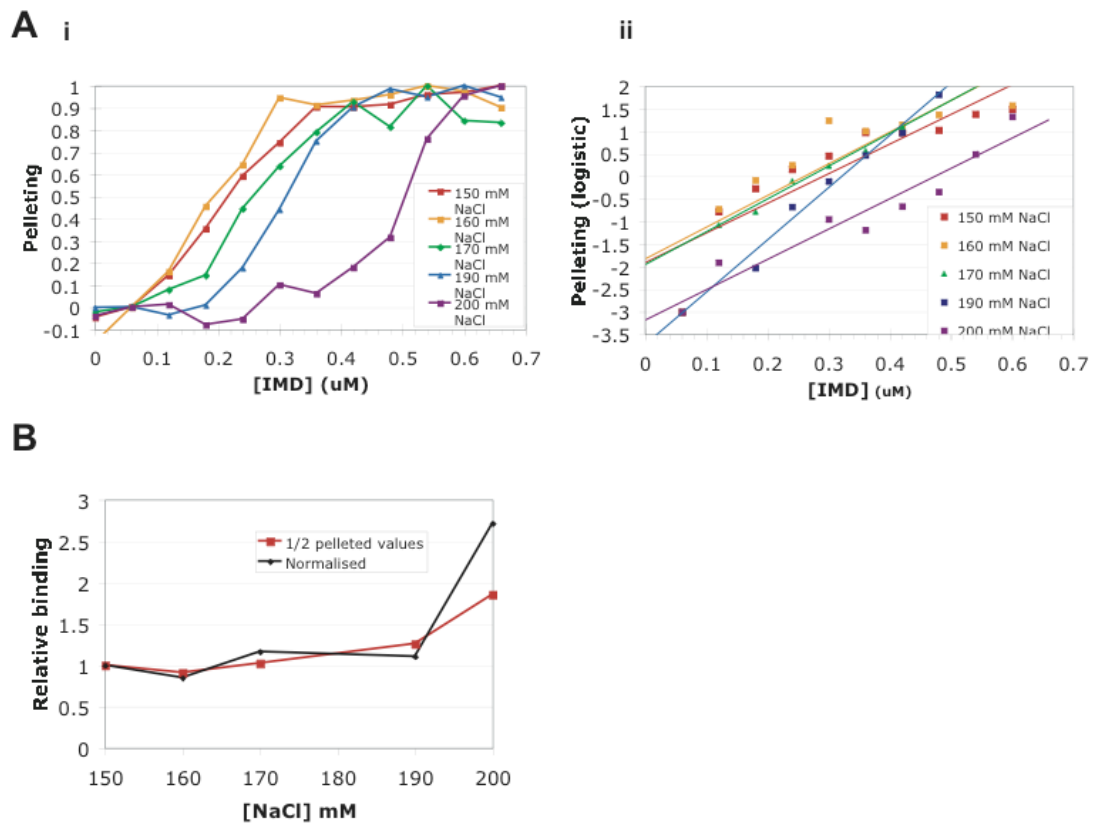


Figure 6.6 Results from IMD and PD vesicle pelleting experiments where the concentration of NaCl was increased. (A) (i) Normalised data from the experiment; (ii) Fitting of the data to estimate concentration of IMD required for pelleting of half the lipid. (B) Chart showing the increased concentration of IMD required for pelleting as a function of NaCl concentration. The normalised values correct for the different levels of intrinsic pelleting seen in lipid samples centrifuged with no IMD present.

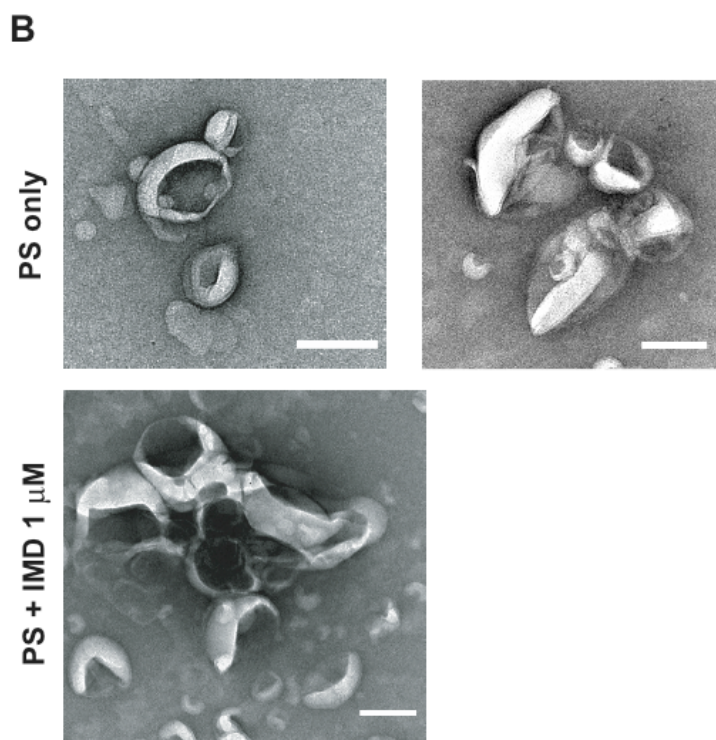
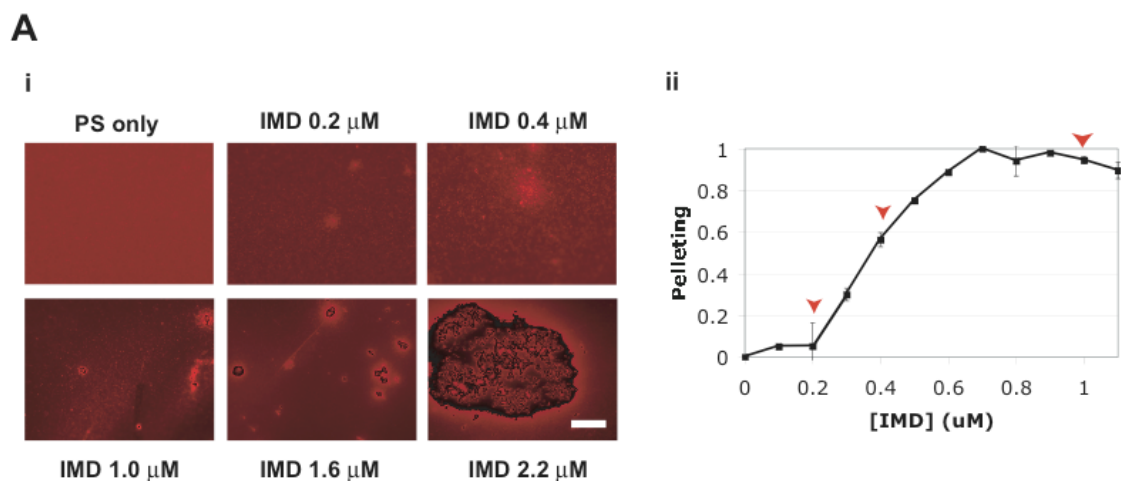


Figure 6.7 Imaging of PS vesicles. (A) (i) 200 nm vesicles (66 μM) were incubated with IMD at concentrations indicated for 15 minutes before imaging by fluorescence microscopy. Scale bar represents 10 μm . (ii) Pelleting experiment done with identical materials and concentrations as used in fluorescence imaging. $N=2$, Error bars represent standard deviation. (B) 200 nm vesicles alone or incubated with 1 μM IMD for 15 minutes were fixed with uranyl acetate, a high electron absorbent stain. Samples were then imaged by transmission electron microscopy. Structures, in this case vesicles, show up in white as they exclude the electron absorbent stain. Scale bar represents 100 nm.

(Suetsugu et al., 2006b; Mattila et al., 2007; Saarikangas et al., 2009). Electron micrograph images of PS vesicles both alone and with IMD are shown in Figure 6.7 (B). Although there is an amount of variation in the size of the vesicles imaged, the vesicles tended to have a diameter of approximately 120 nm. However, the vesicles as seen by T-EM appear to be folded inwards, and so accurate measurement of their dimensions is difficult. The fact that they appear to largely retain structural integrity indicates that the fixing and imaging methods used do not cause major disruption of the vesicles, although the folded – in appearance may indicate that liquid is lost perhaps due to osmotic challenge introduced during fixation. When the lipids were incubated with 1 μ M IMD it was expected that a large amount of aggregation would occur, and that the presence of IMD on the membranes could be observed by the effect on membrane topology, as seen in (Mattila et al., 2007; Saarikangas et al., 2009). Largely, the appearance of the vesicles in presence of IMD was no different to vesicles alone. Some areas of high vesicle density were observed (Figure 6.1 B, bottom), and these possibly correspond to the aggregates observed in Figure 6.1 A.

6.5 Fluorescence resonance energy transfer (FRET) analysis of IMD-vesicle interaction.

In order to measure IMD-vesicle interactions by an alternative technique, a collaboration with Dr. Balazs Visegrady was undertaken in carrying out vesicle-IMD binding experiments probed Förster resonance energy transfer (FRET). IMD was labelled with donor fluorescent dye IEDANS. Under normal conditions, when the fluorophore is excited by light of excitation wavelength (350nm), light at 420-490 nm is emitted and can be detected using a fluorimeter. However, when the fluorophore is in close proximity to a receptor (in these experiments, DiO in vesicles), the energy of the excited state of the donor is transferred directly to the acceptor. This results in a lower level of emitted light from the donor being detected when the donor and acceptor are in close proximity (Figure 6.8 A). FRET data suggest that at 1 μ M IMD and 66 μ M PS not all IMD is bound to vesicles, as observed by FRET efficiency of approximately 70 % of maximal (Figure 6.8 A). However, at higher vesicle: IMD ratios, full FRET efficiency is observed for 100 % PS lipids, suggesting that at lower IMD concentrations in the pelleting experiments, all IMD is bound to membranes. The

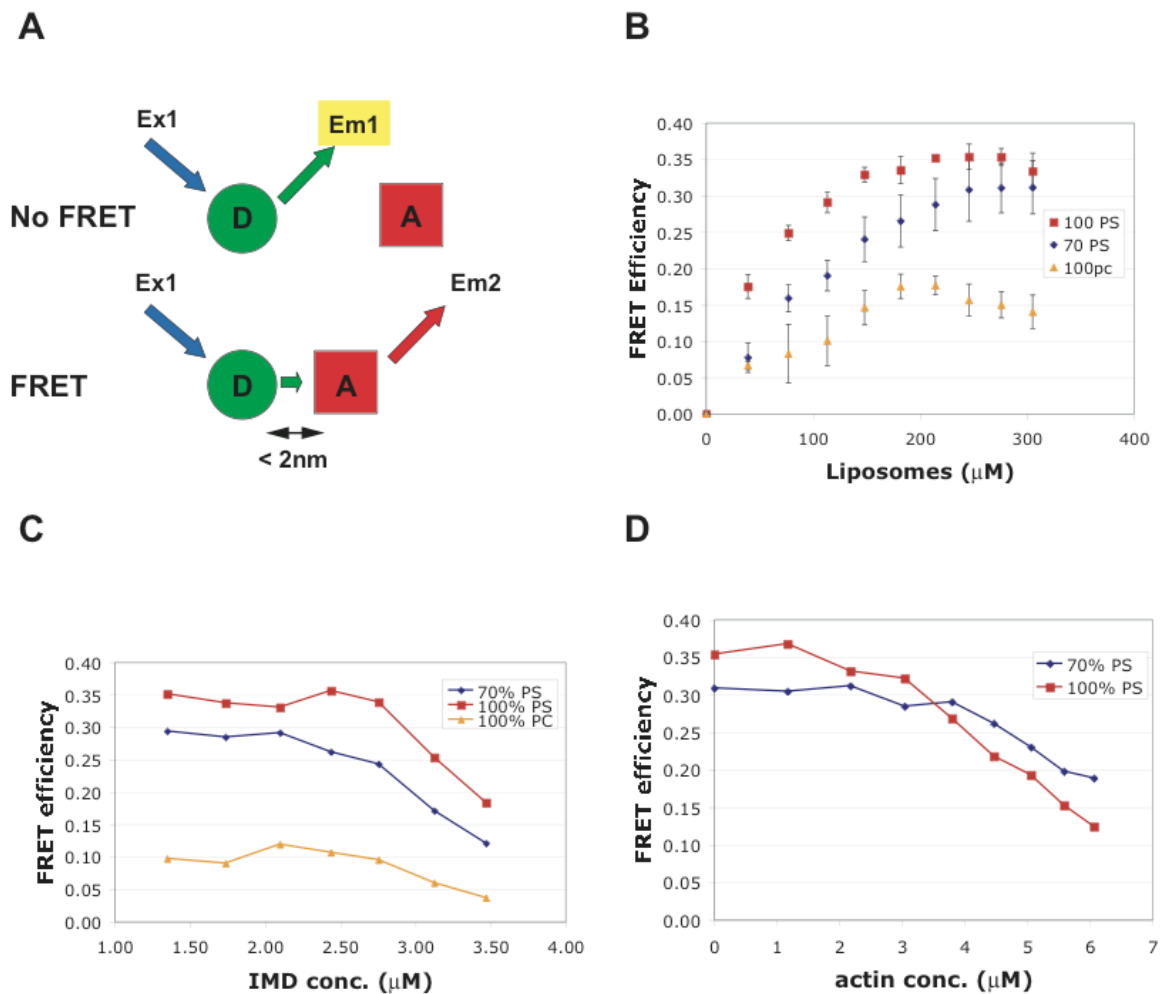


Figure 6.8 FRET experiments carried out on vesicles (receptor) and labelled IMD labelled with FRET donor fluorophore. These experiments were done by Balazs Visegrady. (A) Cartoon of FRET principle. Donor fluorophore *D* is excited by excitation light *Ex1* causing emission of light *Ex1*. This is measured. Top: No FRET occurs and *Ex1* is detected. Bottom: When acceptor *A* is within 2 nm of donor fluorophore, *Ex1* light excites the acceptor, resulting in emission of light from the acceptor, but none from donor – high FRET. In these experiments IMD was labelled with the donor and vesicles with the acceptor. (B) FRET was measured with 1 μM IMD and vesicles were titrated in. Interaction is observed by increase in FRET efficiency. A stronger interaction was observed with 100 % PS vesicles than 70 % vesicles. Only a small increase in FRET efficiency was observed with PC vesicles. (C) Reciprocal experiment of (A). 66 μM vesicles as specified had IMD titrated in. With PS 100 % vesicles, FRET efficiency remained high until more than 2.5 μM was added, suggesting that below this IMD concentration all IMD was in close association with the vesicles. Again, decreased interaction was observed for 70 % PS vesicles, and only a small change was observed when PC vesicles were tested. (D) Actin monomers can compete IMD off vesicles. IMD and vesicles were incubated together to ensure a saturated FRET, as shown in (B). Monomeric actin was then titrated in and FRET measured after 15 minutes to allow equilibration. An actin dependent reduction of FRET efficiency was observed, suggesting that IMD-lipid interactions were disrupted by actin monomers

experiment where IMD was titrated in to vesicles of fixed concentration (Figure 6.8 B), indicates that saturation of IMD-vesicle binding in these conditions occurs at around 3 μ M IMD for 100 % vesicles, and at around 2 μ M for vesicles containing the lower PS concentration. Finally, as shown in Figure 6.8 D, when all IMD (1 μ M) is bound to vesicles, addition of monomeric actin leads to a decrease in FRET efficiency, which suggests that actin displaces IMD from the vesicles.

6.6 Discussion

When the crystal structure of the IMD was determined, it was noted that it shared a high degree of structural similarity to BAR domains (Millard et al., 2005). BAR domains are characterised by a crescent shaped dimer structure and the ability to bind to, and in some cases induce areas of membrane curvature, via the concave face of the structure (McMahon and Gallop, 2005). Many BAR domain containing proteins have been characterised, and all are thought to play roles at various stages of clathrin-mediated endocytosis, where they localize to the curved neck of invaginations. Recent studies of the IMD have revealed that, in line with its structural similarity to the BAR domain family, it too can bind to and modify the architecture of lipid bilayers (Mattila et al., 2007; Suetsugu et al., 2006b; Saarikangas et al., 2009). In contrast to the typical BAR domains, which are involved with invagination of the membrane and bind the exterior of tubules, the IMD is thought to induce or stabilise membrane protrusions by binding to the interior of such structures (Figure 6.9) (Mattila et al., 2007; Saarikangas et al., 2009). This has led the IMD to be classified as a bona fide member of the BAR domain protein superfamily. A feature of all conventional BAR domains is their rigid crescent shape, and the presence of a concave surface with clusters of positively charged residues, with which they interact with negatively charged membranes (McMahon and Gallop, 2005). IMD family domains, in contrast, have no such concave face, and instead present a convex curvature, which is what is postulated to induce curvature in the opposite orientation to conventional BAR domains. The IMD has clusters of positively charged residues located at distal ends of the dimer, which are necessary for formation of protrusions *in vivo* (Millard et al., 2005). These same residues have been shown to be important for binding to and deforming membranes *in vitro*, suggesting that the IMD induces membrane deformation in a manner analogous to BAR domains (Suetsugu et al., 2006b; Mattila et al.,

2007). In addition to the concave face, N-BAR domains possess an amphipathic helix, which inserts into the membrane bilayer and acts as a wedge which contributes to membrane binding and deformation (Ringstad et al., 1997; Farsad et al., 2001; Gallop et al., 2006; Henne et al., 2007). The IMD of IRSp53 does not possess such an N terminal helix, however a recent study has suggested that the IMD of MIM and ABBA do insert an 11 amino acid helix into the membrane bilayer and that this contributes to enhanced lipid binding, drawing yet another parallel between the IMD and BAR domains (Saarikangas et al., 2009).

Although the broad mechanism of membrane deformation by IMD proteins is beginning to be elucidated, particularly through analogies with BAR domains, the membrane components required for this interaction are not clear. The first study to look at lipid binding by IRSp53 was carried out by Suetsugu in 2006. Although this study looked at interactions of a truncated version of the IMD (termed the 'RCB' Rac Binding Domain), the truncation does not affect any regions implicated in lipid binding and so their findings may still apply to IMD. It was found that presence of 10 % PI(3,4,5)P₃ in vesicles containing no other charge was sufficient to allow binding to immobilised lipids. Multilamellar vesicles containing 12 % PS and 4 % PI(3,4,5)P₃ were also found to be bound by RCB at a detectable level, and a K_d of 3 μM of RCB was calculated, indicating a physiologically relevant level of interaction. Another group, which has published two studies regarding the IMD and membranes, postulate that PI(4,5)P₂ specifically is necessary for effective IMD-membrane binding, and that membranes containing other anionic phospholipids, including PI(3,4,5)P₃ and PS are not bound by IMD (Mattila et al., 2007; Saarikangas et al., 2009). This may be somewhat surprising, as the IMD-phospholipid interaction appears to be purely an electrostatic event, and the areas of the IMD responsible for lipid binding do not resemble any known lipid recognition domains, such as the PH (Pleckstrin homology domain) which binds to PI(4,5)P₂. In addition, some F-BAR domains have been shown to simply require anionic lipid headgroups for binding, and can tubulate Folch fraction I brain lipids which contain low PI(4,5)P₂ levels (Tsujita et al., 2006; Frost et al., 2008).

The data presented here show an alternative method to measure interactions of IMD with membrane phospholipids. It was found that absolute results varied between different preparations of protein and lipid (Figure 6.3). In pelleting assays with 100 % PS IMD k_{pell}

values ranged from 0.2 to 0.6 μM . However, within a single preparation results were found to be consistent across experiments, and differences between different conditions could be observed and relative changes quantified. Replacement of a portion of PS in the vesicles with PC was done to reduce the charge density of the vesicles, as the PC headgroup has no overall charge, whereas PS is negatively charged. As expected, even small reductions down to 80 % and 90 % resulted in a decrease in the tendency of the vesicles to pellet, suggesting a reduced interaction with the IMD (Figure 6.4). A relative k_{pell} for 50 % PS was not found due to the interaction with IMD being so weak that even at extremely high IMD concentrations no significant amount of pelleting was measured. This suggests that for relatively highly charged membranes this method is useful, whereas in membranes with less surface charge there is not a measurable amount of aggregation. It remains to be measured whether there is still some IMD binding to the lipids at this proportion of PS. To compare to a BAR domain protein, FBP17 is an F-BAR domain containing protein, and saturated binding to membranes was found at PS concentrations of just 10 % (Itoh et al., 2005). However, at higher charge densities the assay used here is sensitive to relatively small changes in membrane charge. In another set of experiments, more physiological mixture of lipids were tested using the pelleting assay to estimate how they interact with IMD relative to PS (Figure 6.5). Here it was found that the lipid mix and brain lipid share a very similar pelleting profiles (observed k_{pell} of 0.9 (brain lipid) and 1.1 (lipid mix)). When 100 % PS was directly compared with the lipid mix however, a larger difference was observed, and a lower pelleting ability of the IMD of around 3 fold was observed for the lipid mix. When compared with the previous experiments with different concentrations of PS in the lipids, this suggests that the lipid mix shows a similar profile in these experiments to approximately 80 % PS. This indicates that vesicles containing biologically significant charges are prone to pelleting in the conditions used here, and suggests that these assays may have some biological relevance.

Increasing concentration of NaCl was found to have an effect on the ability of IMD to cause aggregation of PS vesicles (Figure 6.6). However the only marked effect was seen at 200 mM NaCl, 50 mM higher than the standard conditions of 150 mM. The disruption of IMD vesicle interaction suggests that the interaction being observed is ionic in nature. However, in retrospect this experiment should have been repeated using higher concentrations of NaCl to completely abrogate interaction. Studies into IMD and BAR domain interactions with

vesicles have used increased NaCl concentration to determine the importance of electrostatic forces in their binding to the vesicles (Henne et al., 2007; Saarikangas et al., 2009). Experiments in these studies have shown that the presence of an amphipathic helix that inserts into the membrane bilayer stabilizes protein-lipid interactions. IRSp53 IMD possesses no such helix, and so is expected to bind solely by electrostatic interactions, and be perturbed by NaCl. In the Saarikangas 2009 study, published after the work reported here was done, IRSp53 and MIM IMD binding to vesicles was found to show different sensitivity to NaCl concentration, with IRSp53 IMD lipid binding reduced from 100 % at 100 mM NaCl to approximately 50 % at 400 mM, whereas approximately 100 % of MIM-IMD remained bound to the vesicles at the higher concentration. This study concluded that the MIM IMD is flanked by an N terminal amphipathic helix which anchors into the lipid bilayer in a manner analogous to N-BAR domains such as endophilin (Gallop et al., 2006; Masuda et al., 2006). The data presented in Figure 6.6 are in accordance with Saarikangas et al 2009, in that the IRSp53 IMD interaction with negatively charged membranes can be perturbed by elevated salt concentration, and therefore the interaction is an electrostatic one. Further experiments with even higher NaCl concentration would add to our knowledge of the strength of interaction, and a more physiological lipid composition would aid our understanding. Based on these data, IRSp53 IMD would appear to induce membrane deformation in a similar manner to F-BAR domains, which also rely solely on electrostatic interactions, whereas MIM IMD may function using the additional helix insertion like N-BARs. Given that membrane protrusion requires a relative compression of the membrane at the site of IMD binding, it is unclear how insertion into the membrane could lead to protrusion. In the case of N-BAR membrane deformation the membrane bends away from the protein, and it is easy to envisage the deformation effect gained by helix insertion. The case for amphipathic helices had been made in the case of MIM and ABBA IMDs, but more work remains to be done to clarify the role.

The data presented here are from experiments looking at aggregation of extruded 200 nm phospholipid vesicles after incubation with IMD. They demonstrate that a decrease in negative charge on the vesicles (Figure 6.4) and increased NaCl concentration (Figure 6.6) both reduce IMD-vesicle interaction as measured by this method. Other studies have used lipid binding experiments to show similar factors to be important in IMD (Suetsugu et al

2006b, Mattila et al 2007; Saarikangas et al 2009), and F-BAR (Henne et al, 2007; Itoh et al 2005) interactions with the membrane, and so the data presented here show that lipid aggregation may be related to binding. In these papers, IMD vesicle binding was done by incubation of protein and lipids followed by ultracentrifugation to remove all vesicles from the supernatant, and binding was measured by amount of protein cosedimented with the lipid in the pellet. A limitation of some studies is that they used multilamellar vesicles to look at interactions of IMD with the membranes (Suetsugu et al., 2006b; Mattila et al., 2007). These are the first products formed after hydration of lipids, and consist of ‘onion-skin’ like structures, with many layers of lipid. This may result in a low proportion of the lipid being exposed to binding the IMD, and so results may underestimate the affinity of IMD for membranes. It is not clear what is being measured. Another limitation of some studies is the use of lipids with excessively high levels of charged lipids, for example 30 % PI(4,5)P₂ (Mattila et al., 2007; Saarikangas et al., 2009).

Although vesicle aggregates were observed by fluorescence microscopy, no evidence for membrane tubulation was observed by electron microscopy (Figure 6.7). This could be due to the fixation conditions used for EM, (fixing in 1 mM uranyl acetate) which may have caused disruption of such structures. Another study that successfully used EM to image these structures was Mattila 2007. In that study an additional fixation step using glutaraldehyde was used, which may have increased stability of the structures. Also, that study used an extremely high amount of PI(4,5)P₂ (30 %) in the membrane, and this was not tested in my experiments. However, the key factor in the lack of tubulation observed in the experiments reported here may be the relatively smaller vesicle size used, as the curvature may be too great for the IMD to bind effectively. Some BAR domains have been shown to require vesicles to be of particular dimensions in order to initiate tubulation (Shimada et al., 2007). The F-BAR domain of FBP17 induces curvature of around 600 Å, and is unable to cause tubulation of vesicles smaller than 400 nm, whereas the amphiphysin BAR domain structure is expected to form smaller tubules of 220 Å, and is unable to tubulate larger vesicles of more than 100 nm. If BAR domains are sensitive to the degree of positive curvature they will bind, then it is perhaps unsurprising that IMD domains, which induce negative curvature would not cause invagination of positively curved vesicles. The smaller the vesicle, the greater the curvature, and so the harder it would be for IMD to bind. The tension in the membrane may

also be much higher in smaller vesicles, rendering invagination unfavourable. Figure 6.9 shows scale representation of the IMD alongside the 200 nm vesicles used in this study, and also much larger GUVs used in other studies.

Although no detectable membrane deformation is observed on vesicles incubated with IMD, due to the concentration-dependent aggregation of vesicles it is clear that some interaction is occurring. A recent study on the F-BAR domain of FCHo2 has indicated that F-BAR domains can bind to membranes by a relatively flat side surface rather than the curved concave face, and remain bound without inducing membrane curvature (Henne et al., 2007). In the case of a BAR domain, the charged residues that are involved in binding the membrane are somewhat hidden and so flat binding must occur at a different face. In the case of the IMD however, the structure shows that it is relatively flat in shape. Therefore it may be that in the system used for this investigation IMD binding to the vesicles by forces that are insufficiently strong to overcome membrane rigidity and therefore tubulation cannot occur. Aggregation of lipids may occur simply because sufficient IMD is bound to neutralise the charge on one vesicle, allowing other vesicles to aggregate with it. In addition to the basic patches, which are known to be important for lipid and actin binding, IMD also carries a generally positive charge all over its surface (Millard et al., 2005). When a sufficient concentration of IMD has bound to a vesicle, it is possible that the combined positive charges present are sufficient to attract another vesicle with a net negative charge. Some studies have suggested that F-BAR domains form intramolecular complexes (Shimada et al., 2007; Frost et al., 2008). It is possible that IMD domains bind vesicles and cause aggregation by binding other IMD molecules attached to other vesicles. However, no such polymerization effect has been observed for IMD domains thus far, and other reasons for aggregation are more probable. Finally, work done on endophilin N-BAR domain has revealed that this domain can cause fusion of vesicles alongside tubulation (Gallop et al., 2006). This could possibly lead to increased pelleting of vesicles as seen here. Although this is an interesting finding in terms of BAR domains, it is unlikely to be the cause of pelleting in this case. Electron microscopy images (Figure 6.7) show that there is no formation of markedly larger vesicles after incubation with IMD, and in order for fused vesicles to show a pelleting activity, one would imagine that they would have to be extremely large and detectable by EM.

Alternatively an assay could be devised whereby an excess of IMD is added to vesicles, and then NaCl added to attempt to reverse the binding.

FRET data suggest that at 1 μM IMD and 66 μM PS not all IMD is bound to vesicles, as observed by FRET efficiency of approximately 70 % of maximal (Figure 6.8 A). However, at higher vesicle: IMD ratios, full FRET efficiency is observed for 100 % PS lipids, suggesting that at lower IMD concentrations in the pelleting experiments, all IMD is bound to membranes. The experiment where IMD was titrated in to vesicles of fixed concentration (Figure 6.8 B), suggests that saturation of IMD-vesicle binding in these conditions occurs at around 3 μM IMD for 100 % vesicles, and at around 2 μM for vesicles containing the lower PS concentration.

The experiment shown in Figure 6.8 C gives some idea of the amount of IMD required to saturate binding of all lipid. It has already been shown that the pelleting assays do not allow us to measure this, as even at 100 % pelleting of all lipid, addition of IMD to 100 % PS vesicles causes more aggregation (Figure 6.7 A). The FRET data suggest that maximal binding of IMD is approximately 3 μM , for 100 % PS and approximately 2.5 μM for 70 % PS. Using these figures it can be estimated that the molar saturation ratio of lipid to IMD binding is approximately 22:1 for 100 % PS and 33:1 for 70 % PS. Rough calculations of IMD flat surface area ($180 \times 25 \text{ \AA} = 4500 \text{ \AA}^2$) and PS headgroup area (40.8 \AA^2) indicate a size ratio of approximately 110 accessible PS molecules per IMD dimer (Petrache et al., 2004; Millard et al., 2005). These figures fit quite well, especially considering that the amount of lipid available for binding is likely to be decreased by aggregation. The actin competition experiment shown in Figure 6.8 D gives an intriguing result. The FRET at the beginning of the experiment was at saturation, that is all IMD was bound to lipid. Addition of actin monomers appears to reduce the amount of IMD bound to the lipids. This appears to be a stable effect, as after each addition of actin the system was left to equilibrate. If this is the case, it suggests that IMD has a higher affinity for actin monomer than for the PS vesicles. A similar effect was seen with the vesicles containing 70 % PS, which IMD aggregates with a similar affinity to natural lipid mixtures (Figure 6.5), suggesting that IMD may bind actin monomers with higher avidity than membranes *in vivo*. The IMD was first believed to induce protrusions by bundling actin filaments (Yamagishi et al., 2004; Disanza et al., 2006),

although a more recent study suggested that IMD mediated actin bundling was an artefact of low salt conditions used causing IMD aggregation (Mattila et al., 2007). This FRET data may provide indirect evidence that IMD does bind actin monomer in physiological salt conditions. This experiment does require further repetition, and further confirmation of the IMD-actin interaction could also be probed by a FRET approach. These FRET data suggest that FRET may be a useful tool for measuring IMD-vesicle interactions, and this technique should be used in future investigations into this interaction. It remains to be seen whether this can also be used to detect interactions at lower concentrations of IMD and lipids level, which is something which the vesicle pelleting assays are unable to address with great accuracy

The experiments described here demonstrate that IMD-lipid interactions can be measured quantitatively by calculating the degree of vesicle aggregation in a pelleting assay. However it is still not entirely clear how the amount of pelleting is related to amount of IMD bound to the lipids. Due to IMD being the limiting factor for pelleting, it was assumed that most IMD was bound to vesicles, although this was not measured. Full understanding of the interaction would require this to be done.

Another limiting factor in these experiments is that the data were not compared to vesicles containing PI(4,5)P₂ as a major anionic constituent of the vesicles, as was used in other studies (Mattila et al., 2007; Saarikangas et al., 2009). However, the study from Mattila et al, 2007 did use an extremely high concentration of PI(4,5)P₂. This should be addressed in order to address the question of how these data relate to findings from other groups. However, vesicles containing both lipid mix and brain lipids were both pelleted by IMD (Figure 6.5), with an interaction of approximately 3-3.5 times less strongly than 100 % PS lipids. This suggests that this assay does have a readout for lipid membranes of biological interest.

The lack of tubulation observed by EM may prove to be useful. Simple binding of the IMD to membranes, with no invagination may make binding more easy to measure, as invagination may render sections of vesicles unable to be bound by IMD. Alternatively, if membranes have too great a curvature, IMD may not be able to bind to them as it would in a cell with relatively flat membrane, and binding could be underestimated. Further studies using

different size vesicles and different methods of measurement of bound IMD may therefore yield interesting results.

6.7 Conclusions and future perspectives

In this chapter, recombinant IMD and extruded vesicles were used to investigate the strength of interaction between the IMD and lipid membranes under several conditions. Strength of interaction was found to be diminished by reduction of surface charge, and by increasing ionic strength, suggesting that the interaction is an ionic one. Vesicles composed of more physiological lipids were shown to interact with IMD with a strength similar to vesicles containing 80 % PS and 20 % PC. A FRET approach was also used to probe this interaction and was found to be a sensitive method for investigating this question. Monomeric actin was found using this technique to decrease IMD binding to vesicles. Future work should define physiologically relevant lipid compositions, and further FRET experiments could also shed more light on the interaction. T-EM studies could be used to confirm the importance of membrane curvature for IMD-mediated tubulation, as the different physical strains imposed on the membranes in different sized vesicles may reveal more about the protrusive force the IMD is able to generate, in the absence of other cellular components.

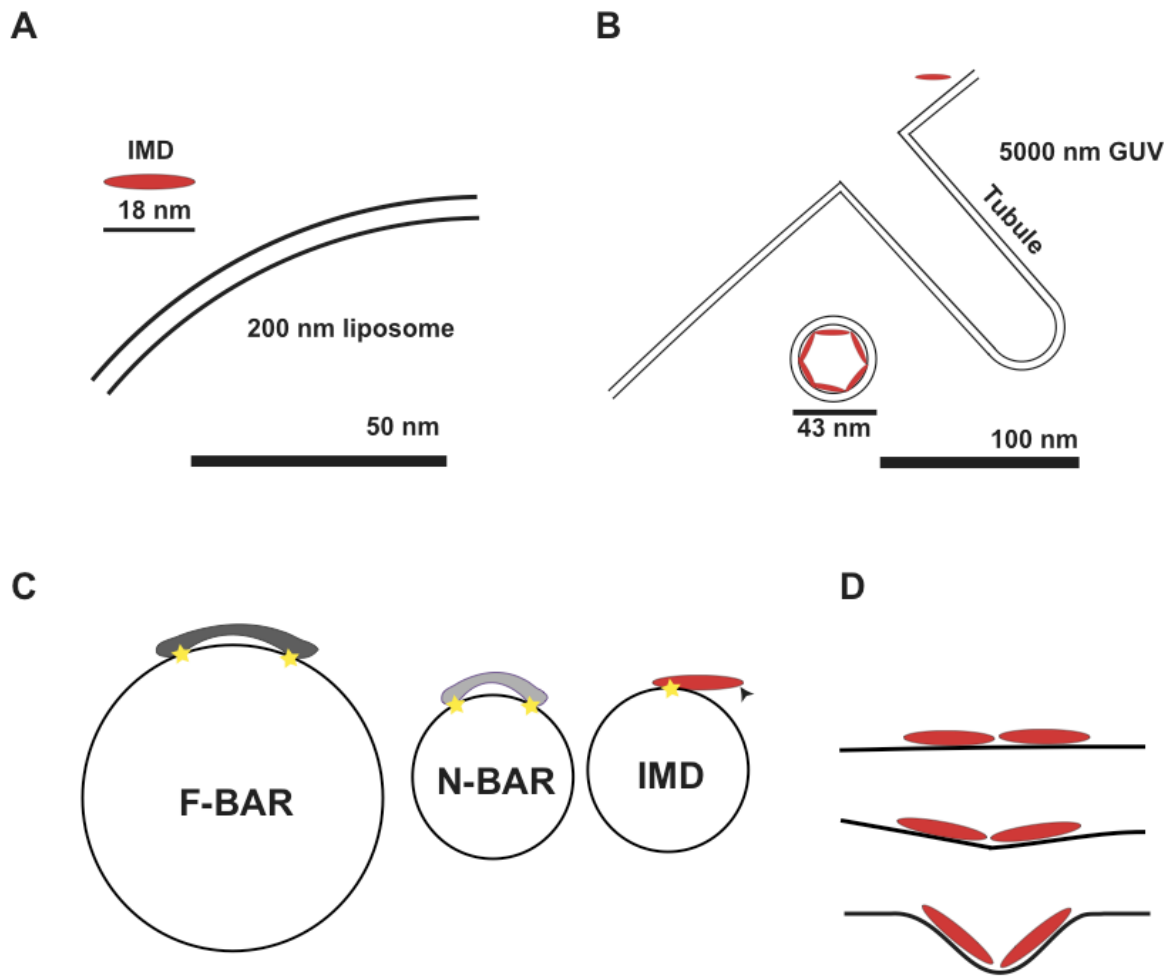


Figure 6.9 (A) Size relationship between the IMD and the vesicles used in the experiments reported above. Note the high degree of curvature of the membrane in the opposite orientation to that normally induced by IMD. (B) Scale cartoon of a 5 μm GUV, at the small end of the scale used in the Saarikangas 2009 study. The membrane surface is of much more neutral curvature, and may also be under less tension. Schematic invaginating tubule is shown, representative of the scale of IRSp53 IMD tubule reported by that study (43 nm). Also shown is cross section of such a tubule indicating how IMD may coat the interior. Black lines represent phospholipid headgroups; white space between them is the hydrophobic centre of the bilayer. (C) Structural basis for importance of vesicle size for membrane deformation to occur. F-BAR has larger span than N-BAR and so is able to bind larger vesicles and make correct contacts (shown as stars). Simplified IMD-vesicle showing that if curvature is too great, IMD cannot bind the lipid by two basic patches at one time (unbound patch denoted by arrowhead), and so cannot induce tubules. (D) Possible action of invagination by IMD on sufficiently uncurved membrane. Note (A) and (B) are to scale; (C) and (D) are schematic.

7 *In vitro* studies of the IMD

Cellular processes such as formation of filopodia are complex, involving many different components. IRSp53 interacts with various proteins, many of which through its SH3 domain, CRIB and PDZ motifs (see Chapter 1). The IMD is sufficient for the formation of filopodia-like protrusions, and for interactions with actin, Rac and membrane phospholipids (Miki et al., 2000; Miki and Takenawa, 2002; Yamagishi et al., 2004; Suetsugu et al., 2006a; Suetsugu et al., 2006b). *In vitro* experiments allow us to measure the strength of interaction between individual components in these systems, which adds to our understanding of the importance of these interactions *in vivo*.

In this chapter the expression and purification of IRSp53 IMD and two IRSp53 truncation proteins are described. These constructs may have a future use in biochemical assays and crystallography studies. Analytical ultracentrifugation (AUC) and native gel approaches to look at the oligomerization state of the IMD were carried out, and interaction studies between the IMD and Rac, also by AUC were also done. Finally, the generation, affinity purification and testing of a polyclonal antibody raised against IRSp53 IMD is described. This provides a useful tool for future study of this domain as it could be used for various experiments, including sensitive detection of IMD in future *in vitro* experiments.

7.1 Expression and purification of recombinant IMD

7.1.1 High affinity chromatography

Human IRSp53 IMD was expressed as a fusion protein with an N terminal GST (glutathione-S-transferase) tag. After expression in *E. coli*, purification was carried out using a high affinity chromatography approach where IMD was expressed as a fusion protein product with GST. This is outlined in Figure 7.1.

7.1.2 Ion exchange chromatography

SDS PAGE analysis of IMD elutions following high affinity chromatography glutathione agarose chromatography revealed the presence of extraneous protein contamination. Therefore, a second purification step was carried out using ion exchange chromatography on a carboxy-methane (CM) sepharose column. This approach allows separation of different

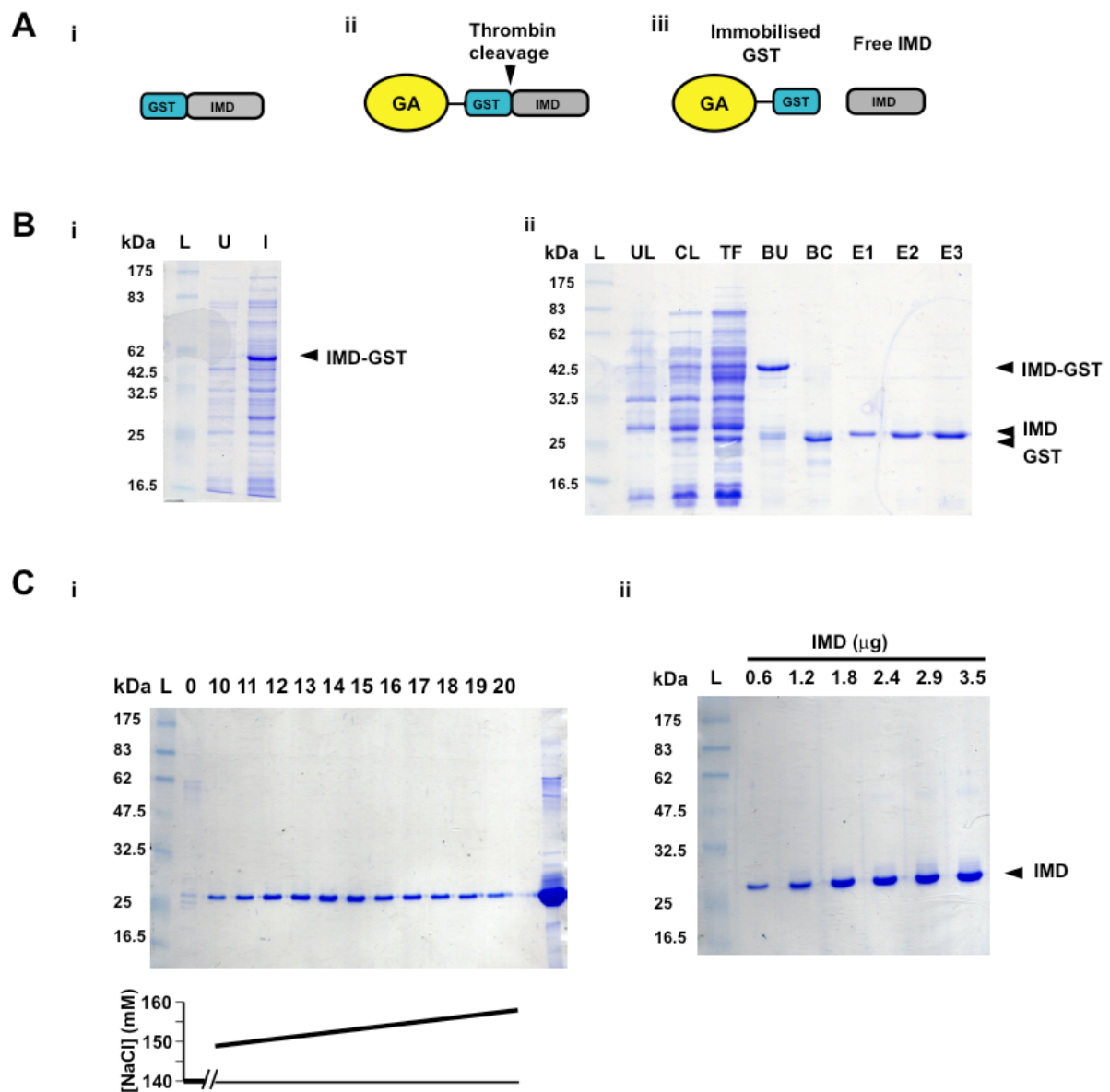


Figure 7.1 Purification of IMD-GST constructs. (A) Overview of the GST expression system (i) IMD was expressed as a fusion protein with GST at its N terminus. (ii) The construct is immobilised on glutathione agarose (GA) beads which GST binds with high affinity. After washing extraneous material, thrombin is added to cleave the fusion at the encoded thrombin cleavage site. (iii) GST remains bound to GA beads and protein is free in solution and is eluted from the column. (B) SDS PAGE gels showing affinity purification of IMD. (i) Induction of expression in BL21 DE3 pLysS cultures. U, uninduced; I, induced cultures after 18 h expression; L, protein size ladder. (ii) SDS PAGE gel showing purification of IMD. UL, uncleared lysate; CL, cleared lysate after centrifugation; TF, through flow – lysate post incubation with GA beads; BU, uncleaved beads with GST-IMD bound; BC, beads following overnight thrombin cleavage; E1-3, subsequent elutions each of 5 ml TRB buffer. (C) SDS PAGE gels used to analyse fractions after ion exchange chromatography on a CM sepharose column. Sample 0 is the sample prior to further purification, and 10-20 are the IMD-containing fractions. NaCl concentration of the column is shown below the gel. (B) increasing concentrations of IMD after pooling and concentration, suggesting that IMD is sufficiently pure for use in *in vitro* experiments.

proteins according to the ionic strength with which they bind to the CM group on the substrate. Many proteins bind at the initial low salt concentration, and are eluted in a NaCl gradient. For this approach to work, the target protein must carry a net positive charge. Thrombin cleavage after affinity purification is carried out at pH 8.0. IMD has a predicted isoelectric point (pI) of 8.83 (ExpASY ProtParam), and so carries only a small positive charge at pH 8.0. It was therefore dialysed into a buffer of pH 7.0 to increase the positive charge on the protein. To enhance binding to the column, a lower NaCl concentration of 140 mM was used. Protein was loaded on the column, followed by washing through with the low NaCl buffer to remove unbound protein. Elution was then started by a linear gradient of 140 NaCl to 320 mM. Fractions were analysed for protein first by Bradford assay and subsequently by SDS PAGE (Figure 7.1 C i). IMD typically was eluted over 10 fractions of 2 ml each, centring on NaCl concentration of 153 mM. Protein was then concentrated and analyzed by SDS PAGE (Figure 7.1 B).

7.2 Expression constructs for truncation mutants of IRSp53

Several studies postulate that IRSp53 is subject to some form of intramolecular inhibition between the SH3 domain and other parts of the protein (Miki et al., 2000; Krugmann et al., 2001; Disanza et al., 2006). Also the extreme C terminus of IRTKS, another IMD family member may have some effect on the function of the protein (Millard et al., 2007). X-ray crystallography studies tend to focus on smaller fragments of proteins, and so if co-crystals of IRSp53 and interacting partners are to be made, truncated IRSp53 constructs will be required. Two N-terminal IRSp53 truncations were generated in the present study – one terminating after the CRIB motif (1-289); and a second one which continued to the end of the SH3 domain (1-438)(Figure 7.1; Figure 7.2). Both constructs were generated as described in Chapter 3. Induction of protein expression for these constructs was initially attempted for 4 hours at 37 °C, and as shown in Figure 7.1, induction of protein expression was sufficiently strong for effective purification. In both cases the GST-IRSp53 truncation bound with high affinity to the glutathione agarose beads,

and cleavage by thrombin was efficient, as indicated by GST band appearing, and loss of the band corresponding to the uncleaved fusions protein. Interestingly, despite thorough elution, the beads retained a small amount of cleaved IRSp53 1-289.

7.3 Presence of thrombin cleavage site in IRSp53 1-438

A more significant problem is the lack of a single large band for the IRSp53 1-438 construct. Based on its amino acid sequence, IRSp53 1-438 is expected to have a molecular weight of 49 kDa (ExPASy ProtParam). However only lower molecular weight bands slightly larger than GST (26 kDa) are observed. To determine whether this was due to unspecific degradation of the polypeptide, samples of IRSp53 1-438 were incubated in different conditions (Figure 7.3 A). No significant degradation of the bands was observed, suggesting that there was no ongoing proteolytic activity. In the sample incubated at room temperature for 18 hours, there was the appearance of a band that ran at a similar size to IMD on the SDS PAGE gel (Figure 7.3 A, grey arrow). The fact that the bands only appeared after thrombin was added to the beads, and the lack of non-specific degradation suggested that a specific endopeptidase may be responsible, and the first peptidase to consider is the thrombin used to cleave the protein from the glutathione agarose. The IRSp53 1-438 protein sequence was searched for presence of a thrombin cleavage site using the Peptide Cutter tool (www.expasy.ch). One thrombin site was found, cutting the polypeptide after Arg 363 (Figure 7.3 B). Examination of the whole IRSp53 sequence revealed that this was the sole thrombin cleavage site. The IRSp53 1-438 truncation protein is predicted to have a molecular weight of 48.8 kDa, and the two fragments after thrombin cleavage are predicted to be 40.4 and 8.4 kDa. The fragments seen on the cleavage gel (Figure 7.2 B iv) have an apparent molecular weight of between 25 kDa and 32.5 kDa, which do not seem to correspond with the expected sized fragments. However as it was clear that this construct would undergo thrombin mediated proteolysis, the construct was cloned using the original restriction sites into a pGEX 4T2 construct which has been altered to include a Rhinovirus S3C protease recognition site in place of the thrombin cleavage site. This construct expressed successfully (Figure 7.3 B I) and appeared to run at the correct molecular weight in SDS PAGE (Figure 7.3 B ii). Cleavage was done with S3C protease,

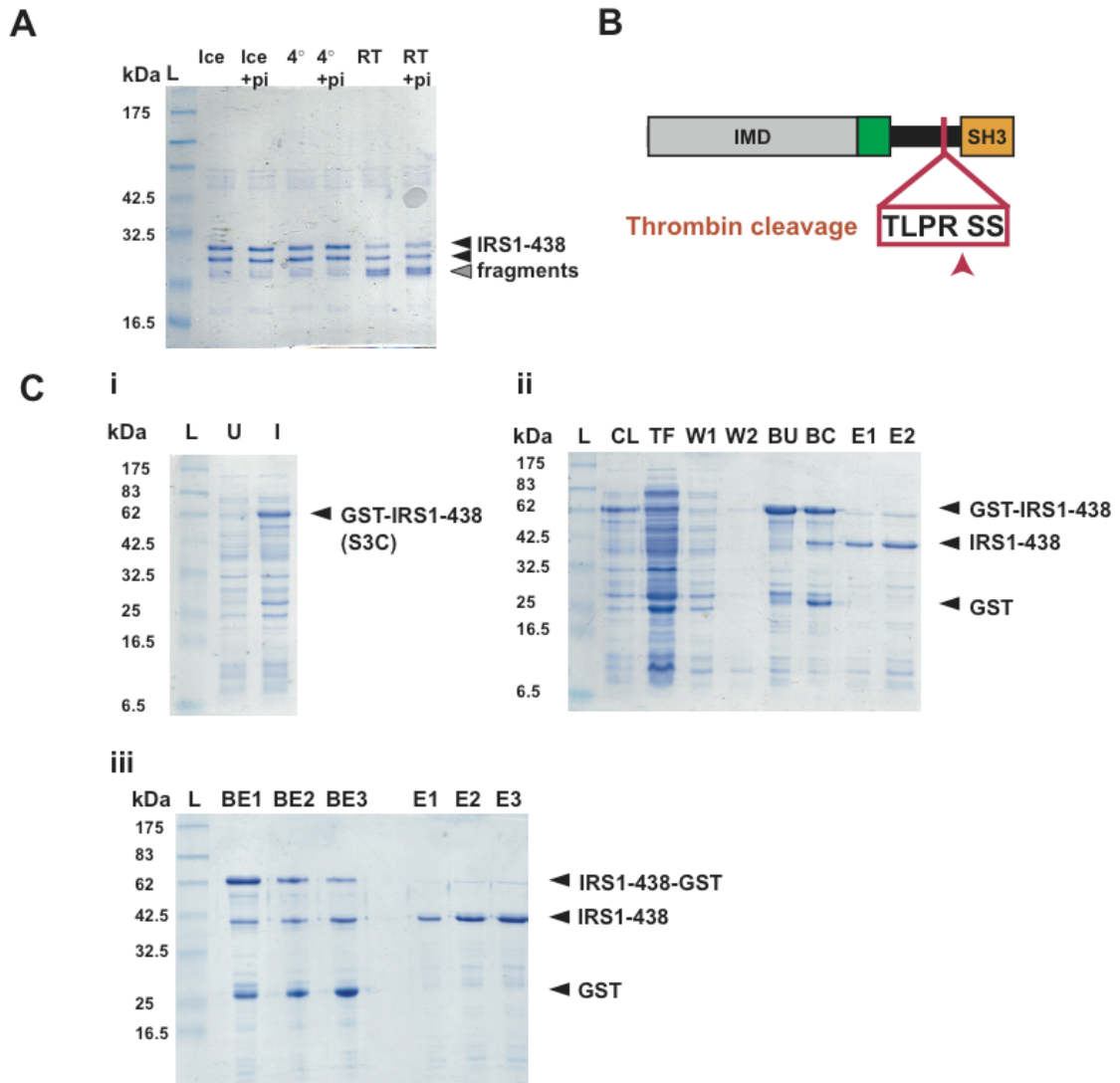


Figure 7.3 (A) Results of a study into the stability of the IRSp53 1-438 protein. IRSp53 1-438 in elution buffer was incubated overnight with or without PMSF protein inhibitor (pi) on ice, at 4 °C or at room temperature. Fragments remained visible, suggesting no large scale degradation is occurring. In room temperature sample an accumulation of protein that ran similarly to IMD was observed. (B) Schematic showing location of thrombin cleavage site in the IRSp53 1-438 construct. (C) (i and ii), induction and purification of IRSp53 1-438 with S3C protease. (iii) Determination of quantity of S3C protease for cleavage. GST-IRSp53 1-438 beads were incubated with 20, 40 and 80 units of protease (1, 2 and 3, respectively), and eluted after incubation for 60 minutes (E1-3). Some uncleaved protein was still present after the final elution suggesting that in excess of 80 units of protease is required, however as can be seen in E3.

using 20 units per 2 l preparation. However, cleavage was not complete, as observed by a significant proportion of the uncleaved protein on the beads post treatment (Figure 7.3 C ii, BC). The beads were divided and incubated with different concentrations of S3C protease (Figure 7.3 C iii) corresponding to total amounts as denoted in the figure legend. These results suggested that the majority of IRSp42 1-438 could be freed from the beads using 80 units of S3C protease.

7.4 Insolubility of IRSp53 truncation constructs

IRSp53 1-438 as eluted from the glutathione agarose beads was not sufficiently pure for use in experiments, as background was visible in samples analyzed by SDS PAGE. An attempt was made to purify it using a CM sepharose column, as used for purification of IMD (7.1.2). IRSp53 1-438 has a predicted pI of 9.00 (ProtParam), which is comparable to that of IMD (8.9). Because of this it was decided to use the same buffer conditions as were used for IMD (including pH 7.0; 140 mM NaCl). A CM sepharose column gel is shown in Figure 7.4. As expected due to the higher pI and larger size than IMD, this construct required a higher NaCl concentration to elute from the column (approx. 166 mM). As the quantity of protein recovered from the column was much lower than anticipated, an attempt was made to estimate sample concentrations by measuring absorbance at 280 nm. However no signal was detected, suggesting that there was a negligible concentration of protein present. Subsequent attempts to purify this construct using CM sepharose chromatography were attempted. Each time however, a white precipitate was observed after dialysis into the CM loading buffer. To attempt to recover any unprecipitated protein filtration was done with a 0.1 μ m filter, and the filtered solution was loaded onto the CM column and the column run as it was initially. No protein elution was observed by Bradford assay, suggesting that the protein was not eluted from the column. An elution with high NaCl (200 mM) buffer was used to try to elute strongly bound protein, but no protein elution was detected, suggesting that any protein loaded had precipitated from solution. The IRSp53 1-289 construct was also found to be unstable in the purification conditions used. The construct showed strong binding to the glutathione substrate and efficient cleavage, such as was observed during purification of the IMD construct. However, precipitation often occurred during dialysis

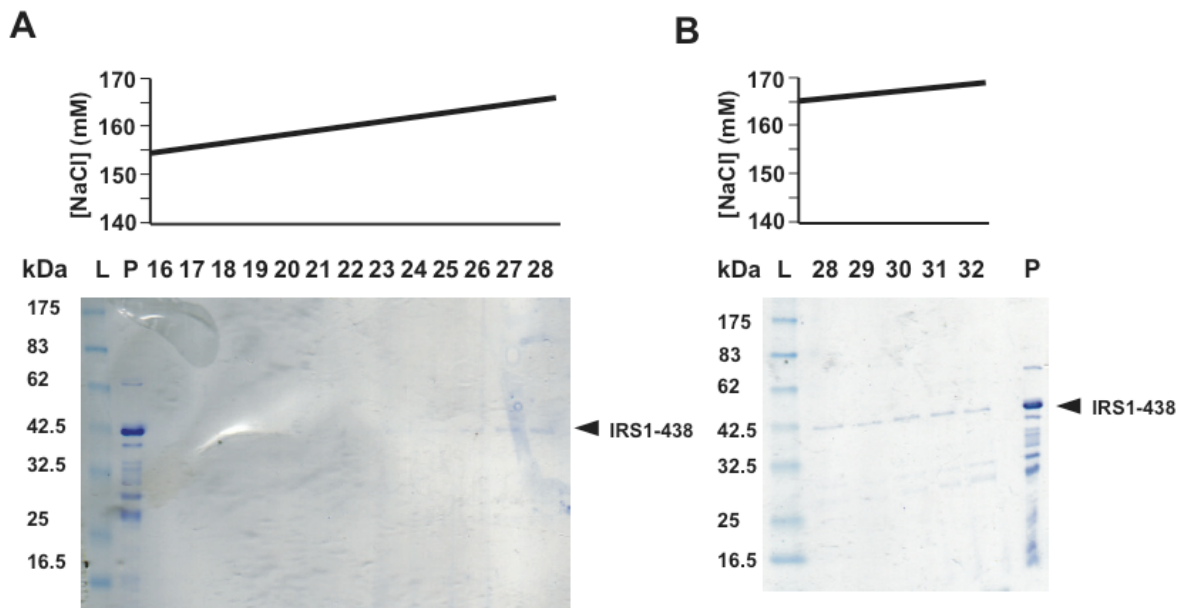
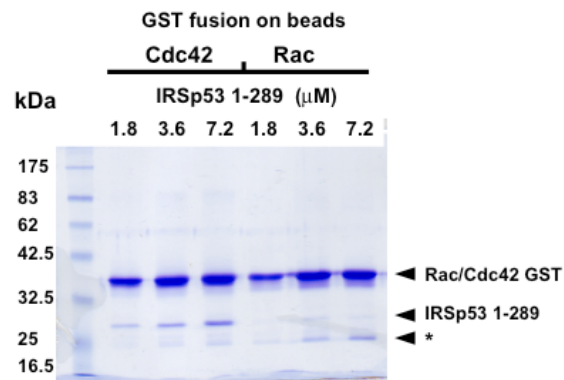


Figure 7.4 Gels from CM sepharose chromatography of IRSp53 1-438. 1.5 mg of protein was loaded at (0). Bradford assay showed significant protein levels only in fractions 26-42, these fractions were then analyzed by SDS PAGE on 12 % gels and stained for protein with Coomassie. Small bands corresponding to IRSp53 1-438 are visible for fractions 36-42. Column was run at 1 ml/minute and washed through with 20 ml low salt buffer to remove unbound protein before elution with a linear NaCl gradient of 140-360 mM, NaCl concentration indicated above the gels.

A Bound



B Unbound

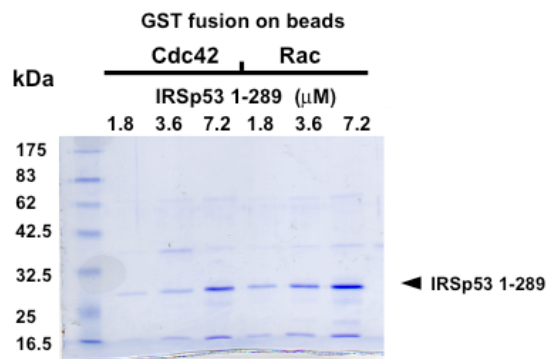


Figure 7.5 A preliminary pulldown experiment suggests IRSp53 1-289 and its breakdown product interact with Rac and Cdc42 differently. IRSp53 1-289 in the concentrations indicated was incubated with 30 μl of saturated GST-Rac wt or GST Cdc42 wt saturated glutathione agarose beads for 30 minutes before pelleting and washing the beads. IRSp53 1-289 appears to bind to wt Cdc42 beads but not Rac beads. The breakdown product, of a similar size to IMD is enriched in the Rac beads but not Cdc42.

prior to loading onto the ion exchange column.

One preparation of IRSp53 1-289 did not precipitate, and it was possible to do a pulldown assay to test binding to wild type small GTPases Rac and Cdc42 (Figure 7.5), although it was not possible to repeat the assay. IRSp53 1-289 was incubated with wild type Rac or Cdc42 immobilised as GST fusions on glutathione agarose beads. The GTPase proteins were pelleted by centrifugation and presence of proteins in supernatant and pellet examined by electrophoresis. IRSp53 1-289 was found to associate with the Cdc42 beads, whereas a smaller breakdown product that was often observed in the IRSp53 1-298 preparations appeared to associate with Rac. This may suggest that the CRIB motif contained in the construct is effective in binding Cdc42 specifically as expected. However, due to the regular precipitation of IRSp53 1-289 it was decided to focus on other aspects of the project.

7.5 Native gel electrophoresis of IRSp53 IMD suggests the IMD is predominantly a dimer in solution.

The IMD has a high degree of structural homology with BAR domains, and is believed to exert its effect on membranes in an analogous fashion, by binding directly to the membrane and causing shape change (Millard et al., 2005; Mattila et al., 2007). A recent structural study has indicated that the BAR domain of FCHO-1 has a dissociation constant of 2.5 μM , which suggests that the dimerisation is reversible, and that a proportion of the domain exists as monomer (Henne et al., 2007). It is currently believed that the IMD exists as a strong dimer, as shown by sedimentation velocity experiments (Millard et al., 2005). This was further investigated using native gel electrophoresis (Figure 7.6). IMD was loaded at concentrations of 1, 5 and 10 μM and rabbit actin at 1 μM was used as a control. Actin has a molecular weight of 42 kDa, which is intermediate between the expected molecular weights of IMD dimer (57 kDa) and monomer (28.5 kDa). Actin was in G buffer, to ensure it was in monomeric G-actin form. A denaturing SDS PAGE gel was run alongside with identical loading volumes and concentrations. The IMD band in the denaturing gel (Figure 7.6 A) runs at a lower molecular weight than the actin. In the native gel (Figure 7.6 B), which does not denature samples, the IMD bands for 5 and 10 μM concentrations can clearly be seen. The

actin band runs at a lower molecular weight, suggesting that the principle band seen in the IMD is the dimer.

7.6 Analytical ultracentrifugation studies of IMD dimerisation.

Analytical ultracentrifugation (AUC) analysis allows determination of the sedimentation coefficient (s) of a molecular species, and has most notably been used in the characterization of ribosomal subunits, whose names derive from their Svedberg values. The s value is a measure of the rate a species migrates through a centrifugal field; the greater its s value the more rapid the migration, and can therefore detect oligomerization state. One method of carrying out AUC experiments is sedimentation velocity (AUC-SV), in which the sample is centrifuged at sufficient velocity to achieve pelleting of the species of interest.

Here, AUC-SV data from experiments carried out are shown in order to address the question of the oligomerization state of IMD in solution. (A) shows a representative experiment where IMD and wild type Rac recombinant proteins were incubated together prior to AUC-SV. The data were fitted using Sedfit to solve the Lamm equation, which describes the migration of species in a centrifugal field, and fits the frictional coefficient (Lamm, 1929). As expected from the different molecular weights of Rac (21 kDa) and IMD (57 kDa dimer), when analysed individually the two proteins had different fitted s values, with the larger IMD having a higher s value of 2.0, compared with the Rac value of approximately 1.4. When the mixture of Rac and IMD was analyzed, the IMD peak remained at the same s value (2.0), whereas the Rac fitted s reduced to 1.2. This change in the lower s value Rac peak was possibly a result of the fitting parameters being more heavily weighed towards the higher s value IMD species. No peak at higher s than 2.0 was detected, suggesting that no larger complex was formed by IMD and Rac interaction. Importantly for addressing the question of IMD dimerisation, only one main population of the protein is observed using this sensitive method, suggesting that IMD does exist principally as a dimer in solution. In the study suggesting that FCHO2 BAR domain exists in a monomer-dimer equilibrium, it was found that dimerisation was decreased under reducing conditions, due to reduction of the disulphide bond between monomers (Shimada et al., 2007). An experiment was done to compare IMD at 5 μ M and 10 μ M in presence and absence of 5 mM DTT (Figure 7.1 B). In absence of added DTT, IMD at both concentrations was fitted to an s of 2.0. In presence of 5 mM DTT,

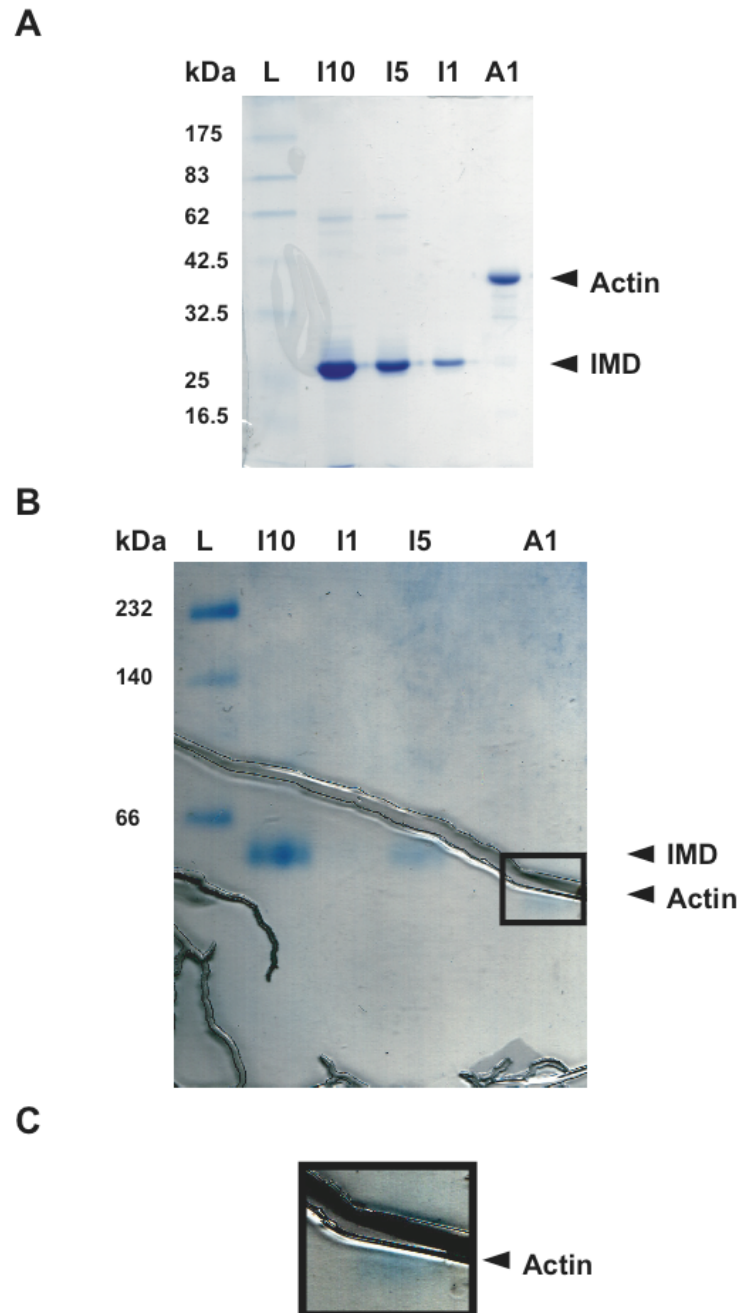


Figure 7.6 Native PAGE and denaturing SDS PAGE of IMD, using rabbit actin as a control. (A) Denaturing SDS PAGE of 1, 5 and 10 μM IMD (I1, I5, I10) and 1 μM G actin (A1). IMD has a molecular weight of 28.5 kDa, and actin of 42 kDa, and the proteins both run at approximately their expected molecular weight. (B) Native PAGE electrophoresis using the blue native system carried out as described in Materials and Methods. (C) shows the band corresponding to G-actin.

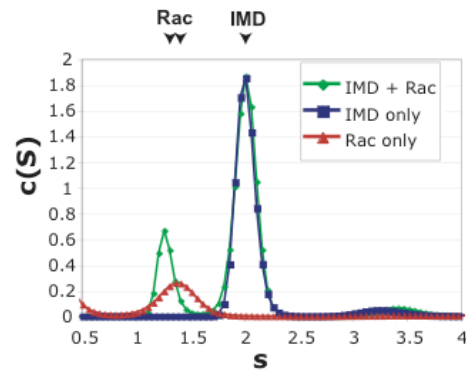
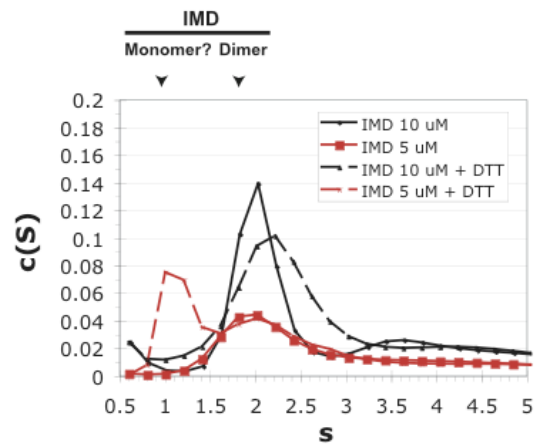
A**B**

Figure 7.7 Analytical ultracentrifugation experiments with IRSp53 IMD and Rac1. (A) Rac alone (4.4 μ M) IMD alone (18 μ M) and a Rac-IMD mixture were analyzed by sedimentation velocity. Rac was fitted to as value of 1-1.4, and frictional coefficient of 1.7 and IMD to a single main peak at 2.0 S, and frictional coefficient 2.34. No interaction between Rac and IMD could be observed as no higher s species was detected. The IMD Rac mixture was fitted with an intermediate frictional coefficient of 2.35. RMSD of fits was lower than 8×10^{-3} , indicating a close fit to the data. (B) Sedimentation velocity experiments with 5 μ M and 10 μ M IMD, both in presence and absence of 5 mM DTT as a reducing agent. Again, IMD was fitted to a peak with S value 2.0. In presence of DTT a lower S value peak is visible, possibly corresponding to monomeric IMD.

a new peak is observed, at lower s value of 1.0. As the main peak at 2.0 s is likely to correspond to IMD dimer, this lower s species may indicate the presence of the monomeric form.

7.7 Affinity purification of a polyclonal antibody raised against IRSp53 IMD

Polyclonal antibodies against specific proteins and domains are a useful tool for research, as they allow sensitive, detection of protein at low concentrations. At the beginning of this work no antibody against the IMD was available, so it was decided to generate one raised in sheep. Antibody raised in sheep was chosen because it has two main advantages. Epitope tags HA and myc are detected in this laboratory using mouse and rabbit antibody, respectively, and so antibody raised in sheep could be used simultaneously with these antibodies, with no cross reaction with the respective secondary antibodies. Also, as sheep is a much larger animal more antiserum can be raised, increasing the chances of obtaining a higher concentration of antibody. One ml of 2 mg/ml IMD purified as described earlier in this chapter was sent to the Scottish Blood Service for inoculation of a sheep according to their standard protocols. Antibody affinity purification was done as described in Materials and Methods. The preimmune serum and first bleed (approx 180 ml) were tested by Western blot against purified recombinant IMD and no detectable interaction was observed. The third and final bleed was tested by Western blot, and found to selectively bind to overexpressed IMD-myc (Figure 7.8 A). To confirm that the band observed was indeed IMD-myc, the lysate was also probed with mouse anti-myc antibody, revealing a band which corresponded to the sheep anti IMD band. The antibody was also tested against beads used in IRSp53-His protein expression, and bound to full-length IRSp53-His (Figure 7.8 B i). This was confirmed using an antibody against the N terminal his tag (Figure 7.8 B i). Purified recombinant IMD was also used to test the antibody, and was found that it was bound, and little background was observed. Finally, IRSp53 1-289 was analyzed by Western blotting and recombinant protein (after only affinity purification stage) was found to be bound by the antibody, although a high amount of background was observed (Figure 7.8 C i). The same construct, overexpressed as an HA tagged protein in cos-7 cells was detected by the antibody and verified by probing the same quantity of lysate on another blot with an anti HA antibody. Thus the affinity purified antibody from bleed 3 can detect IMD recombinant protein, albeit with high background, and also IMD as expressed in cell lines. Preliminary experiments to stain fixed Cos-7 cells

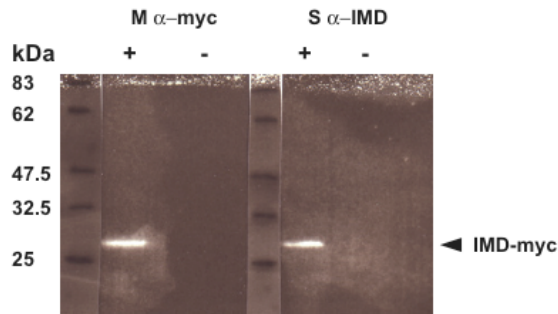
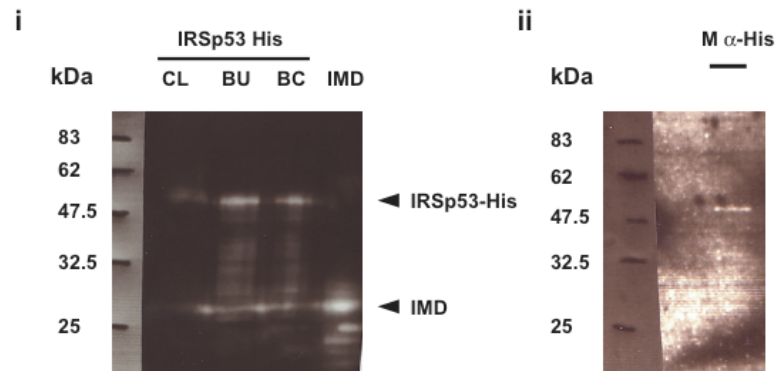
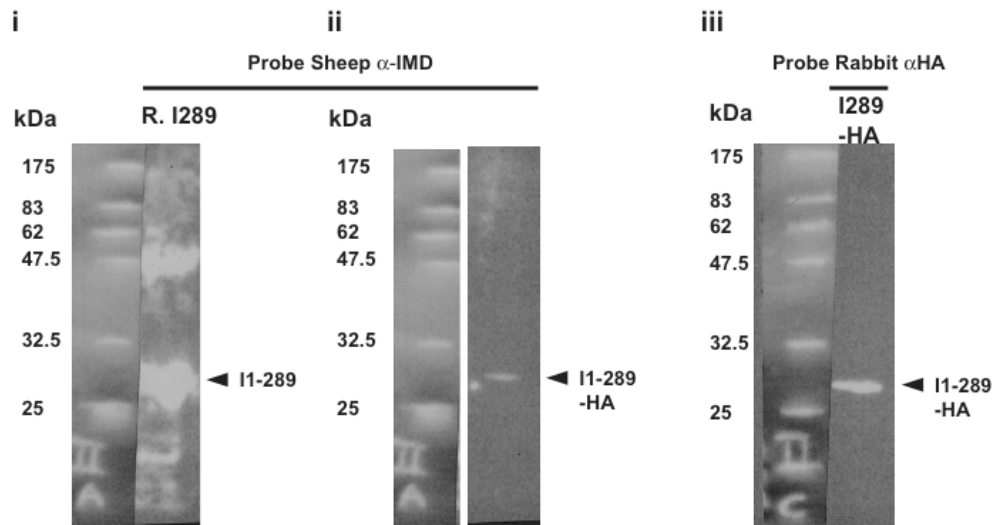
A**B****C**

Figure 7.8 Testing of sheep anti IMD antibody against overexpressed protein in cells and recombinant protein. (A) the third batch of the affinity purified sheep IMD antiserum (1 in 100) was tested by probing Western blot of Cos-7 cells overexpressing IMD-myc (+). A strong and specific band corresponding to the IMD was observed. This was verified by probing with mouse anti myc (1 in 200). No signal was detected in untransfected lysates (-). (B) During early attempts to induce IRSp53-His expression the IMD antibody was used successfully to detect low levels of expression in induced cultures. Purified IMD was also analyzed and was found to be bound by the sheep antibody. (C) IMD antibody binds to first elution of IRSp53 1-289 with a high amount of background. The antibody also binds to IRSp53 1-289 overexpressed as HA-tagged protein in Cos-7 cells.

overexpressing showed the antibody was no better than background, although further studies need to be done to confirm this.

7.8 Discussion

The data presented here describe the generation of several tools which will advance the understanding of the activity of IRSp53 *in vitro*. Although difficulties were had in stability of the IRSp53 1-289 and 1-438 constructs, it is possible that future work could optimise purification conditions and employ them for interaction studies or crystallization attempts. IRSp53 has been shown to readily bind to activated Cdc42, and this may cause some change in the conformation of IRSp53, allowing binding of other partners (Govind et al., 2001; Krugmann et al., 2001). The binding of IRSp53 by the IMD to activated Rac is as yet unclear, although the interaction appears to be weaker than that of the CRIB binding to Cdc42, as several studies have been able to detect Cdc42 binding, but not Rac (Govind et al., 2001; Krugmann et al., 2001; Disanza et al., 2006). The mechanism of Rac binding to the IMD is as yet unclear, whereas the binding of Cdc42 to CRIB domains has been well characterized (Krugmann et al., 2001; Disanza et al., 2006). The understanding of the function of IRSp53 is limited in this respect, and the study of the IRSp53 1-289 or a similar length truncation may yield information about this aspect of IRSp53. The IRSp53 1-438 construct may also provide data on the role of the SH3 domain in the full length protein, as this has not yet been fully investigated. Further pulldown experiments with the IMD and the 1-289 protein are required, however the data shown in Figure 7.5 may suggest that the CRIB motif may affect interactions with the IMD.

The generation of an IMD – specific antibody provides a useful tool for the further study of the IMD. However, its generation does provide a useful tool for further study of the IMD. The affinity purified sheep serum specifically detected IMD and IRSp53 1-289 which was overexpressed in cells, and also IMD and IRSp53 recombinant protein (Figure 7.8). Future studies could utilise the anti-IMD antibody immunoprecipitation experiments in order to identify IMD binding partners, without the requirement for an epitope tag. That the antibody is able to bind to Western blotted recombinant proteins may mean that the antibody can be used for high sensitivity detection of the protein following *in vitro* experiments. Finally, although initial experiments suggested that the antibody was not suitable for immunohistochemistry, further optimization may allow it to be used for this application. The

antibody could also be used for immunogold labelling in conjunction with electron microscopy, which could further aid the understanding of the activity of IMD at the nanometre scale.

The IMD is thought to exist as a tight dimer in solution, as measured by AUC sedimentation equilibrium and SDS PAGE under non-reducing conditions (Millard et al., 2005). The related IMD of MIM has also been determined to be a dimer, as only the dimer form is detected when measured by multi angle light scattering (Lee et al., 2007). However, some studies have suggested that some structurally related BAR domains show a monomer-dimer equilibrium. Work done by Peter et al, 2004 determined a K_d for amphiphysin BAR of 6 μM by analytical ultracentrifugation, and Henne et al in a 2007 study calculated the K_d of F-BAR FCHo2 to be 2.5 μM by analytical gel filtration. Micromolar dissociation constants suggest that these proteins exist in the cell in monomer-dimer equilibrium. In the present study, native gel electrophoresis (Figure 7.6) and AUC (Figure 7.7) showed that the dimer is the main species present. However, under stronger reducing conditions there was a species visible by AUC which may correspond to the monomer. This is in agreement with the findings by Millard et al, 2005 that the disulphide bond is necessary for IMD dimerisation, as gel electrophoresis under non-reducing conditions shows an IMD dimer, which is prevented by mutation of a cysteine which is predicted to form a disulphide bond. However, in the work by Millard et al, DTT was present in the AUC experiments, and no monomer was observed. DTT can be used to induce reducing conditions, resulting in reduction of disulphide bonds. Further investigations are needed to fully address the question of IMD dimerisation but it appears likely that it exists predominantly in the dimer form. This is supported by the structural data which reveal that the IMD dimer has a more substantial dimer interface double the size of that found in amphiphysin, (Tarricone et al., 2001; Millard et al., 2005).

8 General Discussion

IRSp53 functions downstream of both Rac and Cdc42 in the formation of lamellipodia and filopodia, and may induce filopodia-like protrusions directly, making it the focus of considerable interest. It contains protein-protein interaction domains including an SH3 domain, which mediates interactions with many proteins involved in actin cytoskeleton regulation. It also contains the IMD, a novel domain that has homology to BAR domains, and which can induce formation of filopodia-like structures when overexpressed in cells.

8.1 IRSp53 domain structure and family

IRSp53 is a protein of around 53 kDa, and has a modular domain structure that is outlined in Figure 1.2. In addition to the N-terminal IMD, which is described in detail below, IRSp53 possesses several domains through which it interacts with various partners. Adjacent to the C terminal of IMD is a partial CRIB (Cdc42 and Rac interactive binding) motif, through which IRSp53 binds active Cdc42, possibly causing the release of an intramolecular inhibition within the protein (Govind et al., 2001; Krugmann et al., 2001). A canonical SH3 (Src-homology 3) domain is located in the middle of the protein, and has been shown to be responsible for mediating the interactions of IRSp53 with many partners in the formation of lamellipodia and filopodia, including WAVE2, Eps8, and N-WASP (Okamura-Oho et al., 1999; Miki et al., 2000; Funato et al., 2004; Lim et al., 2008). Alternative splicing of the IRSp53 mRNA results in different isoforms of IRSp53, which vary only at the very C terminal, leaving a 511 amino acid portion of the sequence unchanged in all isoforms (Okamura-Oho et al., 2001). The long and medium (L- and M-) isoforms have a WH2 (WASP homology 2), domain, which is able to bind G actin, whereas the short (M) isoform has a PDZ (PSD95, DlgA zo-1) domain-binding motif, which is implicated in the interactions of IRSp53 with PDZ-containing proteins such as PSD-95 (Okamura-Oho et al., 2001; Soltau et al., 2002). The IMD is shared with another family of proteins termed MIM (missing in metastasis) (Yamagishi et al., 2004). The IMD of MIM proteins has a high structural similarity to that of IRSp53, but shares a relatively low sequence identity of 19 %. The two domains are proposed to have similar functions but have some functional differences (Bompard et al., 2005; Mattila et al., 2007; Saarikangas et al., 2009). The IRSp53 and MIM family proteins are also divergent in domain structure, with a major difference being that MIM lacks an SH3 domain (Scita et al., 2008). Similar to some IRSp53 isoforms, MIM has a

proline-rich domain located adjacent to its WH2 domain, which is responsible for its interaction with receptor protein tyrosine phosphatase RPTP δ (Woodings et al., 2003).

IRSp53 is expressed throughout the body with elevated levels of expression in the brain, in the cortex, hippocampus, cerebellum and striatum areas, and is particularly enriched in dendritic spines and the post synaptic density, where it has been implicated in dendritic outgrowth (Abbott et al., 1999; Choi et al., 2005). IRSp53 derives its name from its initial discovery as a protein that is phosphorylated downstream of the insulin receptor (Yeh et al., 1996). Further studies have identified a residue in the predicted unstructured region of the protein as being the principle phosphorylation target, and phosphorylation status has not been found to affect the activity of the protein (Heung et al., 2008).

8.2 Phenotype of IRSp53 in the cell and effect of knockdowns

Overexpression of IRSp53 in cultured cells results in a distinctive filopodia-like phenotype that has been observed by many investigators, with many actin-rich protrusions visible (Govind et al., 2001; Krugmann et al., 2001; Nakagawa et al., 2003; Millard et al., 2005; Disanza et al., 2006; Lim et al., 2008). Antibody staining has also detected endogenous IRSp53 to filopodia and lamellipodia (Nakagawa et al., 2003). Several groups have utilised a knock down strategy to measure the importance of IRSp53 for cellular structures. Reducing levels of IRSp53 in cultured neuronal cells decreases the number and density of dendritic spines, suggesting a role for IRSp53 in initiation of the formation of these structures, which are similar to filopodia (Choi et al., 2005). RNAi has been used to examine the effects of knockdown of IRSp53 on formation of filopodia by active Cdc42, and a decrease of around 40 % in the number of filopodia formed was observed (Disanza et al., 2006). Similarly, Lim et al, in a 2009 study observed a decrease in N-WASP induced filopodia of around 80 % when IRSp53 was knocked out using RNAi, which suggests that IRSp53 is a major interactor in N-WASP induced filopodia formation. Lim et al also reported that no filopodia were observed cells lacking N-WASP, and so these data suggest that IRSp53 is an important component of filopodia. Suetsugu and coworkers, in a 2006 study, found that reduction of cellular IRSp53 by RNAi retarded lamellipodia formation in response to active Rac.

8.3 IRSp53 and lamellipodia

The Scar/WAVE complex has long been known to be important in Arp2/3 complex activation (Machesky and Insall, 1998), and it was known that this was activated by Rac activation, although Rac could not interact directly (Machesky and Insall, 1998). IRSp53 may act as an intermediate in this interaction (Miki et al., 2000). IRSp53 binds WAVE2 via its SH3 domain, and the disruption of this interaction results in a reduction of Rac-mediated lamellipodia (Miki et al., 2000). The work from Miki et al also identified a 229 residue portion of IRSp53 (termed the RCB, Rac binding domain), which is a truncated version of the IMD that binds to active Rac. Rac binding may also be inhibited in the full length IRSp53, giving further evidence for a potential intramolecular inhibition within the protein (Miki and Takenawa, 2002). However, the Rac interaction with IRSp53 has not been observed by other groups.

In addition to providing a direct link between Rac signalling and WAVE-mediated Arp2/3 actin polymerization, there is some evidence that IRSp53 also contributes to Rac activation, and may be involved in local maintenance of active Rac at specific sites (Funato et al., 2004; Connolly et al., 2005). One study found that IRSp53 interacted with Eps8, and that the resultant complex was important for Rac-induced Rac activation, possibly by formation of an Eps8/Abi1/Sos-1 Rac GEF complex (Funato et al., 2004). IRSp53 also interacts with another Rac activating factor, Tiam1 and is required for Tiam1-induced membrane ruffling (Connolly et al., 2005). The work by Connolly et al does not demonstrate enhanced Rac activation as was seen in the work from Funato et al, but it does demonstrate enhanced binding of IRSp53 to both activated Rac and WAVE complex. These studies suggest a complex role for IRSp53 in the mediation of Rac driven actin cytoskeleton modifications.

8.4 IRSp53 and filopodia

The role of IRSp53 in lamellipodia formation would appear to be principally mediated via its interaction with the WAVE complex, as discussed above. The role of IRSp53 in filopodia formation may be mediated through multiple interactions with a large number of different interactors, which are discussed here. Filopodia formation is a complex process, which requires different proteins to interact in order to coordinate actin filament elongation,

formation of parallel actin bundles and assembly of all the required components at the required location and in response to the correct intracellular cues (Faix and Rottner, 2006).

A potent mechanism of initiation of actin filament elongation is by Arp2/3 complex mediated polymerization, which can be activated by N-WASP downstream of Cdc42 activation (Millard et al., 2004). A recent study has demonstrated that IRSp53 interacts with N-WASP, and is important for N-WASP-mediated filopodia formation, as IRSp53 knockdown reduced the filopodia phenotype (Lim et al., 2008). Another mechanism of filopod elongation is the continuous polymerization of actin at the barbed end, which is usually blocked by capping protein (Cooper and Sept, 2008). ENA/VASP proteins prevent filament capping and allow processive extension of the actin filament (Krause et al., 2003). IRSp53 interacts with ena/VASP family member Mena (Krugmann et al., 2001). IRSp53 and Mena were found to increase filopodia formation synergistically, and this was prevented by abrogation of their interaction by mutation of residues in the SH3 domain of IRSp53. This interaction may be controlled by Cdc42, as colocalization of IRSp53 and Mena increased in the presence of activated Cdc42 (Krugmann et al., 2001). Another experiment in this study used a small N terminal fragment of IRSp53 to inhibit the activity of the full length protein, and this was found to disrupt filopodia production induced by Cdc42 activation, again implicating IRSp53 downstream of Cdc42 in filopodia formation.

Filopodia formation requires parallel bundling of the actin filaments (Faix and Rottner, 2006). Eps8 has been identified as a binding partner of IRSp53, and it is proposed that they are able to synergistically bundle actin filaments *in vitro*, with much higher efficiency than either protein in isolation (Disanza et al., 2006). The simultaneous overexpression of the two proteins also results in more protrusions, and the overexpression of IRSp53 may change the localization of Eps8, recruiting it to the sites of filopodia formation (Disanza et al., 2006). This interaction is increased in the presence of active Cdc42, suggesting that this is likely to be physiologically relevant (Disanza et al., 2006).

In addition to having interactions with other proteins involved in filopodia formation, IRSp53 may be able to induce filopodia formation directly via its IMD. This is discussed in the following section.

8.5 The IMD

The IMD is a dimerising helical domain located at the N terminal of IRSp53 and related proteins such as the MIM family proteins, and was the main focus of this thesis. The IMD was first characterised as a Rac-binding domain, in a study by Miki et al, in 2000, when a slightly shortened version of the domain (229 residues; termed the RCB, or Rac Binding domain) was found to bind activated Rac in a pull down assay. The IMD was identified as a conserved 250 residue domain which is sufficient to induce formation of filopodia-like protrusions when expressed in cells (Yamagishi et al., 2004). It was also proposed that the activity of the IMD was mediated by actin filament bundling, and this was substantiated by experiments showing actin filament binding and bundling by IMD *in vitro* (Yamagishi et al., 2004). The determination of the crystal structure of the IMD seemed to provide a structural basis for this theory (Millard et al., 2005). The IMD dimer is approximately 180 angstroms in length, comparable to the distance between filaments in actin bundles. It also has patches of basic residues at the ends of the dimer distal ends, which when mutated result in an inability of the IMD or the full length protein to either induce filopodia in cells, or to bundle actin filaments *in vitro* (Millard et al., 2005).

8.6 The IMD and BAR domains

The structure discovered by Millard *et al* also revealed that the IMD has structural similarity to BAR domains (Figure 1.4). BAR domains are banana-shaped helical dimers that can bind to curved membrane surfaces and are involved in either detection, or induction of curvature by their concave face (Peter et al., 2004). BAR domains have been identified in a large number of proteins, many of which are involved in endocytosis (Peter et al., 2004). BAR domains display a preference for specific vesicle sizes, and it has been hypothesized that one role of the BAR domain is as a mechanism for localizing proteins to regions of specific curvature, such as at different stages of clathrin mediated endocytosis (Peter et al., 2004). The BAR domain superfamily contains several different mechanisms for membrane remodelling. In addition to the induction of membrane curvature by basic patches located on the concave face of the dimer, N-BAR domains also possess an N terminal amphipathic helix, which inserts into the membrane, enhancing curvature and improving binding strength. In recognition of the similarities between the IMD and BAR domains, the IMD is now

considered to be a BAR domain family member, or 'I-BAR', inverted BAR domain (Lim et al., 2008).

The structural similarity of the IMD to BAR domains raises questions about the role of IMD in the cell. In a study by Suetsugu et al 2006, IRSp53 was found to bind to PIP3 and PS vesicles, via the RCB, a truncated IMD. The interaction with PIP3 was found to enhance its interaction with activated Rac and WAVE2, perhaps mimicking the conditions encountered in the cell. In a subsequent study from the same research group, the addition of IMD to lipid vesicles caused disruption of the vesicles, suggesting that like BAR domains the RCB can cause membrane deformation. The work by Suetsugu et al also suggested that activated Rac was required for membrane deformation, although subsequent studies showed that the same phenomenon could be observed in the absence of Rac. This study found that IMD preferentially binds vesicles containing PS and PIP3, although other lipids were not tested. The case for IMD lipid interactions was put forward more strongly in a more recent study (Mattila et al., 2007). In this study, the IMD of MIM was found to cause striking finger-like protrusions on the surface of lipid vesicles, oriented in the opposite sense to tubules formed by BAR domains, reinforcing the theory of inverse BAR activity. Native gel electrophoresis interaction studies were carried out and the IMD of MIM was found to bind to vesicles containing a high concentration of PI(4,5)P₂ and PI(3,4)P₂, but not PIP₃ or PS or a number of other lipid types. In a pelleting assay the IMD of both MIM and IRSp53 was pelleted with vesicles containing PI(4,5)P₂ but not by vesicles containing only PC, PE and PS. This study also performed site directed mutagenesis experiments to attempt to identify the regions of the IMD responsible for actin and lipid binding, and it was found that they could generate a mutant which retained near wild type actin binding ability, but reduced PI(4,5)P₂ binding, and found that this construct produced significantly fewer protrusions. However, it is not clear whether this effect may be due to reduced ability to bind actin. Mattila et al also claimed that the IMD localises to the membrane in cells rather than the actin filaments, although it is questionable whether fluorescence microscopy offers sufficient resolution to make this claim. This study was followed up by another from the same group, which sought to expand upon these findings (Saarikangas et al., 2009). This study used electron microscopy of IMD from different proteins and species to observe the tubules formed. By examining the electron density they were able to locate the IMD to the interior of the tubules formed, suggesting that

the IMD induces tubules in the inverse orientation to BAR domains. The same study also showed that IMD added to large vesicles with fluorescently labelled PI(4,5)P₂ showed formation of focal areas, which is caused by the PI(4,5)P₂ being drawn into local areas of high concentration by the IMD. Saarikangas et al were also able to image the formation of a nascent tubule from one of these foci. However, only PI(4,5)P₂ was tested, and it would be advantageous to know whether this effect would also be seen with other membrane lipids.

In the present study, interaction studies with IRSp53 IMD and vesicles composed of different phospholipids were carried out. An interaction was detected between the IMD and anionic phospholipids, and it was determined that IMD had a similar interaction with vesicles containing 70 % PS as to brain lipids or an artificial lipid mix designed to mimic membranes (Chapter 6). The ionic nature of the IMD-lipid interaction was also supported by the finding that interactions between IMD and lipids is reduced in elevated salt conditions (Figure 6.6). PI(4,5)P₂ was not required for this interaction. Electron microscopy experiments were also carried out to attempt to visualize tubulation, but this was not observed (Figure 6.7). This may be attributable to the smaller extruder pore size (100 nm diameter) used in this study, compared with that used by Mattila et al (1 µm), and which may present an excessively curved surface which prevents tubulation.

Saarikangas et al also looked at the tubules formed by different IMDs using electron microscopy. A range of tubule sizes formed by the different IMDs was observed, and this agrees with the findings by Peter et al that BAR domains form tubules of different sizes. This may provide a reason for some of the small structural differences observed between the IMDs for which structural data already exists, and indicate a reason for divergence between the different IMDs (Millard et al., 2005; Lee et al., 2007). This was backed up by in cell data with differently labelled IMDs from different species, and it was found that IMDs with different approximate diameters segregate into different protrusions. This provides further evidence that the membrane deformation observed in electron microscopy experiments is responsible for filopodia like protrusions seen in cells. This study may also have revealed another facet of the IMD interaction with membranes – a helical insertion similar to that observed in N-BAR domains **Gallop 2006**. This was detected in MIM, and like in N-BAR domains it was found to increase the stability of the protein-membrane interaction, and also

increased the diameter of the tubule formed. This is maybe slightly counterintuitive, as in the case of the N-BAR the helix is thought to provide extra curvature by a “wedge” effect. In the case of the IMD, tubulation must already occur against the resistant force of the internal leaflet of the membrane, and it is unclear how insertion of a wedge would aid in this process.

Fluorescence recovery after photobleaching (FRAP) has been used to investigate the dynamics of different IMDs within cell protrusions, revealing a $t_{1/2}$ of 8.3 s (MIM) and 5.2 (IRSp53), and much slower recovery of around 68 s for *C. elegans* - which correlates with the narrower tubules formed by the *C. elegans* IMD (Saarikangas et al., 2009). This is consistent with the FRAP data obtained in the present study, where IMD was found to recover with a $t_{1/2}$ of 7.3 s. However, Saarikangas et al reported a recovery of approaching 80 %, whereas in this study a lower recovery was detected (37.5 %). It is not clear why this difference is observed, but may be due to differences in cell types used, or the experimental procedures followed, or the precise areas of the cells which were used for the experiments. In the present study, IRSp53 dynamics were also analyzed by FRAP, and suggest that the full-length protein recovers faster than IMD, and to a higher level. This suggests that IRSp53 has a less strong interaction with the protrusions, and may be due to some regulation of the IMD activity within the full length protein. Further studies are required with different conditions to obtain more information on the dynamics of the IMD and IRSp53 in protrusions.

8.7 The IMD and actin

As discussed above, the IMD was initially thought to induce filopodia by actin filament bundling, although recent advances have led some to postulate that actin is not required at all for the activity. When the IMD was first characterised as a filopodia-inducing domain, one of the pieces of evidence that gave this credence was the actin-bundling activity demonstrated in *in vitro* experiments. This was also done in the study by Millard et al, and enhanced by site directed mutagenesis which revealed that a mutant which was unable to bind actin was also unable to induce protrusions in cells. As part of their study on the IMD in 2007, Mattila et al attempted to further probe the nature of the IMD and actin pelleting experiments. They contended that the experiments done by Millard et al, and Yamagishi et al were carried out in low salt conditions which led to precipitation of IMD, and so the actin bundling was an artefact of the experimental conditions. This was reinforced by dynamic light scattering

(DLS) data which showed that IMD precipitation occurs below 100 mM KCl. The bundling experiments done by Millard et al were done in F-buffer, which has an ionic strength of 50 mM, and according to the DLS data from Mattila, this would have led to some precipitation of the IMD. However, in studies by Yamagishi and Disanza 100 mM KCl was used, and actin bundling was observed. In addition, as described above that work by Disanza et al showed that IRSp53 and Eps8 appear to work synergistically to bundle actin filaments, suggesting a physiological role for IRSp53 in filament bundling. This may suggest that IRSp53-mediated filament bundling requires other components, and the work from Lim et al, 2009 which compared the binding efficiencies of IRSp53 and actin-bundling protein, Fascin, and found that while a concentration of only 60 nM of fascin was required for actin bundling, 5 to 10 μ M of IRSp53 was required.

In addition to the *in vitro* work done to look at IMD-actin interactions, work has been done in cells. Actin has been observed in IRSp53 and IMD-induced protrusions, using both phalloidin staining, which binds to filamentous actin in fixed cells, and fluorescently labelled beta actin, which labels both filamentous and monomeric actin. However, the presence of actin in these protrusions does not necessarily signify that it is required, and so functional studies and higher resolution techniques are required to determine its role. Several groups have used drugs to disrupt actin dynamics and observe the effect this has on the protrusions mediated by IMD and IRSp53. Mattila et al found that treatment of cells with Latrunculin A reduced the number of extending protrusions, and Yang et al 2009 found that Latrunculin B caused cells to round up entirely, suggesting that actin is required for extension and long term persistence are dependent on actin filaments. Suetsugu et al, 2006b, on the contrary, could still observe protrusions in the presence of Latrunculin, and concluded that actin is not required for these structures and that they are purely membrane-based.

In the experiments conducted as part of the present work, cells were treated with cytochalasin D, another actin destabilizing compound, and this was found to prevent extension of IMD rich protrusions (Figures 4.8 and 4.9). Prior to treatment, many of the protrusions displayed growth of an average of 0.15 μ m per second, however treatment with cytD 5 μ M prevented all extension, and caused a small amount of retraction. Treatment of cells with a high concentration of cytD for an extended period of time caused some retraction of protrusions,

but many protrusions still persisted. This suggests that although actin polymerization is required for extension of IMD-mediated protrusions, actin filaments may not be required for long-term maintenance of the structures. This is in agreement with the conclusions of Mattila et al, but in disagreement with Suetsugu 2006, who concluded that actin is not required for these structures. FRAP experiments carried out in the present study suggest that treatment of cells with cytochalasin D does not have a significant effect on the recovery rate of IMD (Figure 5.4). This may suggest that the immobile fraction of IMD is not affected by actin dynamics in the protrusion.

It appears that the requirement for actin in these protrusions is a complex issue, and another recent study has shown that the presence of actin may be transient in some cases (Yang et al., 2009). Yang et al used time-lapse microscopy and fluorescently labelled IMD and actin and found that actin filaments sometimes leave the protrusions after formation, and can be replaced by other filaments. IMD-induced protrusions, although containing actin, were found to have fewer filaments, and in a less ordered array, suggesting that filament formation is not well regulated, and may be the result of actin filaments entering the protrusions by chance. These detailed EM images indicate that detection actin by phalloidin staining is not sufficient to understand its role in these protrusions. The literature surrounding the IMD suggests that the contribution of actin to the formation of IMD-mediated and IRSp53-mediated protrusions may be complex.

8.8 Open questions for IRSp53 and the IMD

Despite an ever-growing body of literature on the study of IRSp53, many questions on its role in the cell remain unanswered. Many studies have examined the interactions of IRSp53 with binding partners involved in cytoskeleton regulation (Table 1.1). However, the regulation of IRSp53 activity has not yet been closely examined. Future work could focus on determining the effect of binding of other proteins on the conformation of IRSp53, possibly involving structural studies of IRSp53 in complex with its binding partners. It would be of particular interest to determine the effect of Rac and Cdc42 binding to IRSp53, as these are the two master switches for filopodia and lamellipodia formation, and may have significantly different effects on IRSp53 conformation.

The role of the IMD in the context of the full-length protein is yet to be fully elucidated, and this should be a priority of future studies in this field. The IMD may play roles in localization of IRSp53; detection, induction or stabilization of membrane curvature; localization or binding to actin filaments; or some combination of these roles. It also needs to be determined whether the IMD is strongly involved in protrusion formation or it is principally important for the localization of IRSp53. The regulation of the IMD protrusive activity in the full-length protein also remains to be properly investigated. It is likely that this is subject to some regulation, because IRSp53 is localized to the tips of lamellipodia, and yet does not constitutively induce formation of filopodia (Nakagawa et al., 2003). Further work is required to investigate factors regulating the protrusive activity of the IMD.

Whilst the present study attempted to examine the importance of lipid composition for IMD-mediated protrusions, it is still not clear what effect lipid composition has on IMD mediated membrane deformation in the cell. Further studies on the lipid specificity of the IMD binding are required in order to determine whether IMD-mediated protrusion formation is dependent on membrane composition, and therefore if this is partially responsible for the regulation of IMD-mediated membrane deformation. The data presented in Chapter 4 suggest that the protrusions generated by IMD are at least partly dependent on actin filaments, and this is in agreement with other studies (Mattila et al., 2007; Saarikangas et al., 2009; Yang et al., 2009). Future studies should attempt to investigate the involvement of actin filaments on protrusions mediated by the full-length IRSp53 protein.

Much is now known about individual properties of IRSp53 and the IMD. Future work should be focussed on integrating these various aspects to elucidate the regulation and formation of actin structures by this protein.

9 References

- Abbott, M.A., D.G. Wells, and J.R. Fallon. 1999. The insulin receptor tyrosine kinase substrate p58/53 and the insulin receptor are components of CNS synapses. *J Neurosci.* 19:7300-8.
- Abo, A., J. Qu, M.S. Cammarano, C. Dan, A. Fritsch, V. Baud, B. Belisle, and A. Minden. 1998. PAK4, a novel effector for Cdc42Hs, is implicated in the reorganization of the actin cytoskeleton and in the formation of filopodia. *Embo J.* 17:6527-40.
- Abou-Kheir, W., B. Isaac, H. Yamaguchi, and D. Cox. 2008. Membrane targeting of WAVE2 is not sufficient for WAVE2-dependent actin polymerization: a role for IRSp53 in mediating the interaction between Rac and WAVE2. *J Cell Sci.* 121:379-90.
- Alpi, E., E. Landi, M. Barilari, M. Serresi, P. Salvadori, A. Bachi, and L. Dente. 2009. Channel-interacting PDZ protein, 'CIPP', interacts with proteins involved in cytoskeletal dynamics. *Biochem J.* 419:289-300.
- Aratyn, Y.S., T.E. Schaus, E.W. Taylor, and G.G. Borisy. 2007. Intrinsic dynamic behavior of fascin in filopodia. *Mol Biol Cell.* 18:3928-40.
- Aspenstrom, P., U. Lindberg, and A. Hall. 1996. Two GTPases, Cdc42 and Rac, bind directly to a protein implicated in the immunodeficiency disorder Wiskott-Aldrich syndrome. *Curr Biol.* 6:70-5.
- Bishop, A.L., and A. Hall. 2000. Rho GTPases and their effector proteins. *Biochem J.* 348 Pt 2:241-55.
- Bockmann, J., M.R. Kreutz, E.D. Gundelfinger, and T.M. Bockers. 2002. ProSAP/Shank postsynaptic density proteins interact with insulin receptor tyrosine kinase substrate IRSp53. *J Neurochem.* 83:1013-7.
- Bompard, G., S.J. Sharp, G. Freiss, and L.M. Machesky. 2005. Involvement of Rac in actin cytoskeleton rearrangements induced by MIM-B. *J Cell Sci.* 118:5393-403.
- Brown, P.H., and P. Schuck. 2006. Macromolecular size-and-shape distributions by sedimentation velocity analytical ultracentrifugation. *Biophys J.* 90:4651-61.
- Chesarone, M.A., and B.L. Goode. 2009. Actin nucleation and elongation factors: mechanisms and interplay. *Curr Opin Cell Biol.* 21:28-37.

- Choi, J., J. Ko, B. Racz, A. Burette, J.R. Lee, S. Kim, M. Na, H.W. Lee, K. Kim, R.J. Weinberg, and E. Kim. 2005. Regulation of dendritic spine morphogenesis by insulin receptor substrate 53, a downstream effector of Rac1 and Cdc42 small GTPases. *J Neurosci.* 25:869-79.
- Connolly, B.A., J. Rice, L.A. Feig, and R.J. Buchsbaum. 2005. Tiam1-IRSp53 complex formation directs specificity of rac-mediated actin cytoskeleton regulation. *Mol Cell Biol.* 25:4602-14.
- Cooper, J.A. 1987. Effects of cytochalasin and phalloidin on actin. *J Cell Biol.* 105:1473-8.
- Cooper, J.A., E.L. Buhle, Jr., S.B. Walker, T.Y. Tsong, and T.D. Pollard. 1983. Kinetic evidence for a monomer activation step in actin polymerization. *Biochemistry.* 22:2193-202.
- Cooper, J.A., and D. Sept. 2008. New insights into mechanism and regulation of actin capping protein. *Int Rev Cell Mol Biol.* 267:183-206.
- Crepin, V.F., F. Girard, S. Schuller, A.D. Phillips, A. Mousnier, and G. Frankel. 2010. Dissecting the role of the Tir:Nck and Tir:IRTKS/IRSp53 signalling pathways in vivo. *Mol Microbiol.* 75:308-23.
- Cullen, P.J., J.J. Hsuan, O. Truong, A.J. Letcher, T.R. Jackson, A.P. Dawson, and R.F. Irvine. 1995. Identification of a specific Ins(1,3,4,5)P4-binding protein as a member of the GAP1 family. *Nature.* 376:527-30.
- Disanza, A., S. Mantoani, M. Hertzog, S. Gerboth, E. Frittoli, A. Steffen, K. Berhoerster, H.J. Kreienkamp, F. Milanesi, P.P. Di Fiore, A. Ciliberto, T.E. Stradal, and G. Scita. 2006. Regulation of cell shape by Cdc42 is mediated by the synergic actin-bundling activity of the Eps8-IRSp53 complex. *Nat Cell Biol.* 8:1337-47.
- Faix, J., and K. Rottner. 2006. The making of filopodia. *Curr Opin Cell Biol.* 18:18-25.
- Farsad, K., N. Ringstad, K. Takei, S.R. Floyd, K. Rose, and P. De Camilli. 2001. Generation of high curvature membranes mediated by direct endophilin bilayer interactions. *J Cell Biol.* 155:193-200.
- Frankel, G., and A.D. Phillips. 2008. Attaching effacing Escherichia coli and paradigms of Tir-triggered actin polymerization: getting off the pedestal. *Cell Microbiol.* 10:549-56.
- Frost, A., R. Perera, A. Roux, K. Spasov, O. Destaing, E.H. Egelman, P. De Camilli, and V.M. Unger. 2008. Structural basis of membrane invagination by F-BAR domains. *Cell.* 132:807-17.
- Fujiwara, T., A. Mammoto, Y. Kim, and Y. Takai. 2000. Rho small G-protein-dependent binding of mDia to an Src homology 3 domain-containing IRSp53/BAIAP2. *Biochem Biophys Res Commun.* 271:626-9.

- Funato, Y., T. Terabayashi, N. Suenaga, M. Seiki, T. Takenawa, and H. Miki. 2004. IRSp53/Eps8 complex is important for positive regulation of Rac and cancer cell motility/invasiveness. *Cancer Res.* 64:5237-44.
- Gallop, J.L., C.C. Jao, H.M. Kent, P.J. Butler, P.R. Evans, R. Langen, and H.T. McMahon. 2006. Mechanism of endophilin N-BAR domain-mediated membrane curvature. *Embo J.* 25:2898-910.
- Govind, S., R. Kozma, C. Monfries, L. Lim, and S. Ahmed. 2001. Cdc42Hs facilitates cytoskeletal reorganization and neurite outgrowth by localizing the 58-kD insulin receptor substrate to filamentous actin. *J Cell Biol.* 152:579-94.
- Habermann, B. 2004. The BAR-domain family of proteins: a case of bending and binding? *EMBO Rep.* 5:250-5.
- Henne, W.M., H.M. Kent, M.G. Ford, B.G. Hegde, O. Daumke, P.J. Butler, R. Mittal, R. Langen, P.R. Evans, and H.T. McMahon. 2007. Structure and analysis of FCHO2 F-BAR domain: a dimerizing and membrane recruitment module that effects membrane curvature. *Structure.* 15:839-52.
- Hering, H., and M. Sheng. 2001. Dendritic spines: structure, dynamics and regulation. *Nat Rev Neurosci.* 2:880-8.
- Heung, M.Y., B. Visegrady, K. Futterer, and L.M. Machesky. 2008. Identification of the insulin-responsive tyrosine phosphorylation sites on IRSp53. *Eur J Cell Biol.* 87:699-708.
- Hill, T.L., and M.W. Kirschner. 1982. Subunit treadmill of microtubules or actin in the presence of cellular barriers: possible conversion of chemical free energy into mechanical work. *Proc Natl Acad Sci U S A.* 79:490-4.
- Hori, K., D. Konno, H. Maruoka, and K. Sobue. 2003. MALS is a binding partner of IRSp53 at cell-cell contacts. *FEBS Lett.* 554:30-4.
- Itoh, T., K.S. Erdmann, A. Roux, B. Habermann, H. Werner, and P. De Camilli. 2005. Dynamin and the actin cytoskeleton cooperatively regulate plasma membrane invagination by BAR and F-BAR proteins. *Dev Cell.* 9:791-804.
- Jaiswal, J.K., and S.M. Simon. 2003. Total internal reflection fluorescence microscopy for high-resolution imaging of cell-surface events. *Curr Protoc Cell Biol.* Chapter 4:Unit 4 12.
- Krause, M., E.W. Dent, J.E. Bear, J.J. Loureiro, and F.B. Gertler. 2003. Ena/VASP proteins: regulators of the actin cytoskeleton and cell migration. *Annu Rev Cell Dev Biol.* 19:541-64.
- Krugmann, S., I. Jordens, K. Gevaert, M. Driessens, J. Vandekerckhove, and A. Hall. 2001. Cdc42 induces filopodia by promoting the formation of an IRSp53:Mena complex. *Curr Biol.* 11:1645-55.

- Lamm, O. 1929. Die differentialgleichung der ultrazentrifugierung. *Arkiv for matematik, astronomi och fysik*. 21 B:1-4.
- Lazarides, E., and K. Weber. 1974. Actin antibody: the specific visualization of actin filaments in non-muscle cells. *Proc Natl Acad Sci U S A*. 71:2268-72.
- Lee, S.H., F. Kerff, D. Chereau, F. Ferron, A. Klug, and R. Dominguez. 2007. Structural basis for the actin-binding function of missing-in-metastasis. *Structure*. 15:145-55.
- Leung, I.W., and N. Lassam. 1998. Dimerization via tandem leucine zippers is essential for the activation of the mitogen-activated protein kinase kinase kinase, MLK-3. *J Biol Chem*. 273:32408-15.
- Lim, K.B., W. Bu, W.I. Goh, E. Koh, S.H. Ong, T. Pawson, T. Sudhakaran, and S. Ahmed. 2008. The Cdc42 effector IRSp53 generates filopodia by coupling membrane protrusion with actin dynamics. *J Biol Chem*. 283:20454-72.
- Machesky, L.M., S.J. Atkinson, C. Ampe, J. Vandekerckhove, and T.D. Pollard. 1994. Purification of a cortical complex containing two unconventional actins from *Acanthamoeba* by affinity chromatography on profilin-agarose. *J Cell Biol*. 127:107-15.
- Machesky, L.M., and A. Hall. 1997. Role of actin polymerization and adhesion to extracellular matrix in Rac- and Rho-induced cytoskeletal reorganization. *J Cell Biol*. 138:913-26.
- Machesky, L.M., and R.H. Insall. 1998. Scar1 and the related Wiskott-Aldrich syndrome protein, WASP, regulate the actin cytoskeleton through the Arp2/3 complex. *Curr Biol*. 8:1347-56.
- Machesky, L.M., and S.A. Johnston. 2007. MIM: a multifunctional scaffold protein. *J Mol Med*. 85:569-76.
- Massari, S., C. Perego, V. Padovano, A. D'Amico, A. Raimondi, M. Francolini, and G. Pietrini. 2009. LIN7 mediates the recruitment of IRSp53 to tight junctions. *Traffic*. 10:246-57.
- Masuda, M., S. Takeda, M. Sone, T. Ohki, H. Mori, Y. Kamioka, and N. Mochizuki. 2006. Endophilin BAR domain drives membrane curvature by two newly identified structure-based mechanisms. *Embo J*. 25:2889-97.
- Matsuda, S., S. Yokozaki, H. Yoshida, Y. Kitagishi, N. Shirafuji, and N. Okumura. 2008. Insulin receptor substrate protein 53 (IRSp53) as a binding partner of antimetastasis molecule NESH, a member of Abelson interactor protein family. *Ann Oncol*. 19:1356-7.
- Mattila, P.K., and P. Lappalainen. 2008. Filopodia: molecular architecture and cellular functions. *Nat Rev Mol Cell Biol*. 9:446-54.

- Mattila, P.K., A. Pykalainen, J. Saarikangas, V.O. Paavilainen, H. Vihinen, E. Jokitalo, and P. Lappalainen. 2007. Missing-in-metastasis and IRSp53 deform PI(4,5)P2-rich membranes by an inverse BAR domain-like mechanism. *J Cell Biol.* 176:953-64.
- Matus, A. 2000. Actin-based plasticity in dendritic spines. *Science.* 290:754-8.
- May, R.C. 2001. The Arp2/3 complex: a central regulator of the actin cytoskeleton. *Cell Mol Life Sci.* 58:1607-26.
- May, R.C., and L.M. Machesky. 2001. Phagocytosis and the actin cytoskeleton. *J Cell Sci.* 114:1061-77.
- McMahon, H.T., and J.L. Gallop. 2005. Membrane curvature and mechanisms of dynamic cell membrane remodelling. *Nature.* 438:590-6.
- Miki, H., S. Suetsugu, and T. Takenawa. 1998. WAVE, a novel WASP-family protein involved in actin reorganization induced by Rac. *Embo J.* 17:6932-41.
- Miki, H., and T. Takenawa. 2002. WAVE2 serves a functional partner of IRSp53 by regulating its interaction with Rac. *Biochem Biophys Res Commun.* 293:93-9.
- Miki, H., H. Yamaguchi, S. Suetsugu, and T. Takenawa. 2000. IRSp53 is an essential intermediate between Rac and WAVE in the regulation of membrane ruffling. *Nature.* 408:732-5.
- Millard, T.H., G. Bompard, M.Y. Heung, T.R. Dafforn, D.J. Scott, L.M. Machesky, and K. Futterer. 2005. Structural basis of filopodia formation induced by the IRSp53/MIM homology domain of human IRSp53. *Embo J.* 24:240-50.
- Millard, T.H., J. Dawson, and L.M. Machesky. 2007. Characterisation of IRTKS, a novel IRSp53/MIM family actin regulator with distinct filament bundling properties. *J Cell Sci.* 120:1663-72.
- Millard, T.H., S.J. Sharp, and L.M. Machesky. 2004. Signalling to actin assembly via the WASP (Wiskott-Aldrich syndrome protein)-family proteins and the Arp2/3 complex. *Biochem J.* 380:1-17.
- Miyahara, A., Y. Okamura-Oho, T. Miyashita, A. Hoshika, and M. Yamada. 2003. Genomic structure and alternative splicing of the insulin receptor tyrosine kinase substrate of 53-kDa protein. *J Hum Genet.* 48:410-4.
- Morita-Ishihara, T., J. Terajima, H. Watanabe, and H. Izumiya. 2009. Interaction between enterohemorrhagic Escherichia coli O157:H7 EspFu and IRSp53 induces dynamic membrane remodeling in epithelial cells. *Jpn J Infect Dis.* 62:351-5.
- Morton, W.M., K.R. Ayscough, and P.J. McLaughlin. 2000. Latrunculin alters the actin-monomer subunit interface to prevent polymerization. *Nat Cell Biol.* 2:376-8.

- Mullins, R.D., J.A. Heuser, and T.D. Pollard. 1998. The interaction of Arp2/3 complex with actin: nucleation, high affinity pointed end capping, and formation of branching networks of filaments. *Proc Natl Acad Sci U S A*. 95:6181-6.
- Nakagawa, H., H. Miki, M. Nozumi, T. Takenawa, S. Miyamoto, J. Wehland, and J.V. Small. 2003. IRSp53 is colocalised with WAVE2 at the tips of protruding lamellipodia and filopodia independently of Mena. *J Cell Sci*. 116:2577-83.
- Nobes, C.D., and A. Hall. 1995. Rho, rac, and cdc42 GTPases regulate the assembly of multimolecular focal complexes associated with actin stress fibers, lamellipodia, and filopodia. *Cell*. 81:53-62.
- Oda, K., T. Shiratsuchi, H. Nishimori, J. Inazawa, H. Yoshikawa, Y. Taketani, Y. Nakamura, and T. Tokino. 1999. Identification of BAIAP2 (BAI-associated protein 2), a novel human homologue of hamster IRSp53, whose SH3 domain interacts with the cytoplasmic domain of BAI1. *Cytogenet Cell Genet*. 84:75-82.
- Okamura-Oho, Y., T. Miyashita, K. Ohmi, and M. Yamada. 1999. Dentatorubral-pallidoluysian atrophy protein interacts through a proline-rich region near polyglutamine with the SH3 domain of an insulin receptor tyrosine kinase substrate. *Hum Mol Genet*. 8:947-57.
- Okamura-Oho, Y., T. Miyashita, and M. Yamada. 2001. Distinctive tissue distribution and phosphorylation of IRSp53 isoforms. *Biochem Biophys Res Commun*. 289:957-60.
- Paavilainen, V.O., E. Bertling, S. Falck, and P. Lappalainen. 2004. Regulation of cytoskeletal dynamics by actin-monomer-binding proteins. *Trends Cell Biol*. 14:386-94.
- Penzes, P., R.C. Johnson, R. Sattler, X. Zhang, R.L. Huganir, V. Kambampati, R.E. Mains, and B.A. Eipper. 2001. The neuronal Rho-GEF Kalirin-7 interacts with PDZ domain-containing proteins and regulates dendritic morphogenesis. *Neuron*. 29:229-42.
- Peter, B.J., H.M. Kent, I.G. Mills, Y. Vallis, P.J. Butler, P.R. Evans, and H.T. McMahon. 2004. BAR domains as sensors of membrane curvature: the amphiphysin BAR structure. *Science*. 303:495-9.
- Petrache, H.I., S. Tristram-Nagle, K. Gawrisch, D. Harries, V.A. Parsegian, and J.F. Nagle. 2004. Structure and fluctuations of charged phosphatidylserine bilayers in the absence of salt. *Biophys J*. 86:1574-86.
- Pollard, T.D. 1986. Rate constants for the reactions of ATP- and ADP-actin with the ends of actin filaments. *J Cell Biol*. 103:2747-54.
- Prendergast, F.G., and K.G. Mann. 1978. Chemical and physical properties of aequorin and the green fluorescent protein isolated from *Aequorea forskalea*. *Biochemistry*. 17:3448-53.
- Rappoport, J.Z., S.M. Simon, and A. Benmerah. 2004. Understanding living clathrin-coated pits. *Traffic*. 5:327-37.

- Redecker, P., J. Bockmann, and T.M. Bockers. 2007. Secretory granules of hypophyseal and pancreatic endocrine cells contain proteins of the neuronal postsynaptic density. *Cell Tissue Res.* 328:49-55.
- Ridley, A.J. 2001. Rho family proteins: coordinating cell responses. *Trends Cell Biol.* 11:471-7.
- Ringstad, N., Y. Nemoto, and P. De Camilli. 1997. The SH3p4/Sh3p8/SH3p13 protein family: binding partners for synaptojanin and dynamin via a Grb2-like Src homology 3 domain. *Proc Natl Acad Sci U S A.* 94:8569-74.
- Roy, B.C., N. Kakinuma, and R. Kiyama. 2009. Kank attenuates actin remodeling by preventing interaction between IRSp53 and Rac1. *J Cell Biol.* 184:253-67.
- Saarikangas, J., H. Zhao, A. Pykalainen, P. Laurinmaki, P.K. Mattila, P.K. Kinnunen, S.J. Butcher, and P. Lappalainen. 2009. Molecular mechanisms of membrane deformation by I-BAR domain proteins. *Curr Biol.* 19:95-107.
- Sakamuro, D., K.J. Elliott, R. Wechsler-Reya, and G.C. Prendergast. 1996. BIN1 is a novel MYC-interacting protein with features of a tumour suppressor. *Nat Genet.* 14:69-77.
- Sala, C., V. Piech, N.R. Wilson, M. Passafaro, G. Liu, and M. Sheng. 2001. Regulation of dendritic spine morphology and synaptic function by Shank and Homer. *Neuron.* 31:115-30.
- Sambrook, D. 2000. *Molecular Cloning: A Laboratory Manual.* Cold Spring Harbor Laboratory Press, U.S.; .
- Sampath, P., and T.D. Pollard. 1991. Effects of cytochalasin, phalloidin, and pH on the elongation of actin filaments. *Biochemistry.* 30:1973-80.
- Sanda, M., A. Kamata, O. Katsumata, K. Fukunaga, M. Watanabe, H. Kondo, and H. Sakagami. 2009. The postsynaptic density protein, IQ-ArfGEF/BRAG1, can interact with IRSp53 through its proline-rich sequence. *Brain Res.* 1251:7-15.
- Schirenbeck, A., T. Bretschneider, R. Arasada, M. Schleicher, and J. Faix. 2005. The Diaphanous-related formin dDia2 is required for the formation and maintenance of filopodia. *Nat Cell Biol.* 7:619-25.
- Scita, G., S. Confalonieri, P. Lappalainen, and S. Suetsugu. 2008. IRSp53: crossing the road of membrane and actin dynamics in the formation of membrane protrusions. *Trends Cell Biol.* 18:52-60.
- Shimada, A., H. Niwa, K. Tsujita, S. Suetsugu, K. Nitta, K. Hanawa-Suetsugu, R. Akasaka, Y. Nishino, M. Toyama, L. Chen, Z.J. Liu, B.C. Wang, M. Yamamoto, T. Terada, A. Miyazawa, A. Tanaka, S. Sugano, M. Shirouzu, K. Nagayama, T. Takenawa, and S. Yokoyama. 2007. Curved EFC/F-BAR-domain dimers are joined end to end into a filament for membrane invagination in endocytosis. *Cell.* 129:761-72.

- Sivadon, P., F. Bauer, M. Aigle, and M. Crouzet. 1995. Actin cytoskeleton and budding pattern are altered in the yeast *rvs161* mutant: the Rvs161 protein shares common domains with the brain protein amphiphysin. *Mol Gen Genet.* 246:485-95.
- Slepnev, V.I., and P. De Camilli. 2000. Accessory factors in clathrin-dependent synaptic vesicle endocytosis. *Nat Rev Neurosci.* 1:161-72.
- Soltau, M., D. Richter, and H.J. Kreienkamp. 2002. The insulin receptor substrate IRSp53 links postsynaptic shank1 to the small G-protein cdc42. *Mol Cell Neurosci.* 21:575-83.
- Suetsugu, S., S. Kurisu, T. Oikawa, D. Yamazaki, A. Oda, and T. Takenawa. 2006a. Optimization of WAVE2 complex-induced actin polymerization by membrane-bound IRSp53, PIP(3), and Rac. *J Cell Biol.* 173:571-85.
- Suetsugu, S., H. Miki, and T. Takenawa. 2002. Spatial and temporal regulation of actin polymerization for cytoskeleton formation through Arp2/3 complex and WASP/WAVE proteins. *Cell Motil Cytoskeleton.* 51:113-22.
- Suetsugu, S., K. Murayama, A. Sakamoto, K. Hanawa-Suetsugu, A. Seto, T. Oikawa, C. Mishima, M. Shirouzu, T. Takenawa, and S. Yokoyama. 2006b. The RAC binding domain/IRSp53-MIM homology domain of IRSp53 induces RAC-dependent membrane deformation. *J Biol Chem.* 281:35347-58.
- Svitkina, T.M., and G.G. Borisy. 1999. Progress in protrusion: the tell-tale scar. *Trends Biochem Sci.* 24:432-6.
- Svitkina, T.M., E.A. Bulanova, O.Y. Chaga, D.M. Vignjevic, S. Kojima, J.M. Vasiliev, and G.G. Borisy. 2003. Mechanism of filopodia initiation by reorganization of a dendritic network. *J Cell Biol.* 160:409-21.
- Symons, M., J.M. Derry, B. Karlak, S. Jiang, V. Lemahieu, F. McCormick, U. Francke, and A. Abo. 1996. Wiskott-Aldrich syndrome protein, a novel effector for the GTPase CDC42Hs, is implicated in actin polymerization. *Cell.* 84:723-34.
- Takei, K., V.I. Slepnev, V. Haucke, and P. De Camilli. 1999. Functional partnership between amphiphysin and dynamin in clathrin-mediated endocytosis. *Nat Cell Biol.* 1:33-9.
- Tarricone, C., B. Xiao, N. Justin, P.A. Walker, K. Rittinger, S.J. Gamblin, and S.J. Smerdon. 2001. The structural basis of Arfaptin-mediated cross-talk between Rac and Arf signalling pathways. *Nature.* 411:215-9.
- Teodorof, C., J.I. Bae, S.M. Kim, H.J. Oh, Y.S. Kang, J. Choi, J.S. Chun, and W.K. Song. 2009. SPIN90-IRSp53 complex participates in Rac-induced membrane ruffling. *Exp Cell Res.* 315:2410-9.
- Tsujita, K., S. Suetsugu, N. Sasaki, M. Furutani, T. Oikawa, and T. Takenawa. 2006. Coordination between the actin cytoskeleton and membrane deformation by a novel

membrane tubulation domain of PCH proteins is involved in endocytosis. *J Cell Biol.* 172:269-79.

Verkleij, A.J., R.F. Zwaal, B. Roelofsen, P. Comfurius, D. Kastelijn, and L.L. van Deenen. 1973. The asymmetric distribution of phospholipids in the human red cell membrane. A combined study using phospholipases and freeze-etch electron microscopy. *Biochim Biophys Acta.* 323:178-93.

Vignjevic, D., S. Kojima, Y. Aratyn, O. Danciu, T. Svitkina, and G.G. Borisy. 2006. Role of fascin in filopodial protrusion. *J Cell Biol.* 174:863-75.

Vingadassalom, D., A. Kazlauskas, B. Skehan, H.C. Cheng, L. Magoun, D. Robbins, M.K. Rosen, K. Saksela, and J.M. Leong. 2009. Insulin receptor tyrosine kinase substrate links the *E. coli* O157:H7 actin assembly effectors Tir and EspF(U) during pedestal formation. *Proc Natl Acad Sci U S A.* 106:6754-9.

Visegrady, B., D. Lorinczy, G. Hild, B. Somogyi, and M. Nyitrai. 2004. The effect of phalloidin and jasplakinolide on the flexibility and thermal stability of actin filaments. *FEBS Lett.* 565:163-6.

Weiss, S.M., M. Ladwein, D. Schmidt, J. Ehinger, S. Lommel, K. Stading, U. Beutling, A. Disanza, R. Frank, L. Jansch, G. Scita, F. Gunzer, K. Rottner, and T.E. Stradal. 2009. IRSp53 links the enterohemorrhagic *E. coli* effectors Tir and EspFU for actin pedestal formation. *Cell Host Microbe.* 5:244-58.

Woodings, J.A., S.J. Sharp, and L.M. Machesky. 2003. MIM-B, a putative metastasis suppressor protein, binds to actin and to protein tyrosine phosphatase delta. *Biochem J.* 371:463-71.

Yamagishi, A., M. Masuda, T. Ohki, H. Onishi, and N. Mochizuki. 2004. A novel actin bundling/filopodium-forming domain conserved in insulin receptor tyrosine kinase substrate p53 and missing in metastasis protein. *J Biol Chem.* 279:14929-36.

Yanagida-Asanuma, E., K. Asanuma, K. Kim, M. Donnelly, H. Young Choi, J. Hyung Chang, S. Suetsugu, Y. Tomino, T. Takenawa, C. Faul, and P. Mundel. 2007. Synaptopodin protects against proteinuria by disrupting Cdc42:IRSp53:Mena signaling complexes in kidney podocytes. *Am J Pathol.* 171:415-27.

Yang, C., M. Hoelzle, A. Disanza, G. Scita, and T. Svitkina. 2009. Coordination of membrane and actin cytoskeleton dynamics during filopodia protrusion. *PLoS One.* 4:e5678.

Yeh, T.C., W. Ogawa, A.G. Danielsen, and R.A. Roth. 1996. Characterization and cloning of a 58/53-kDa substrate of the insulin receptor tyrosine kinase. *J Biol Chem.* 271:2921-8.

Zigmond, S.H. 1993. Recent quantitative studies of actin filament turnover during cell locomotion. *Cell Motil Cytoskeleton.* 25:309-16.

10 Appendix

10.1 PCR Primers

IMD-GFP	pEGFP N2	BglII	EcoRI	PCR	F: TAAGATCTATGTCTCTGTCTCGCTCA R: CAGAATTCGTTGCTGGCCACCTGCTG	Sequenced
IRSp53-GFP	pEGFP N1	BglII	BamHI	PCR	F: TAAGATCTATGTCTCTGTCTCGCTCA R: ATGGATCCGCACTGTGGACACCA	Sequenced
IMD-mCherry	pmCherry N1	BglII	BamHI	PCR	F: TAAGATCTATGTCTCTGTCTCGCTCA R: ATGGATCCCGTTGCTGGCCACCT	Sequenced
IMD K4E GFP	pEGFP N1	BglII	BamHI	PCR	F: TAAGATCTATGTCTCTGTCTCGCTCA R: ATGGATCCCGTTGCTGGCCACCT	Sequenced
IMD-GFP	pEGFP N1	BglII	BamHI	PCR	F: TAAGATCTATGTCTCTGTCTCGCTCA R: ATGGATCCCGTTGCTGGCCACCT	Sequenced
IRSp53 1-289 pGEX	PGEX4T2	BamHI	EcoRI	PCR	F: CGGGATCCATGTCTCTGTCTCGCTCAGAG R: GGAATTCTCACC GCCC CACGAACGGTGC	Sequenced
IRSp53 1-438 pGEX	PGEX4T2	BamHI	EcoRI	PCR	F: CGGGATCCATGTCTCTGTCTCGCTCAGAG R: GGAATTCTCAATCGCTGTCCAAGACCCGGGT	Sequenced
IRSp53 1-438-pGEX S3C	PGEX4T2 (S3C)	BamHI	EcoRI	Subcloned	-	
IMD-pGEX	PGEX4T2	BamHI	EcoRI	Generated by Tom Millard	-	

10.2 SDS PAGE buffers

Coomassie stain for SDS PAGE:

0.1 % Coomassie brilliant blue

45 % v/v Methanol

10 % v/v Acetic acid

Destain:

10 % Methanol

10 % Acetic acid

Gel Drying Solution

20 % (v/v) Methanol

2 % (v/v) Glycerol

Protein loading buffer

1 M Tris-Cl, pH8

1 M β -mercaptoethanol

75 % v/v Glycerol

10 % SDS

0.05 % Bromophenol blue dye

DNA loading buffer

40 % w/v Sucrose

0.05 % Bromophenol blue dye

Ladders

DNA: 1 Kb ladder,

Protein: Prestained protein marker (NEB)

Antibiotics

Ampicillin 1000 x stock solution 50 mg/ml in distilled water

Chloramphenicol 1000 x stock solution 30 mg/ml in ethanol

Kanamycin 1000 x stock solution 50 mg/ml in distilled water

10.3 Protein purification buffers

GTLB 1:

50 mM Tris-Cl, pH 8.0

40 mM EDTA

2.5 % (w/v) Sucrose

0.02 % NaN₃

1 mM PMSF

GTLB 2:

50 mM Tris-Cl, pH 8.0

100 mM MgCl₂

0.2 % (w/v) Triton X-100

0.02 % NaN₃

1 mM PMSF

PBS + DTT + Tween

0.2 % Tween

1 mM DTT

Thrombin Resuspension Buffer (TRB)

50 mM Tris-Cl, pH 8.0

150 mM NaCl
5 mM MgCl₂
2.5 mM CaCl₂
1 mM DTT

CM Sepharose column loading buffer

140 mM NaCl (150 mM for IMD-CRIB construct)
20 mM HEPES, pH 7.0
5 mM MgCl₂
2.5 mM CaCl₂
1 mM DTT

CM Sepharose column gradient buffer

500 mM NaCl (600 mM NaCl for IMD-CRIB)
20 mM HEPES, pH 7.0
5 mM MgCl₂
2.5 mM CaCl₂
1 mM DTT

AUC buffer

150 mM NaCl
50 mM Tris-Cl pH 8.0
1 mM DTT

10.4 Western blotting buffers

Anode I

300 mM Tris-Cl
20 % (v/v) Methanol
pH 10.4

Anode II

25 mM Tris-Cl
20 % (v/v) Methanol
pH 10.4

Cathode

25 mM Tris-Cl
40 mM Caproic acid
20 % Methanol
pH 9.4